UNIVERSITÀ
DI TORINO

UNIVERSITA' DEGLI STUDI DI TORINO

DEPARTMENT OF ONCOLOGY

PHD PROGRAM IN MOLECULAR MEDICINE

XXXV CYCLE

TFEB DRIVES CHEMO-IMMUNO-RESISTANCE IN LUNG CANCER

THESIS AUTHOR: MUHLIS AKMAN

SUPERVISOR: PROF. CHIARA RIGANTI

PHD PROGRAM COORDINATOR: PROF. FRANCESCO NOVELLI

ACADEMIC YEARS OF ENROLLMENT 2019-2023

CODE OF SCIENTIFIC DISCIPLINE: BIO/10

ABSTRACT

Introduction: With approximately 2 million fatalities per year worldwide, lung cancer is the second most prevalent malignancy and the leading cause of cancer-related death. Despite the advancements in lung cancer treatments, the five-year survival rate remains at 16% for men and 23% for women in Italy. Multidrug resistance (MDR) is one of the causes of failure in lung cancer treatment and the ATP Binding Cassette (ABC) transporters, which are responsible for the efflux of chemotherapeutic drugs, are key players in MDR. Transcription factor EB (TFEB) is a leucine zipper protein and a major regulator of lysosomal biogenesis and autophagy. These two events confer chemoresistance in solid tumors, by sequestrating chemotherapeutic drugs. Moreover, TFEB modulates the immune-recognition of cancer cells by the host immune-system. In endothelial cells, ChIP-Seq assays revealed that several ABC transporters are transcriptional targets of TFEB, but nothing is known for cancer. The aim of this study is to clarify if and how TFEB influences the expression and activity of ABC transporters as ABCB1, ABCC1, which determine chemosensitivity or resistance, and ABCA1, which determine sensitivity to Vγ9δ2 T lymphocyte-mediated immunological killing in non-small cell lung cancer (NSCLC).

Material and Methods: Changes in the expression of TFEB and ABC transporters (ABCA1, ABCB1, ABCC1), and their gene networks, as well as their effect on survival were analyzed by using TCGA-LUAD dataset. The results were validated in a cohort of NSCLC patients receiving chemotherapy, present at the Department of Oncology, University of Torino. After screening NSCLC cell lines, we silenced TFEB in the top 2 TFEB-expressing cell lines, NCI-H441 and NCI-H2228 cells. Changes in ABC transporters, in the upstream signaling pathways and the metabolic pathways involved in chemo-immunoresistance were measured by RT-PCR, immunoblotting, metabolic radiolabeling

and spectrophotometric assays, ELISA and ChIP. Sensitivity to cisplatin and paclitaxel was evaluated by the WST-1 assay. Co-cultures between NSCLC cells and Vγ9δ2 T-lymphocytes were set-up to measure their expansion and tumor cell killing. Wild-type (WT) and shTFEB NSCLC xenografts implanted in Hu-CD34^{+} NSG mice were used for in vivo validation of new chemo-immuno-sensitizing strategies.

Results and Discussion: The bioinformatic analysis showed that TFEB^{low}ABCA1^{low}ABCC1^{high} phenotype predicts poor overall survival in both TCGA-LUAD and in our patient cohort. ChIP assay indicated that ABCA1 is a direct target of TFEB, while ABCB1 and ABCC1 are not. By reducing the activation ofERK1/2 and Akt, TFEB silencing decreased the phosphorylation and the nuclear translocation of HIF-1α, which in turns down-regulate ABCB1 and ABCC1. Consistently, shTFEB cells had decreased expression of ABCB1 and ABCC1. In parallel, shTFEB cells had a reduced ERK-1/2-mediated activation of SREBP2, a master regulator of genes involved in cholesterol homeostasis. As such, TFEB silencing down-regulated genes of cholesterol synthesis, decreased the expression and the activity of ABCA1, which effluxes cholesterol and isopentenyl pyrophosphate (IPP), the endogenous activator of Vγ9δ2 T-lymphocytes. Consequently, TFEB silenced cells were less immune-killed by Vγ9δ2 T-cells.

The decreased cholesterol levels in mitochondria were paralleled by an increased activity of the oxidative phosphorylation (OXPHOS) and production of mitochondrial ATP (mtATP), the main fuel of drug efflux transporters. Notwithstanding the reduced expression of ABCB1 and ABCC1 in TFEB-silenced cells, we found a higher enzymatic activity that determines a slightly higher IC50 to cisplatin. Interestingly, these effects were reversed by low doses of nano-assembled zoledronic

acid (NZ) that increased IPP efflux and re-activated Vγ9δ2 T-lymphocytes killing, without reducing cholesterol synthesis and therefore maintaining low OXPHOS, mtATP and ABCB1/ABCC1 activity.

The results of immune xenografts, i.e., NCI-H2228 NSCLC cells implanted in Hu-CD34^{+}NSG mice, confirmed that shTFEB tumors were more resistant to cisplatin than wild-type counterpart. Conversely, they responded well to NZ. . The combination of cisplatin an NZ was effective in reversing the chemo-immuno-resistance of shTFEB tumors.

Conclusion: We propose TFEB as a driver of chemo-immuno-resistance in NSCLC. We dissected the intracellular signaling and molecular pathways controlled by TFEB and linked to the differential expression of ABC transporters involved in drug resistance and immune-killing. From this analysis we identified an unexpected and innovative chemo-immune-sensitizing approaches in NSCLC with TFEB^{low}ABCA1^{low}ABCC1^{high} phenotype that are associated with the worst prognosis. Further bioinformatic analysis predicted additional networks controlled by TFEB: if validated at biological levels, novel chemo-sensitizing tools may be discovered.

TABLE OF CONTENTS

LIST OF TABLES AND FIGURES

LIST OF ABBREVIATIONS

ASR	Age-Standardized Rate
ABCA1	Adenosine Triphosphate (ATP)-Binding Cassette (ABC) Transporter A1
ABCB1	Adenosine Triphosphate (ATP)-Binding Cassette (ABC) Transporter B1
ABCC1	Adenosine Triphosphate (ATP)-Binding Cassette (ABC) Transporter C1
ADGRF5	Adhesion G Protein-Coupled Receptor F5
ALK	Anaplastic Lymphoma Kinase
APC	Antigen-Presenting Cell
BRAF	V-Raf Murine Sarcoma Viral Oncogene Homolog B
BSA	Bovine Serum Albumin
CTLA-4	Cytotoxic T Lymphocyte Antigen-
CYP4F11	Cytochrome P450 4F11
DEG	Differentially Expressed Genes
DNA	Deoxyribonucleic Acid
EGFR	Epidermal Growth Factor Receptor
ENDS	Electronic Nicotine Dispensing Systems
EPD	Eucaryotic Promoter Database
ERK1/2 (MAPK)	Extracellular Signal-Regulated Kinase 1/2
ETC	Electron Transport Chain
FNIP2	Folliculin Interacting Protein 2
FPPS	Farnesyl Pyrophosphate Synthase
GAPDH	Glyceraldehyde 3-Phosphate Dehydrogenase
GO-BP	Gene Ontology Biologic Processes
GSVA	Gene Set Variation Analysis
GTF2A2	General Transcription Factor Iia Subunit 2
HER2	Epidermal Growth Factor Receptor 2
HIF1α	Hypoxia-Inducible Factor 1 Alpha
HMGCR	HMG-Coa Reductase
IC50	Half Maximal Inhibitory Concentration
ICI	Immune Checkpoint Inhibitors
IHC	Immunohistochemistry
IKZF1	Ikaros Family Zinc Finger 1
IL-18	Interleukin 18
IL-6	Interleukin 6
IL-8	Interleukin 8
IPP	Isopentenyl Pyrophosphate
KRAS	Kirsten Rat Sarcoma Viral Oncogene
LUAD	Lung Adenocarcinoma
LUSC	Lung Squamous Cell Carcinoma
MAPK	Mitogen-Activated Protein Kinase
MDR	Multidrug Resistance
MDR1	Multidrug Resistance Protein 1

MRP1	Multidrug Resistance-Associated Protein 1
mtATP	Mitochondrial ATP
mtDNA	Mitochondrial DNA
mTOR	Mammalian Target of Rapamycin
mTORC1	Mammalian Target of Rapamycin Complex 1
NGS	Next-Generation Sequencing
NSCLC	Non-Small Cell Lung Cancer
NZ	Nano-Assembled Zoledronic Acid
OCR	Oxygen Consumption Rate
OS	Overall Survival
OSGIN1	Induced Growth Inhibitor 1
OXPHOS	Oxidative Phosphorylation
PBMC	Peripheral Blood Mononuclear Cells
PD1	Programmed Death-1
PDL1	Programmed Death Ligand 1
PFS	Progression-Free Survival
PGD	Phosphogluconate Dehydrogenase
PI3K	Phosphoinositide 3-Kinases
RNA	Ribonucleic Acid
SASH3	Sam And Sh3 Domain Containing 3
SCLC	Small Cell Lung Cancer
SNX20	Sorting Nexin 20
SREBP2	Sterol Regulatory Element-Binding Protein 2
TBP	Tata Box Binding Protein
TCGA	The Cancer Genome Atlas Program
TFEB	Transcription Factor EB
TGFα	Transforming Growth Factor A
TME	Tumor Microenvironment
TNF-α	Tumor Necrosis Factor Alpha
VST	Variance-Stabilized Transformation
WGCNA	Weighted Correlation Network Analysis
WT	Wild-Type

1. INTRODUCTION

1.1. Lung Cancer Epidemiology and Risk Factors

Lung cancer is the second most common cancer, and it is the first cause of cancer-related death, with nearly 2 million deaths per year worldwide[1]. In Italy, the general cancer incidence rate was reported as in age-standardized rate (ASR) of 278,3 per 100.000 persons in both sexes, meanwhile the mortality rate was 90,6 ASR per 100.000 persons for all cancer types. With 25,3 ASR per 100.000 persons, lung cancer is the fourth most common cancer in Italy; however, the estimated mortality data shows that lung cancer leads the cancer-related death in Italy as in the rest of the world[2,3].

The one-year overall survival (OS) rate is 50%, while the five-year survival rate drops to 19% for both women and men in the US and Europe, and closer to these rates, five-year survival rate remains at 16% for men and 23% for women in Italy[3,4].

The incidence of lung cancer is often associated with tobacco consumption and in fact, it has been reported that 85-90% of the lung cancer cases were caused by smoking in Italy[5]. Smoking also increases cancer risk in other organs but its effect on lung is the highest impact amongst all sites. Lung cancer also affects non-smokers who were exposed to tobacco smoke because of its high carcinogenic content such as free radicals namely quinones and its derivatives, inorganic agents like nickel, arsenic, and chromium, as well as polycyclic aromatic hydrocarbons, N-nitrosamines, heterocyclic and aromatic amines, and aldehydes[6–8]. In recent years, electronic nicotine dispensing systems (ENDS) mostly known as e-cigarettes have risen to popularity as they are considered to be “safer” compared to conventional tobacco use because of its dispersion of nicotine by heating the liquid rather than burning. However, e-cigarettes still lead to numerous

lung complications, namely lung oedema, tissue hypoxia and airway epithelial injury[9]. In vitro studies indicate that e-cigarettes can induce apoptosis through lipid peroxidation, and similar to conventional cigarettes, e-cigarettes can activate pro-inflammatory signaling such as IL-6, IL-8, and TNF-α to increase inflammation, which further increases the self-renewal capabilities of lung cancer cells[10].

Prior studies have found a positive relationship between air pollution and the incidence of lung cancer, but the underlying causes remain unclear. According to a new study by Hill and colleagues, mutagens in air pollution promote lung cell mutations over the EGFR or KRAS genes in lung cells to facilitate their proliferation, and at the same time pollution enables macrophage recruitment to release IL-1β, leading to inflammation to further promotes the cancer formation[11]. In addition to air pollution, over 100 carcinogenic agents were associated with human cancers and especially acid mists, exposure to asbestos, and silica[12].

Studies have shown that hereditary factors play a significant role in the development of lung cancer. An analysis based on data from the International Lung Cancer Consortium revealed that people with a familiar history of lung cancer are at a higher risk, particularly the strongest association was among individuals who have a sibling who has lung cancer[13]. Although the mechanism of the hereditary factors are complex, genetic polymorphisms can provide insight into these complex systems. Studies indicated that germline mutations in p53 tumor suppressor gene plays crucial role in the promotion of lung cancer formation and chromosome 6q23-25 locus is identified as “susceptibility genes” for hereditary lung cancer[14,15].

1.2. Lung Cancer Screening and Molecular Classification

One of the causes why lung cancer leads to cancer-related deaths is the fact that lung cancer is diagnosed at late-stages. In US, the Center for Disease Control and Prevention organization implemented lung cancer screening program by using "*low-dose computed tomography*" (LDCT) to detect the cancer at early-stage if the patient has a history of smoking and is 50 to 80 years old, However, a comparable screening program has yet to be developed in Italy[16,17]. The multicentric Italian Lung Detection (MILD) trial findings indicated that LDCT screening reduced the lung cancer risk by 39% at 10 years, and overall mortality decreased by 20%, meaning that screening for lung cancer is crucial for early detection and overall survivability[18].

1.3 Main Genetic Alterations in Lung Cancers

KRAS

Up to 26% of the lung adenocarcinoma cases show Kirsten rat sarcoma viral oncogene homolog (KRAS) mutations[19]. KRAS is one of the members of the RAS superfamily that is activated upon GTP binding, subsequently activates RAS/RAF/MAPK2/MAPK and PI3K/Akt pathways to trigger cell proliferation and survival in both normal and cancer cells. In addition KRAS mutations were found to be associated with poorer survival and resistance to therapies[20].

EGFR-HER2

Epidermal growth factor receptor (EGFR) is a transmembrane receptor tyrosine kinase that belong to ErbB family of receptors, which consisted of three other receptors namely Human epidermal growth factor receptor 2 (HER2) - also known as ErbB2 (or neu in rodents) -, HER3 and HER4[21]. When EGFR binds to its ligands such as transforming growth factor α (TGFα) or phospholipase C, it forms heterodimers with the other members of the ErbB family, then it

activates mitogen-activated protein kinase (MAPK) as well as PI3K/Akt/mTOR pathways that promotes cell proliferation, survival and migration[22]. 15–25% of cases of lung adenocarcinoma patients have mutations in the EGFR, which results with continuous ATP binding and receptor activation[23]. Similar to EGFR, heterodimerization activates HER2 that activates RAS/MAP/MEK and PI3K/AKT pathways. However, Her2 genetic alterations are not common as EGFR, in fact HER2 mutations in lung cancer are reported in 3% of the cases[24]

ALK

Another member of the receptor tyrosine kinase family, anaplastic lymphoma kinase (ALK), is frequently found to be expressed in the nervous system but not in the lung. However EML4-ALK chimeric mutations are expressed in 3-7% of lung cancer patients[25,26]. This fusion is responsible for increased cell growth, proliferation and cell survival in lung cancer, often in young patients or non-smokers[27].

BRAF

V-Raf murine sarcoma viral oncogene homolog B (*BRAF*) kinase is associated with RAS/RAF/MEK/ERK pathway that is activated when BRAF is mutated, resulting in increased cell prolifetation[28]. BRAF mutations were detected up to 3% of lung cancer cases[29].

ROS1

As a member of the insulin receptor family, ROS1 is a receptor tyrosine kinase that may have a role in growth or differentiation. SLC34A2 and CD74 genes were found to be fuse with ROS1 and these fusions are potential driver for the non-small cell lung cancer, although only 1-3% of the cases show ROS1 rearrangements[30,31].

Other genetic alterations

Genes such as Ret Proto-Oncogene (RET), NTRK1 (TrkA), MET, v-AKT Murine Thymoma Viral Oncogene Homolog 1 (AKT1), Mitogen-Activated Protein Kinase 1 (MAP2K1) and Phosphatidylinositol-4,5-Bisphosphate 3-Kinase, Catalytic Subunit Alpha (PIK3CA) are also reported to be tumor driver genes in lung cancer, however they are usually upregulated in 1-3% of all the lung cancer cases[32].

1.4. Lung Cancer Subtypes

The tumors of cancer patients differ from one another in a variety of ways, and as new molecular and pathological diagnostic methods become available, new discoveries should be categorized; in fact the guidelines of the World Health Organization are accepted worldwide and are adapted for new diagnoses and treatments by other countries[33].

Squamous cell carcinoma	Small cell carcinoma	Adenocarcinoma	Large cell carcinoma
Clear cell	Combined	Adenocarcinoma, mixed subtype	Large cell neuroendocrine
Small cell		Acinar	Basaloid
Basaloid		Papillary	Lymphoepithelioma-like
		Bronchioloalveolar	Clear cell
		Nonmucinous	Large cell carcinoma with rhabdoid phenotype
		Mucinous	
		Mixed	
		Solid	
		Fetal	
		Mucinous cystadenocarcinoma	
		Signet ring	
		Clear cell	

Adenosquamous carcinoma	Sarcomatoid carcinoma	Carcinoid	Salivary gland tumors
	Pleomorphic carcinoma	Typical	Mucoepidermoid carcinoma
	Spindle cell	Atypical	Adenoid cystic carcinoma
	Giant cell		Epithelial-myoepithelial carcinoma
	Carcinosarcoma		
	Pulmonary blastoma		

Table 1: Several classes and subclasses of lung cancers shown in the table which adapted from the latest guideline of World Health Organization[34].

Lung cancers is divided in two main categories histologically: 15% of the cases belong to small-cell lung cancer (SCLC), the remaining 85% of the cases are Non-small cell lung cancer (NSCLC) that can be further divided in three different histologic subtypes: lung adenocarcinoma (LUAD), which is the most common, lung squamous cell carcinoma (LUSC) and large cell carcinoma[35].

Immunohistochemistry (IHC) is frequently used to support the classification. First, hematoxylin–eosin-stained tissue sections are evaluated to identify the morphology of the cancer cells, and then thyroid Transcription Factor 1 (TTF-1), p40 and mucicarmine staining are applied to distinguish the lung cancer subtype[32]. Molecular testing is also proven to be quite important for further classification of NSCLC, ADC or Squamous subtypes of lung cancers. Currently EGFR, ALK and ROS mutations as well as mutations and rearrangements on PD-L1, KRAS and BRAF-V600E are detected with IHC, however FISH, multiplex-PCR platforms and next-generation sequencing (NGS) techniques are now used quite often[36].

As the new biomarkers and new drugs discovered, precision medicine becomes increasingly important to improve treatment success. Each patient is unique and has different characteristic both genetically and molecularly, and their genetic and protein expression profiles, medical conditions and their lifestyle information can be analyzed with bioinformatics tools such as machine learning-algorithms artificial intelligence applications that can allow physicians to detect tumor tissues at early stages and moreover, they can adapt new treatment options or rearrange the treatment to improve their quality of life and success of treatment[37].

1.5. Staging Lung Cancer

After determining the type of cancer, the tumor is staged to determine its size and potential for metastasis. There are three abbreviations used to identify the tumor: T states the size of the

tumor which can go up to 7 cm or more, M states whether tumor has spread one or multiple part of the body, and N states whether lymph nodes have tumor tissue or not[38].

T (Primary Tumor)	
TX	Primary tumor cannot be assesed
T0	No primary tumor
Tis	In situ carcinoma
T1	size is <3 cm
T1mi	adenocarcinoma is minimally invasive
T1a	size is <1 cm
T1b	size is >1 cm but <2 cm
T1c	size is >2 cm but <3 cm
T2	size is >3 cm but <5 cm
T2a	size is >3 cm but <4 cm
T2b	size is >4 cm but <5 cm
T3	Tumor size is >5 cm but <7 cm or invades chest wall, diaphragm, phrenic nerve, parietal pericardium or main bronchus
T4	Tumor size is >7 cm or that invades heart, great vessels, trachea, laryngeal nerve, esophagus or vertebral body

Distant Metastasis (M)	
M0	No distant metastasis
M1	Distant metastasis
M1a	Separate tumor nodule(s) in a contralateral lobe tumor with pleural nodules or malignant pleural (or pericardial) effusion
M1b	Single distant extrathoracic organ metastasis
M1c	Multiple metastases

Regional Lymph Nodes (N)	
NX	Regional lymph nodes cannot be assessed
N0	No regional lymph node metastases
N1	Metastasis in ipsilateral peribronchial and/or ipsilateral hilar lymph nodes and intrapulmonary nodes, including involvement by direct extension
N2	Metastasis in ipsilateral mediastinal and/or subcarinal lymph node(s)
N3	Metastasis in contralateral mediastinal, contralateral hilar, ipsilateral or contralateral scalene, or supraclavicular lymph node(s)

Anatomic Stage and Prognostic Groups			
Occult Carcinoma	TX	N0	M0
Stage 0	Tis	N0	M0
Stage IA1	T1mi	N0	M0
	T1a	N0	M0
Stage IA2	T1b	N0	M0
Stage IA3	T1c	N0	M0
Stage IB	T2a	N0	M0
Stage IIA	T2b	N0	M0
Stage IIB	T1a	N1	M0
	T1b	N1	M0
	T1c	N1	M0
	T2a	N1	M0
	T2b	N1	M0
	T3	N0	M0
Stage IIIA	T1a	N2	M0
	T1b	N2	M0
	T1c	N2	M0
	T2a	N2	M0
	T2b	N2	M0
	T3	N1	M0
	T4	N0	M0
	T4	N1	M0
Stage IIIB	T1a	N3	M0
	T1b	N3	M0
	T1c	N3	M0
	T2a	N3	M0
	T2b	N3	M0
	T3	N2	M0
	T4	N2	M0
Stage IIIC	T3	N3	M0
	T4	N3	M0
Stage IVA	Any T	Any N	M1a
	Any T	Any N	M1b
Stage IVB	Any T	Any N	M1c

Table 2: Primary tumor, regional lymph nodes, distant metastasis and histopathologic grades make the staging of lung cancers as Stage 0 to Stage IV which adapted from the eight edition of American Joint Committee on Cancer Manual[39].

1.6. Treatment Options for NSCLC

Following the staging and the molecular classification of the lung cancer, treatment options have to be evaluated. Currently, the options for treating NSCLC include adjuvant chemotherapy with carboplatin/cisplatin, docetaxel/paclitaxel for early stages, and neoadjuvant chemotherapy followed by surgical resection. For patients who are not candidates for surgical resection and have

tumors that lack oncogenes, adjuvant chemotherapy followed by radiation therapy is the standard of care[40,41]. At early stages of NSCLC, namely Stage I and Stage II, surgery is considered as first treatment option to decrease mortality. Depending on the size of the tumor, following operations are considered: lobectomy, bilobectomy, pneumonectomy, segmentectomy or wedge resections[42]. However, surgical resection of SCLC is excluded from treatment options due to poor outcome[43].

Although new surgical techniques are introduced such as robotic lobectomy or video-assisted thoracoscopic surgery, some patients are remain inoperable therefore stereotactic body radiation therapy (SBRT), also known as stereotactic ablative (SABR) radiotherapy is often applied concurrently or sequentially[42,44].

On the other hand, chemotherapy remains one of the standards for locally advanced or metastatic lung cancers, and when patients are not eligible for target therapy or immunotherapy. As a first line therapy option, platinum-based drugs especially cisplatin and carboplatin are proven effective against many solid tumors including lung cancer, while crosslinking with DNA to interfere with DNA repair mechanisms to create DNA damage and eventually initiating apoptosis for the cancer cell[45]. Cisplatin is one of the oldest and widely used chemotherapeutic drug that can also binds to mitochondrial DNA (mtDNA) to stop the replication of DNA, mRNA and proteins which lead to necrosis or apoptosis while it is effective against many tumors, cisplatin-received cancer patients can display serious side effects and resistance to chemotherapy. Cisplatin is often combined with other drugs such as taxanes[46].

Paclitaxel and docetaxel are natural taxanes extensively used in NSCLC treatment, that can bind to microtubules and arrest the cell in mitosis, resulting cytostatic or cytotoxic responses[47]. A

meta-analysis showed that nab (nanoparticle-albumin bound)-paclitaxel combined with carboplatin increased overall response rate as well as OS in NSCLC[48]. The results of CAPITAL phase-III trial on Japanese patients aged over 70 with advanced squamous NSCLC revealed that OS was better in patients who received nab-paclitaxel plus carboplatin compared to patients treated with carboplatin-docetaxel combination[41].

Gemcitabine is a pyrimidine analog approved by FDA as a first-line treatment for advanced NSCLC which can be incorporated into DNA strands during S phase of cell cycle and results with single-strand breaks of DNA. It is often used to combine with cisplatin or carboplatin due to its low toxicity[49].

Pemetrexed which is a pyrrolopyrimidine antifolate that inhibits thymidylate synthase, glycinamide ribonucleotide formyltransferase, and dihydrofolate reductase. Also, it is used as second line treatment along with docetaxel, in fact phase III trials reports that pemetrexed has better improved OS compared to docetaxel in NSCLC patients who has been received chemotherapy before[50,51]. Also, KEYNOTE-189 trial updates showed that pembrolizumab which is an anti-programmed death-1 (PD-1) antibody combined with pemetrexed-platinum treatment increased the OS to 22 months compared to placebo combined with pemetrexed-platinum treatment, which had a median of 10.7 months of OS in metastatic non-squamous NSCLC[52].

In the recent years, there has been a rapid development in the targeted therapy field due to novel biomarker discoveries. More than 65% of people with advanced NSCLC are estimated to have a potentially treatable genetic mutations, thus targeting these alterations and rearrangements could be beneficial for these patients[53]. There are several drugs (shown in Table 3) that are already

approved by FDA to be used in advanced NSCLC, essentially, these drugs inhibit activity of their target thus reduce the tumor burden and improve the OS of the patient[36].

Target	FDA Approved Drug
EGFR	Gefitinib Erlotinib Afatinib Dacomitinib Osimertinib
ALK	Crizotinib Alectinib Brigatinib Ceritinib Loratinib
ROS1	Crizotinib Loratinib Entrectinib Brigatinib
RET	Pralsetinib Selpercatinib
HER2	Pyrotinib Tucatinib Trastuzumab Trastuzumab deruxtecan
KRAS	Adagrasib Sotorasib
BRAF	dabrafenib plus trametinib
NTRK	Larotrectinib Entrectinib
MET	Crizotinib

Table 3: Rearrangements or mutations in genes commonly observed in NSCLC and their respective drugs which are approved by FDA are shown. Table is adapted from Guo et al, 2022[36].

1.7. Immunotherapy

Recent research has shown that patients with lung cancer can benefit from immunotherapies belonging to "Immune checkpoint inhibitors (ICIs)". A number of targets and antibodies were proposed to have immunotherapeutic use, as:

- programmed cell death protein-1/programmed cell death ligand-1(PD-1/PD-L1) pathway
- cytotoxic T lymphocyte antigen-4 (CTLA-4) pathways

can be used for immunotherapy of NSCLC[54].

PD1/PDL1 Pathway

A T cell family inhibitory receptor called programmed cell death protein 1 (PD1) is expressed on antigen-activated T cells. Antigen presenting cells (APCs), tissue cells and bone marrow-derived APCs all express its ligands, PD-L1 and PD-L2, respectively. When PD1 binds to its ligands, T cells are made anergic as a result of PD-1's interference with the kinase-dependent signals from the TCR-coreceptor complex, CD28, and other costimulatory receptors[55]. In tumor microenvironment (TME), PD1 overexpression regulates tumor-specific T cell immunity which causes immune system anergy[56]. So far,

- Nivolumab
- Pembrolizumab
- Cemiplimab

Are approved for PD1 therapy in NSCLC. Anti-PDL1 agents Atezolizumab and Durvalumab are approved for the patients who has metastatic NSCLC[57].

CTLA-4

All T cells have CD28 receptor that transduces co-stimulatory signals necessary for T cell activation and survival. Its ligands CD80 (B7-1) and CD86 (B7-2) are located on APCs for activation of T cells[58]. A further member of the CD28 receptor family, cytotoxic T lymphocyte antigen-4 (CTLA-4) serves as a competitive inhibitor of CD28 and lowers the availability of B7 for the CD28 receptor in normal conditions. Chronic inflammation and cancer are frequently associated to CTLA-4

overexpression suggesting that CTLA-4 in the TME may be responsible for the suppression of the anti-tumor immune response[59]. So far only anti-CTLA4 antibody Ipilimumab combined with Nivolumab therapy is approved for NSCLC patients with no EGFR or ALK genomic tumor mutations[60].

1.8. Resistance to Treatment

Drug resistance is one of the main barriers to an effective cancer treatment. It occurs when the disease develops a tolerance to chemotherapy. Numerous causes, including genetic mutations and/or epigenetic modifications, increased drug efflux, and various other cellular and molecular pathways, contribute to the development of resistance to anticancer drugs. To overcome this phenomenon, an increasing number of targeted agents have been produced in recent years to accurately target/block the alterations that fuel cancer growth and proliferation. Although many medications exhibit impressive positive effects when used at the beginning of treatment, the majority of patients eventually acquire resistance[61]. Multidrug resistance (MDR), i.e., the simultaneous resistance to different agents unrelated for structures and mechanisms of action, can be either intrinsic or acquired. The latter is more clinically significant, and it has been attributed mostly to the increased efflux of the anticancer agent, which results in lower intracellular drug accumulation. This event is mainly controlled by adenosine triphosphate (ATP)-binding cassette (ABC) transporters superfamily[62].

ABC transporters

ABC transporters superfamily consists of seven subfamilies from ABCA to ABCG and 48 genes in total. ABCB1, also known as P-glycoprotein (Pgp) or multidrug resistance protein 1 (MDR1), has been identified as the first transporter involved in the ABC transporter structure is made by two

transmembrane domains (TMDs), which recognize and transport substrates, and two cytoplasmic nucleotide-binding domains (NBDs), which bind and hydrolyze ATP to exert their function[63]. Multidrug resistance-associated protein 1 (MRP1), which is encoded by ABCC1 gene, was the second ABC transporter to be identified and studied extensively due to the variety of xenobiotics and biological substances effluxed along with ABCB1[64]. In physiological conditions, these transporters are responsible for transporting lipids, peptides, vitamins, steroids[65], as well as toxic metabolites and xenobiotics. Carboplatin, cisplatin and paclitaxel are substrates for both ABCB1 and ABCC1[66,67].

According to an earlier study, ABCB1 is expressed in 15–50% of lung cancers[66]. In the lung cancer tissue of NSCLC patients, ABCC1 expression was noticeably increased compared to non-transformed tissue. ABCC1 is functionally active in NSCLC cells, and the increased drug efflux may be related with poor treatment outcomes in NSCLC patients, according to a meta-analysis, although it is not known how MRP1 expression is regulated in NSCLC[68]. At first, pharmacological inhibitors of ABC transporters were developed to challenge MDR. Some of them underwent clinical trials over the past three decades but they had only little therapeutic success because of various heavy adverse effects due to the physiological block of ABC transporters in healthy tissues[69].

Recent studies show that alterations in the metabolism of cancer cells, particularly aberrant cholesterol metabolism, play a significant role in their increased ability to proliferate and migrate. ABCA1 is another ABC transporter localized in the plasma membrane and a significant factor controlling intracellular cholesterol levels[70]. In the context of cholesterol homeostasis, ABCA1 is most known for its roles in the efflux of intracellular cholesterol and the formation of nascent

HDL. Additionally, it is in charge of the efflux of the tiny isoprenoid isopentenyl pyrophosphate (IPP), which is the natural activator of γ9δ2 T-lymphocytes, a T-cell subset endorsed with anti-tumor properties[71]. This mechanism allows ABCA1 to improve immune killing[72–74]. While the roles of ABCB1 and ABCC1 in cancer is well established, ABCA1 role in cancer is rather tumor-dependent: there are few studies examining the role of ABCA1 in NSCLC. It has been reported that ABCA1 increases the sensitivity of NSCLC to cisplatin, but it is associated to poor prognosis in triple-negative breast cancer and ovarian cancer[75–77].

TFEB

The maintenance of the physiologic status of the cell depends on the homeostasis of nutrients., To maintain this homeostasis, the autophagy pathway is activated under nutritional stress, such as stress brought on by nutrient deficiency or excess. As a result, the nutrients or damaged organelles are recycled for cell survival after the autophagy pathway is activated[78]. Autophagosomes are heavily interconnected with lysosomes: the autophagosomal substrates that is generated at the end of autophagic pathway are eliminated upon fusing with the lysosome. Recently, it has been reported that several pathways activating autophagy, autophagosome formation, and degradation of damaged organelles are controlled by Transcription factor EB (TFEB), a leucine zipper protein which belongs to microphthalmia family of basic helix-loop-helix–leucine-zipper (bHLH-Zip) transcription factors (MiT family)[79]. TFEB can control lysosomal biogenesis, autophagy, lipid catabolism and lysosomal exocytosis in addition to promoting intracellular clearance of damaged organelles[80]. Recent works have shown that TFEB has an emerging player in metabolic homeostasis and organelle biogenesis[81].

When inactive, TFEB is retained in the cytosol; however, upon starvation, exercise and lysosomal stress TFEB translocate into the nucleus and becomes active as transcription factor[82]. Extracellular signal-regulated kinase 1/2 (ERK1/2, also known as MAPK1) and mammalian target of rapamycin complex 1 (mTORC1) have been found to phosphorylate TFEB[83,84], but the functional meaning of these phosphorylations and the linkage with TFEB activation are still under investigation.

There are few studies examining the role of TFEB in NSCLC. Strong expression of TFEB on adenocarcinomas and poor prognosis were noted in one study, where silenced TFEB cells resulted had reduced migration abilities, with no change in their proliferation potential[85]. However, in another recent study a low TFEB expression was associated with poor prognosis in NSCLC patients[86]. Thus, the role of TFEB in NSCLC is still remain unclear.

TFEB also controls cholesterol homeostasis and modulates immune response[87,88]. Until now, no data correlate TFEB with the homeostasis of cholesterol mediated by ABCA1 and with the anti-tumor activity of γ9δ2 T-lymphocytes[71]. Lysosomal biogenesis and autophagy are known to confer chemoresistance in solid tumors, by sequestrating chemotherapeutic drugs and/or triggering a cytoprotective autophagy[89], but currently there are not studies investigating of TFEB could also modulate the activity and expression of ABCB1 and ABCC1, involved in chemotherapeutic drug efflux and chemoresistance[63].

2. Aim of the Study

Despite novel biomarker discoveries and optimizations in the chemotherapy and immunotherapy regimens, NSCLC remains lethal and often shows resistance to chemotherapy and immune-evasive. One of the causes of resistance is represented by ABCB1 and ABCC1 that are not promising druggable targets. Modulating the cancer-specific pathways that control ABC transporters activity and expression seems nowadays a more promising strategy to fight MDR.

Since TFEB, which is more expressed in NSCLC than in non-transformed tissue, affects cholesterol homeostasis, which is crucial in regulating both chemoresistance and tumor cell immune-killing by Vγ9δ2 T-lymphocytes, it could be regarded as a good target to manipulate within NSCLC to induce chemo- and immune-sensitization.

The aim of this work is to unravel the role of TFEB on regulating expression and activity of ABC transporters which dictate the resistance/sensitivity to chemotherapy (ABCB1, ABCC1) and to Vγ9δ2 T-lymphocyte-mediated immune-killing (ABCA1). Starting from the interrogation of TCGA database (LUAD cohort), we found that patients with low levels of TFEB, low levels of ABCA1 and high levels of ABCC1 had the worst OS. This association was confirmed in a retrospective analysis of NSCLC patients receiving chemotherapy at the Department of Oncology, University of Torino, and was supported by the in vitro finding that TFEB silencing induced a chemo-immuno-sensitization, mediated by the changes in the expression and activity of ABCB1, ABCC1 and ABCA1. We examined the metabolic and molecular circuitries controlled by TFEB that modulate activity and expressions of these ABC transporters, and the impact that targeting TFEB may have on chemo- and immuno-resistance of NSCLC cells. Finally, by disrupting such metabolic circuitries, particularly linked to cholesterol homeostasis, we set up a new pharmacological strategy that

induces chemo-immuno-sensitization even in NSCLC with low levels of TFEB that have the worst response to chemotherapy and poorest immune-killing efficacy.

3. Material & Methods

3.1. Bioinformatic analysis: Publicly available three lung cancer datasets, provided by The Cancer Genome Atlas (TCGA), were identified, and lung adenocarcinoma cases were selected (https://portal.gdc.cancer.gov/projects/TCGA-LUAD). Transcriptome profiling of the TCGA-LUAD project was downloaded via query, then the database was imported to the R working environment. Count matrices and clinical information of TCGA-LUAD sequencing reads were extracted and exported. Count matrices were read, and Ensembl IDs of the genes was set. Feature annotations were created by querying “org.Hs.eg.db”, which is an annotation package based on mapping using Entrez Gene identifiers of human genes to obtain "ENSEMBL", "ENTREZID", "SYMBOL", "GENENAME" features of the genes[90]. After checking if all features and the samples were present, counts matrices and feature annotations were synced to create a “dds” object. The dds object, which was created during data preprocessing was normalized via the DESeq2 package. DESeq2 package provides several methods to test differential expression by using negative binomial linear models, and estimation of dispersion as well as logarithmic fold changes[91]. After creating a variance-stabilized transformed (VST) dds object, distributions of TFEB, ABCA1, and ABCC1 were compared between normal tissue and tumor tissue. From these findings, "high" and "low" levels of the genes were estimated. Following gene dispersion, clinical data including survival times and the vital status of the cases were extracted. Then the correlation of TFEB, ABCA1, ABCC1 and survival in lung cancer was calculated.

Differentially expressed genes (DEG) were calculated by comparing high vs low levels of TFEB, ABCA1, and ABCC1. To identify the pathways linked to these DEGs, gene set variation analysis (GSVA) transformation was done from gene expression profiles[92]. After transformation, GSVA

scores were extracted and differentially activated pathways as per GSVA were calculated by using the "limma" package[93]. Weighted correlation network analysis (WGCNA) is a package in the R environment to find clusters (hence modules) of highly correlated genes and summarize these clusters using the module "eigengene". In addition to that, it can be used to correlate modules from one cluster to another and external sample traits by using the methodology of eigengene network[94]. The same dds objects were filtered from microRNA, pseudogenes, and uncharacterized genes and loaded into variance stabilized transformation. After calculation, genes which have a base mean < 0 were filtered out. Filtered VST object was used to construct the network by the WGCNA package. Modules were set into biologic context by term enrichment analysis, then the correlation between module eigengene and traits were calculated. Significantly differing module eigengenes were calculated by high vs low expression of the genes of interest, followed by the estimation of the connectivity and the determination of hub genes.

3.2. Retrospective analysis on NSCLC patients: A cohort of patients with stage III-IV non-resectable NSCLC, treated with Cisplatin (n=32) or immunotherapy (Pembrolizumab; n=43) as a first-line treatment was examined in terms of progression free survival (PFS; time from the beginning of chemotherapy to the first sign of disease's progression) and OS (survival from the beginning of chemotherapy until patients' death)**.** From each tumor samples the RNA was extracted and the levels of TFEB, ABCC1 and ABCA1 were measured by qRT-PCR, as indicated in the dedicated paragraph. A multiparametric analysis was applied to correlate the levels of TFEB, ABCC1 and ABCA1 with TTP and OS of the patients. The study was conducted in accordance with the Declaration of Helsinki and was approved by the local ethics committee (San Luigi Gonzaga Hospital, Orbassano, Torino; IRB n. 73/2018).

3.3. Cells: Calu-3, NCI-H1975, NCI-H3122, NCI-NCI-H2228, NCI-NCI-H441, NCI-H1650, A549 NSCLC cell lines were purchased from ATCC (Manassas, VA). Cells were monitored by a contrast phase Leica DC100 microscope (Leica Microsystems GmbH, Wetzlar, Germany) and maintained in RPMI-1640 (Gibco-Thermo Fisher Scientific, Waltham, MA) medium supplemented with 10% v/v fetal bovine serum (FBS), 1% v/v penicillin-streptomycin, 1% v/v L-glutamine.

3.4. TFEB Silencing: A shRNA lentiviral vector produced in house was used to silence TFEB[95]. NCI-NCI-H441 and NCI-NCI-H2228 cells were seeded at $2.5x10^5$ cells/well. 24 hours after seeding, cells were transduced with the vector targeting TFEB or with the corresponding empty vector (pLKO) for 6 hours, in medium with 10 µg/mL Polybrene/hexadimethrine bromide (Sigma-Aldrich, USA). After incubation, the medium containing was removed and replaced by new medium containing puromycin (Sigma-Aldrich, USA) at the respective IC50 values (250 ng/mL for NCI-NCI-H441, 1 µg/mL for NCI-NCI-H2228), determined in previous viability assays on these cell lines. After incubation, cells were removed with either trypsin for subsequent passaging or with RiboZol (VWR International Srl, Milan, Italy) for RNA extraction. The efficiency of TFEB silencing were checked with qRT-PCR at 24, 48 and 72 h. The best silencing conditions were: 48 h for NCI-NCI-H441 cells, 24 h for NCI-NCI-H2228 cells.

3.5. Flow cytometry. $1×10^4$ cells were washed in phosphate-saline buffer (PBS), pH 7.2, 0.5% bovine serum albumin (BSA) and 2 mM EDTA, centrifuged at 300×g for 10 min, incubated 20 min at room temperature in the dark with 250 µl of Inside Fix reagent (Inside Stain Kit, Miltenyi Biotec., Bergisch Gladbach, Germany), centrifuged at 300×g for 5 minutes, washed with 1 mL of Inside Perm (Inside Stain Kit), centrifuged at 300×g for 5 minutes, and incubated 30 minutes at room temperature with the following antibodies (all from Miltenyi): anti-CD243/ABCB1 antibody (PE-

Vio® 770-conjugated); anti-MRP1/ABCC1 antibody (PE-conjugated); anti-ABCA1 (DyLight 488-conjugated). Cells were washed with 1 mL of Inside Perm reagent, centrifuged at 300×g for 5 minutes and read using a Guava® EasyCyte flow cytometer (Millipore, Billerica, MA), equipped with the InCyte software (Millipore).

3.6. Immunoblotting and Co-Immunoprecipitation: The cells were lysed in MLB buffer (125 mM Tris-HCl, 750 mM NaCl, 1% v/v NP40, 10% v/v glycerol, 50 mM $MgCl_2$, 5 mM EDTA, 25 mM NaF, 1 mM $NaVO_4$, 10 mg/mL leupeptin, 10 mg/mL pepstatin, 10 mg/mL aprotinin, 1 mM phenylmethylsulphonyl fluoride PMSF, pH 7.5), sonicated and centrifuged at 13,000 g for 10 min at 4°C. 50 µg of proteins were subjected to immunoblotting and probed with the following antibodies: anti-TFEB (Bethyl Laboratories, Inc., Montgomery, TX, dilution 1/1000), anti-phospho(Ser211)-TFEB(Invitrogen Carlsbad CA, dilution 1/1000), anti-ULK1 (Invitrogen Carlsbad CA, dilution 1/1000), anti-phospho(Ser555)-ULK1 (Invitrogen Carlsbad CA, dilution 1/1000), anti-AMPK-α-1 (Invitrogen Carlsbad CA, dilution 1/1000), anti-phospho(Thr183/Thr172)-AMPK-α-1/2 (Invitrogen Carlsbad CA, dilution 1/1000), anti-HMGCR (Santa Cruz Biotechnology Inc., Santa Cruz, CA, dilution 1/1000), anti-ABCA1 (HJI, Abcam, dilution 1/500), anti-ABCB1 (C219, Novus Biologicals, Littleton, CO, dilution 1/250), anti-ABCC1 (Santa Cruz Biotechnology Inc., Santa Cruz, CA, dilution 1/1000), anti-phospho(Ser473)Akt (6F5, Millipore, dilution 1/1000), anti-Akt (SKB1, Millipore, dilution 1/500), anti-phospho(Thr389)-p70 S6K (Cell Signaling, Technology, Danvers, MA, dilution 1/1000), anti-phospho(Thr421/Ser424)-p70 S6K (Cell Signaling Technology, dilution 1/1000), anti-p70 S6K (Cell Signalling Technology, dilution 1/1000), anti-phospho(Thr202/Tyr204) ERK1/2 (Cell Signalling Technology, dilution 1/1000), anti-ERK1/2 (Cell Signaling Technology, dilution 1/1000), anti-α-ubiquitin (R&D Systems, dilution 1/1000), anti-phospho-serine (Abcam,

dilution 1/1000), anti-HIF1α (dilution 1/1000), anti-sterol regulatory element binding protein 2 (SREBP2; NBP1-71880, Novusbio, USA, 1/500, which recognizes both uncleaved and cleaved SREBP2) antibody. Anti-GAPDH (Santa Cruz Biotechnology Inc., Santa Cruz, CA, dilution 1/1000) was employed as a control of equal protein loading. The proteins were detected by enhanced chemiluminescence (Bio-Rad Laboratories). The immunoprecipitated samples (100 µg of whole cell lysates) were incubated with an anti-phospho (Thr202/Tyr204) ERK1/2 antibody (Cell Signaling Technology, dilution 1/1000), or anti-phospho-serine antibody (Abcam, dilution 1/1000) with the PureProteome Protein A/G Mix Magnetic Beads (LSKMAGAG10, Millipore) for 3 h at 4°C. pERK 1/2 immunoprecipitated samples were immunoblotted with an anti-SREBP2 antibody to detect the interaction between phosphor-ERK1/2 and SREBP2. pSer immunoprecipitated samples were immunoblotted with an anti-HIF1α antibody, to measure the phosphorylation of HIF1α. 50 µg of proteins prior immunoprecipitation were subjected to immunoblotting using the anti-SREBP2 or anti-HIF1α antibodies, to check the equal protein loading.

3.7. Cell viability: Cell viability of NCI-NCI-H441 and NCI-NCI-H2228 against increasing concentrations of cis-Diammine Platinum (II) dichlorate (Cisplatin, Sigma-Aldrich, USA) and Paclitaxel (Sigma-Aldrich, USA) was measured by using WST-1 kit (Roche, USA) as per manufacturer's instructions, using a Synergy HT Multi-Detection Microplate Reader (Bio-Tek Instruments, Winooski, VT). The relative absorbance units of untreated cells were considered as 100% viability; the results were expressed as a percentage of viable cells versus untreated cells.

3.8. Synthesis of cholesterol, farnesyl pyrophosphate (FPP) and isopentenyl pyrophosphate (IPP): Cells were labeled with 1 µCi of [^{3}H]-acetate (3600 mCi/mmol; Amersham International, Piscataway, NJ) for 24 h. The synthesis of radiolabeled cholesterol, FPP and IPP was measured after lipid extraction, separation by thin layer chromatography (TLC) and liquid scintillation count[96]. Results were expressed as pmoles/mg cell proteins, according to the relative calibration curves.

3.9. HMGCR activity: 10 x 10^6 cells were rinsed with the lysis buffer (10 mM Tris, 100 mM NaCl, 20 mM KH2PO4, 30 mM EDTA, 1 mM EGTA, 250 mM sucrose, pH 7.5) supplemented with protease inhibitor cocktail set III (100 mM AEBSF, 80 mM aprotinin, 5 mM bestatin, 1.5 mM E-64, 2 mM leupeptin and 1 mM pepstatin; Merck), 1 mM Na_3VO_4, 1 mM NaF, 1 PMSF, 10 mM aprotinin and 10 mM dithiothreitol (DTT). After sonication, cell lysates were centrifuged at 13,000 x g for 15 min at 4°C. The supernatants were centrifuged at 100,000 x g for 1 h at 4°C, using an Optima L-90K Beckman Coulter Ultracentrifuge (Beckman Coulter Inc, Fullerton, CA) to collect the microsomal fraction, which was re-suspended in 250 µL lysis buffer and stored at -80°C until the use. For HMGCR activity, microsomal protein extracts were re-suspended in lysis buffer (12.5 µg proteins in 25 µL), supplemented with 10 mM DTT, 5 mM NADP and a NADPH-generating system (1.3 mM glucose 6-phosphate, 0.67 U/mL glucose-6 phosphate dehydrogenase, 33 mM MgCl2). The reaction was started by adding 60 nCi [^{14}C]HMG-CoA (50–62 mCi/mmol, Amersham Bioscience). After a 20-min incubation at 37°C, the reaction was stopped with 25 µL 10 N HCl. The samples were stirred for 30 min at 37°C to ensure complete lactonization of mevalonic acid, centrifuged at 13,000 x g for 2 min and separated by TLC on silica gel plates (LK6D Whatman silica gels (Merck, Darmstadt, Germany) with hexane/acetone (1:1, v/v) as mobile phase. A 1 mM solution of

purified mevalonolactone was used as standard. The labeled product, [^{14}C]mevalonolactone, was recovered from the TLC plates and quantified by liquid scintillation. HMGCR activity was expressed as nmol HMGCoA/mg cell proteins, according to a titration curve previously set.

3.10. Release of cholesterol and IPP: To measure the efflux of an exogenous pulse of cholesterol or IPP, 1 x 10^6 cells/ml were labeled for 1 h with 0.02 mCi of [^{14}C]-cholesterol (60 mCi/mmol; Amersham International)[96] or [^{14}C]-IPP (50 mCi/mmol; Amersham International)[97], washed five times with PBS and left for 24 h in fresh medium. After this incubation time, supernatants were collected, lipids were extracted, subjected to separation by TLC and quantified by liquid scintillation to measure the effluxed cholesterol or IPP. Results were expressed as pmoles/ml, according to the relative calibration curves.

3.11. Total and mitochondrial cholesterol: 10 x 10^6 cells were lysed in 0.5 mL of 10 mM Tris, 100 mM NaCl, 20 mM KH2PO4, 30mM EDTA, 1 mM EGTA, 250 mM sucrose, pH 7.5) and sonicated with 2 bursts of 10 s (Labsonic sonicator, Sartorius Stedim Biotech S.A., Aubagne Cedex, France), then centrifuged at 13,000 x g for 15 min at 4°C. The supernatants were centrifuged at 100,000 g for 1 h at 4°C, using an Optima L-90K Beckman Coulter Ultracentrifuge (Beckman Coulter Inc, Fullerton, CA) to collect the membrane fractions. In case of mitochondrial cholesterol mitochondrial extracts were prepared as detailed below. The pellets of membranes or mitochondria were resuspended in 250 µL of the assay buffer provided by fluorometric Cholesterol/Cholesteryl Ester Assay Kit – Quantitation (Abcam) and used to measure free cholesterol in the membrane, as per manufacturer's instructions. An aliquot of 50 µL were sonicated again and used to measure the membrane proteins. Results were expressed as mg cholesterol/mg membrane proteins.

3.12. Electron transport chain (ETC) activity: Mitochondria were isolated from 10^7cells, lysed in 0.5 mL lysis buffer (5 mM Tris-HCl, 100 mM KCl, 5 mM $MgCl_2$, 1.8 mM ATP, 1 mM EDTA, pH7.2, Protease Inhibitor Cocktail III, 1 mM PMSF and 250 mM NaF). Samples were centrifuged at 650×g for 3 minutes at 4°C, the supernatants were re-centrifuged at 13000×g for 5 min at 4°C. Mitochondria containing pellets were resuspended in 0.25 mL resuspension buffer (250 mM sucrose, 15 mM K_2HPO_4, 2 mM $MgCl_2$, 0.5 mM EDTA). 50 µL aliquots were sonicated and used for the measurement of protein content. 10 µg of each sonicated sample were analyzed by SDS-PAGE and immunoblotting with an anti-porin antibody (clone 20B12AF2, Abcam, Cambridge, UK, dilution 1/1000) to confirm the presence of mitochondrial proteins in the extracts. The electron efflux from complex I to complex III, taken as an index of the mitochondrial respiratory activity[98] was measured on 50 µg of non-sonicated mitochondrial samples, re-suspended in 0.2 mL of buffer A (5 mM KH_2PO_4, 5 mM $MgCl_2$, 5% w/v BSA; pH 7.2) and 0.1 ml of buffer B (25% w/v saponin, 50 mM KH_2PO_4, 5 mM $MgCl_2$, 5%w/v BSA, 0.12 mM oxidized cytochrome c, 0.2 mM NaN_3, which blocks complex IV allowing the accumulation of reduced cytochrome c; pH7.5). The reaction mix was allowed to equilibrate for 5 min at room temperature. The cytochrome c reduction reaction was monitored for 5 min after adding 0.15 mM NADH, reading the absorbance changes at 550nm by a Synergy HT Multi-Detection Microplate Reader (Bio-Tek Instruments). Results were expressed as nanomoles of reduced cytochrome c/min/mg mitochondrial proteins.

3.13. O_2 consumption rate (OCR): 5×10^4 NCI-H441 and NCI-H2228 cells were seeded in 96-well microplates (Nunc, Rochester, NY). After 24 h, the Resipher oxygen sensing lid (Lucid Scientific, Atlanta, MA) was positioned upon the plate[99]. Cells were incubated with IC25-IC50-IC75 doses of

Cisplatin to monitor the O_2 consumption over 5 days. Live OCR was monitored continuously for 120 h by measuring the flux of O_2 diffusing into the cells from the air above the well. The measurement was performed by sensing the O_2 concentration gradient across a range of heights throughout the media and then calculating the flux of O_2. Data were analyzed using the Resipher web application (Lucid Scientific).

3.14. Mitochondrial ATP: ATP levels in mitochondrial extracts were measured with the ATP Bioluminescent Assay Kit (FLAA; Sigma Aldrich), as per manufacturer's instructions. Results were expressed as nanomoles/mg mitochondrial proteins.

3.15. MAPK Activity Assay: MAP Kinase Assay Kit (17-191, Millipore, CA) was used to measure ERK1/2 activity. 200 µg of cell lysates of NCI-NCI-H441 and NCI-NCI-H2228 cells were immunoprecipitated with anti-ERK1/2 (137F5, Cell Signaling Technology, dilution 1/1000). Then Mg^{2+}/ATP cocktail and MAP kinase substrate from the kit were added to the samples and incubated for 30 minutes, in the absence or presence of the inhibitor cocktail supplied. After incubation, 1 µg protein were subjected to immunoblotting and probed with the anti-phospho-MBP antibody (1/1000, supplied by the kit). The intensity of the immunoblot band was considered an index of ERK1/2 activity.

3.16. Akt Kinase Activity Assay: Akt Kinase Activity Assay Kit (ab139436, Abcam, UK) was used to assess the kinase activity, in the absence or presence of 0.1, 1, 5, 10 and 20 µM Akt inhibitor Capivasertib (AZD5363, cat#S8019 Selleckchem). $2x10^6$ cells were seeded and incubated for 24 h, then washed with 2xPBS and incubated with lysis buffer (pH 7.2 [20 mM MOPS, 50 mM β-glycerolphosphate, 50 mM NaF, 1 mM $NaVO_4$, 5 mM EGTA, 2 mM EDTA, 1% NP40, 1 mM

dithiothreitol (DTT), 1 mM benzamidine, 1 mM PMSF and 10 µg/mL leupeptin and aprotinin]) for 10 min on ice. Cells were scraped and collected. Samples were centrifuged at 13000 x g for 15 min then the supernatants were transferred to new pre-chilled 1.5 mL tubes. 30 µL of samples were added to pre-coated 96-well plates in duplicates and the reaction were initiated by adding 10 µL of diluted ATP (supplied by the kit). After 90 min, the wells content was discarged and 40 µL of Phosphospecific Substrate Antibody added for 60 min, followed for 4 washing steps and incubation with then Anti-rabbit IgG:HRP for 30 min. The TMB substrate were added for 30 min, and the reaction was stopped by adding the stop solution of the kit. Absorbance was measured at 450 nm wavelength by using a Synergy HT Multi-Detection Microplate Reader (Bio-Tek Instruments). Results were expressed as absorbance units/cells number.

3.17. Nuclear Isolation: Nuclear extracts were prepared according to Nuclear Extract Kit (Active Motif, Carlsbad, CA). 85-90% confluent dishes were washed with ice-cold PBS/Phosphatase Inhibitors, then pellets were collected by gently scraping with 3 mL PBS/Phosphatase Inhibitors. Cell suspensions centrifuged for 5 min at 200 x g in a centrifuge pre-cooled at 4°C. Supernatants were discarded and cell pellets resuspend cells in 500 µL 1X Hypotonic Buffer by pipetting up and down to incubate for 15 min on ice. Following incubation, 25 µL detergent were added to suspensions and vortexed for 10 s. Suspensions were centrifuged at 14,000 x g for 30 s in a microcentrifuge pre-cooled at 4°C. Supernatants were discarded and pellets were resuspended 50 µL Complete Lysis Buffer by pipetting up and down then vortexed 10 s at the highest setting. Suspensions were incubated for 30 min on ice on a rocking platform set at 150 x g, followed by vortex 30 s at the highest setting. Vortexed suspensions were centrifuged for 10 min at 14,000 x g in a microcentrifuge pre-cooled at 4°C. Supernatants (nuclear fraction) transferred into a pre-

chilled microcentrifuge tube. Protein calculation was done Bicinchoninic Acid Kit (Sigma Aldrich, USA). Equal amount of protein was used for both immunoblotting and ELISA. Anti-HIF1α (dilution 1/1000) antibody was used to determine the changes in nuclear translocation of HIF1α. Anti-TATA Box Binding Protein (TBP, Santa Cruz Biotechnology, dilution 1/500) was used as housekeeping protein.

3.18. Vγ9δ2 T-lymphocytes induced-cytotoxicity: Peripheral blood samples were obtained from healthy blood donors; the samples were provided by the local Blood Bank (Fondazione Strumia, AOU Città della Salute e della Scienza, Torino). After isolation on a Ficoll-Hypaque density gradient, peripheral blood mononuclear cells (PBMC) were subjected to an immuno-magnetic sorting with the TCRγ/δ+T Cell Isolation Kit (Miltenyi Biotec., Bergisch Gladbach, Germany). The phenotypic characterization of Vγ9δ2 T-lymphocytes was confirmed by staining 5 x 10^5 isolated cells with anti-TCR Vγ9 (clone B6, BD, dilution 1/50) and anti-CD3 (clone BW264/56, Miltenyi Biotec, dilution 1/10) antibodies[97]. Cells were counted with a Guava® easyCyte flow cytometer (Millipore), equipped with the InCyte software (Millipore). Vγ9δ2 T-lymphocyte killing was measured according to Cimini et al., 2011[100] with minor modifications. 5 x 10^5 Vγ9δ2 T-lymphocytes were cultured overnight with NSCLC cells at 1:1 ratio. After this co- incubation, the supernatant containing Vγ9δ2 T-lymphocytes was removed, while adherent (i.e., NSCLC) cells were washed twice with PBS, detached with gentle scraping, and stained with the Annexin V/Propidium Iodide kit (APOAF, Sigma-Merck), as per manufacturer's instruction. The fluorescence was acquired using Guava® EasyCyte flow cytometer and InCyte software. The percentage of Annexin V^+/Propidium $Iodide^+$ cells were considered an index of Vγ9δ2 T-lymphocyte killing. The results were expressed as killing fold change, i.e., percentage of Annexin

V^+/Propidium $Iodide^+$ cells in each experimental condition/percentage of Annexin V^+/Propidium $Iodide^+$ I-NCI-H441 and -NCI-H2228 untreated cells.

3.19. qRT-PCR: Total RNA was extracted and reverse-transcribed using iScriptTM cDNA Synthesis Kit (Bio-Rad Laboratories). The qRT-PCR was performed with the IQ SYBR Green Supermix (Bio-Rad Laboratories). Lipoprotein signaling and cholesterol metabolism PrimePCR array were ready-to-use plates, and the arrays were conducted according to supplier's protocol (Bio-Rad Laboratories). The relative quantification of each gene of interest was performed by comparing each PCR product with the housekeeping PCR product of β-2-microglobulin (B2M), using the Bio-Rad Software Gene Expression Quantitation (Bio-Rad Laboratories). Primers that are used in qRT-PCR were shown in table 4.

Primers	**Forward**	**Reverse**
TFEB	5'-GACTCAGAAGCGAGAGCTAACA	5'-TGTGATTGTCTTTCTTCTGCCG
ABCA1	5'-CAGAGCTCACAGCAGGGAC	5'-CTTCTCCGGAAGGCTTGTC
PGP (ABCB1)	5'-GAGGAAGACATGACCAGGTATGC	5'-CCCACCCACCAAAATGAAACC
MRP1 (ABCC1)	5' -TCTGGTCAGCCCAACTCTCT	5'-CCTGTGATCCACCAGAAGGT
HMGCR	5'-GTCATTCCAGCCAAGGTTGT	5'-GGGACCACTTGCTTCCATTA
B2M	5'-AGCAAGGACTGGTCTTTCTATCTC	5'-ATOTCTCCATCCCACTTAAGTATCTT

Table 4: Forward and reverse sequences of the primers that used in qRT-PCR.

3.20. Chromatin Immunoprecipitation: 90% confluent NCI-H441 and NCI-H2228 cells were collected with trypsin and washed with PBS. $5x10^6$ cells were resuspended with PBS and

formaldehyde was added to a final concentration of 1% to cross-link the cells. Cross-link reaction has stopped by adding glycine (0.125M) after 7 minutes of incubation. Cross-linking reaction centrifuged at 3000 g for 1 minutes at 4°C. Supernatant was discarded and cell pellets were resuspended in 1 mL chilled 1X PBS containing 1 mM PMSF and 1X protease inhibitor cocktail III (Merck), then the suspensions were centrifuged at 3000 x g for 1 min at 4°C. This step was repeated for 2 times, then supernatants were discarded. Zymo-Spin ChIP Kit (D5209-D5210, Zymo Research, Orange, CA) was used to obtain ChIP-ready DNA. Nuclei preparation and chromatin shearing was done as per manufacturer's instructions. ZymoMag Protein A beads were incubated with anti-HIF1α or anti-TFEB antibodies for 3 h at 4°C for each sample. Samples were then incubated at 75°C for 5 min with 5M NaCl and centrifuged at 10,000 x g for 30 s. ChIP DNA eluates were incubated at 65°C for 30 min, then 1 µL Proteinase K was added for additional 90 min. The DNA was recovered with Zymo-Spin IC column with the DNA elution buffer of the kit. The promoter sequences were identified from the Eucaryotic Promoter Database (EPD) using as inputs "ABCA1", "ABCB1", "ABCC1". Binding sites for HIF1α and TFEB to these promoter sites were identified from Jaspar database (https://jaspar.genereg.net/). Primers used for qRT-PCR after ChIP are shown in the table.

Primers for ChIP-PCR	Forward	Reverse
HIF1a to promoter of		
ABCA1	AAATTCCACTGGTGCCCTTG	CCACGACACATCTAGGGAGT
ABCB1	ATGCGCGTTTCTCTACTTGC	CTTCCTGTGGCAAAGAGAGC
ABCC1	AGTGATTAGCCAGGTGACCC	CCCTGCGACCACTTTTCAAA
TFEB to promoter of		
ABCA1	GGACCCTAAGACACCTGCTG	TTCCCGGCCTCTGTTTATGT
ABCC1	ACCTCAGTTTCCCCATCTGT	AAGAAACCCAGGTGCAGAGA

Table 5: Forward and reverse sequences of the primers that used in qRT-PCR for ChIP assay.

3.21. ABCB1/ABCC1 activity: To prepare plasma-membrane vesicles enriched of ABC transporters, 10 x 10^6 cells (after overnight starvation) were washed with Ringer's solution (148.7 mM NaCl, 2.55 mM K_2HPO_4, 0.45 mM KH_2PO_4, 1.2 mM $MgSO_4$; pH 7.4), lysed on crushed ice with lysis buffer (10 mM Hepes/Tris, 5 mM EDTA, 5 mM EGTA, 2 mM DTT; pH 7.4) supplemented with 2 mM PMSF, 1 mM aprotinin, 10 µg/mL pepstatin, 10 µg/mL leupeptin, and subjected to nitrogen cavitation at 1200 psi for 20 min. Samples were centrifuged at 300 x g for 10 min, diluted 1:4 in the pre-centrifugation buffer (10 mM Tris/HCl, 25 mM sucrose; pH 7.5), overlaid on a sucrose cushion (10 mM Tris/HCl, 35% w/v sucrose, 1 mM EDTA; pH 7.5) and centrifuged at 14,000 x g for 10 min. The interface was collected, diluted 1:5 in the centrifugation buffer (10 mM Tris/HCl, 250 mM sucrose; pH 7.5) and subjected to a third centrifugation at 100,000 x g for 45 min (Optima L-

90K Beckman Coulter Ultracentrifuge). The vesicles pellet was re-suspended in 0.5 ml centrifugation buffer and stored at -80°C until the use, after the quantification of the protein content. 100 µg proteins were immunoprecipitated in non-denaturing conditions using anti-ABCB1 (MA5-28587, Invitrogen Thermos Scientific, dilution 1/100) and anti-ABCC1 (#ab263865, Abcam, dilution 1/100) antibodies, in the presence of 25 µL of PureProteome Magnetic Beads. The ATPase activity of immunopurified ABCB1 and ABCC1 was measured by a spectrophotometric method: samples (containing 20 µg proteins) were incubated for 30 min at 37°C with 50 µl of the reaction mix (25 mM Tris/HCl, 3 mM ATP, 50 mM KCl, 2.5 mM $MgSO_4$, 3 mM DTT, 0.5 mM EGTA, 2 mM ouabain, 3 mmol/L NaN_3; pH 7.0). In each set of experiments, a blank containing 0.5 mM Na_3VO_4 was included. The reaction was stopped by adding 0.2 ml ice-cold stopping buffer (0.2% w/v ammonium molybdate, 1.3% v/v H_2SO_4, 0.9% w/v SDS, 2.3% w/v trichloroacetic acid, 1% w/v ascorbic acid). After a 30-min incubation at room temperature, the absorbance of the phosphate hydrolyzed from ATP was measured at 620 nm, using a Packard EL340 microplate reader (Bio-Tek Instruments, Winooski, MA). The absorbance was converted into µmol hydrolyzed phosphate/min/mg proteins, according to the titration curve previously prepared. ATPase activity in control cells was considered 100%; results were expressed as percentage towards mock/control cells.

3.22. [^{3}H-PT] accumulation: Cells were incubated for 3 h with 1 µCi/mL [^{14}C]-carboplatin (20 Ci/mmol; Amersham Bioscience, Piscataway, NJ), washed twice in PBS, detached with trypsin, centrifuged at 1,300 x g for 2 min and sonicated. The amount of [^{14}C]-carboplatin was measured using a Tri-Carb Liquid Scintillation Analyzer (PerkinElmer). Radioactivity was converted in nmol/mg cell proteins.

3.23. Self-assembled zoledronic acid nanoformulations: Self-assembling nanoparticles encapsulating zoledronic acid (termed NZ) were prepared as previously reported[101], by Prof. Giuseppe De Rosa, University Federico II of Naples, Italy. Briefly, an aqueous solution of 18 mM $CaCl_2$ was added, dropwise and under magnetic stirring, to an aqueous solution of 10.8 mM Na_2HPO_4. The resulting suspension (termed CaPNPs) was filtered through a 0.22 μm polycarbonate filter (Millipore) and stored at 4°C before use. Zoledronic acid (Sigma) was then complexed with CaPNPs (to obtain CaPZNPs), at a volume ratio of 50:1, with a final concentration of 50 mg/mL. Cationic liposomes (N-[1-(2,3-dioleoyloxy) propyl]-N,N,N-trimethylammonium chloride/cholesterol/1,2-distearoyl-sn-glycero-3-phosphoethanolamine-N-[amino(polyethylene glycol)-2000] at a ratio of 1:1:0.5) were prepared by hydration of a thin lipid film followed by extrusion. The lipid mixture dissolved in chloroform/methanol (2:1 v/v) was added to a 50 mL round-bottom flask and the solvent was removed under reduced pressure by a rotary evaporator (Laborota 4010 digital, Heidolph, Schwabach, Germany) in nitrogen atmosphere. The resulting lipid film was hydrated with 1 mL of 0.22 μm-filtered distilled water and the resulting suspension was gently mixed in the presence of glass beads followed by incubation at room temperature for 2 h. The liposome suspension was then extruded using a thermobarrel extruder system (Northern Lipids Inc., Vancouver, BC, Canada) passing repeatedly the suspension under nitrogen atmosphere through polycarbonate membranes with decreasing pore sizes from 400 to 100 nm (Nucleopore Track Membrane 25 mm, Whatman, Brentford, UK). The liposomes were stored at 4°C. Each formulation was prepared in triplicate. Finally, equal volumes of suspensions of the liposomes and CaPZNPs, respectively, were mixed in a glass tube and the resulting dispersion was maintained at room temperature for 10 min, to obtain the so-called NZ formulation.

3.24. In Vivo Experiments and Immunohistochemistry: 1×10^6 NCI-NCI-H2228 wild-type (WT) and TFEB-silenced (shTFEB) cells, mixed with 100 µL Matrigel (Sigma Aldrich), were injected subcutaneously (s.c.) in female NOD SCID-γ (NSG) mice engrafted with human hematopoietic $CD34^+$ cells (Hu-$CD34^+$; The Jackson Laboratories, Bar Harbor, MA). Mice were housed (5 per cage) under 12 h light/dark cycle, with food and drinking provided ad libitum. Tumor growth was measured weekly by caliper, according to the equation (LxW2)/2, where L = tumor length and W = tumor width. In a preliminary experimental set, when tumors reached the volume of 50 mm^3, animals (4/group) were randomized and treated for 3 weeks as it follows: control group (CTRL), treated with 0.1ml saline solution intravenously (i.v.), once a week; cisplatin group (PT), treated with 2 mg/kg cisplatin i.v. once a week; Nanozol group (NZ), treated with 1 mg/kg i.v. NZ once a week; Nanozol and Cisplatin (NZ+PT) group, receiving the same doses i.v. once a week simultaneously. Animals were euthanized at day 28 after randomization with zolazepam (0.2ml/kg) and xylazine (16mg/kg). Animal weights were monitored throughout the study. Tumors were excised, weighted, and photographed. Tumor sections, fixed in 4% v/v paraformaldehyde, were stained with hematoxylin/eosin (Sigma Aldrich) and anti-Ki67 antibody (Merck, dilution 1/100) followed by a peroxidase-conjugated secondary antibody (Dako, Santa Clara, CA; dilution 1/1000). Nuclei were counterstained with hematoxylin (Sigma Aldrich). Tumor tissues were also stained with *in situ* Cell Death Detection Kit also known as TUNEL Assay (Roche, Basel, Switzerland), followed by nuclei counterstaining with 4',6-diamidino-2-phenylindole (DAPI). Sections were examined with a LeicaDC100 microscope.

Immediately after the euthanasia, 200 µL blood were collected to measure the following parameters: red blood cells (RBC), white blood cells (WBC), hemoglobin (Hb), platelets (PLT), as

indexes of bone mar ow function; lactate dehydrogenase (LDH), aspartate aminotransferase (AST), alanine aminotransferase (ALT), alkaline phosphatase (AP), as indexes of liver function; creatinine, as index of kidney function; creatine phosphokinase (CPK), as index of muscle/heart damage, using commercially available kits from Beckman Coulter Inc. (Miami, FL). Heart, lungs, liver, kidneys, and spleen were collected, fixed in 4% v7v paraformaldehyde and the sections were stained with hematoxylin-eosin (Sigma Aldrich), using a LeicaDC100 microscope. Animal care and experimental procedures were approved by the Italian Ministry of Health (#627/2018-PR, 10/08/2018).

3.25. Statistical analysis: All data in the text and figures are provided as means ± SEM. The results were analyzed by Two-way analysis of variance (ANOVA), using GraphPad Prism 9 (Dotmatics, v9.5.1). $p<0.05$ was considered significant throughout the study. Pearson correlation coefficients were calculated based on fold-changes of TFEB, ABCA1, ABCB1, and ABCC1 mRNA levels, then the matrix was created based on coefficients ranging from -1 to +1. -1 means negative correlation while +1 means perfect correlation. The differences between gene density were compared by T-test, and the Kaplan-Meier survival analysis were performed used to calculate the PFS and OS. Log-rank test was used to compare the outcome of $TFEB^{low}ABCA1^{low}ABCC1^{high}$ and $TFEB^{high}ABCA1^{high}ABCC1l^{ow}$. Module eigengenes were compared by T-test, and to adjust the p-value "Benjamini–Hochberg method" was used. The software used in this study was R version 4.2.2.

4. Results

4.1. TFEB and ABC transporters expression in NSCLC patients

There are 585 cases in the TCGA-LUAD Transcriptome Profiling dataset that was used in this investigation. Due to unreported staging, eight instances were disqualified, while 59 cases were labeled as "normal tissue". "Primary solid tumor" was assigned to the remaining 531 cases (Table 6). In both patient groups, there were a balanced number of men and women (271 men and 321 women), however sex was not considered as variable.

TCGA-LUAD Dataset (n = 585)	Male	Female
Patients with Primary Tumor (n=531)	246	287
Patients with Normal Tissue (n=59)	25	34

Table 6: Patient numbers of the TCGA-LUAD cohort.

First, we investigated the changes in TFEB, ABCA1 and ABCC1 in tumors. ABCB1 was excluded from the analysis since it was coinciding with the literature data. We examined the effects of TFEB, ABCA1, ABCC1 on OS (Fig 1). High TFEB expression significantly predicted a better OS (Fig 1A). A similar trend, although not significant, was observed for the immuno-sensitizing gene ABCA1 (Fig 1B). By contrast, high levels of ABCC1 are associated with poor OS (Fig 1C). In a subsequent co-expression analysis, we found $TFEB^{low}ABCA1^{low}ABCC1^{high}$ phenotype was the poorest in terms of OS amongst all phenotypes, likely because of the high levels of the well-known inducer of chemoresistance ABCC1 and the low levels of ABCA1, which promotes the immuno-killing by the host immune system[74]. Conversely, the opposite $TFEB^{high}ABCA1^{high}ABCC1^{low}$ phenotype is significantly better for the patient OS (Fig 1D).

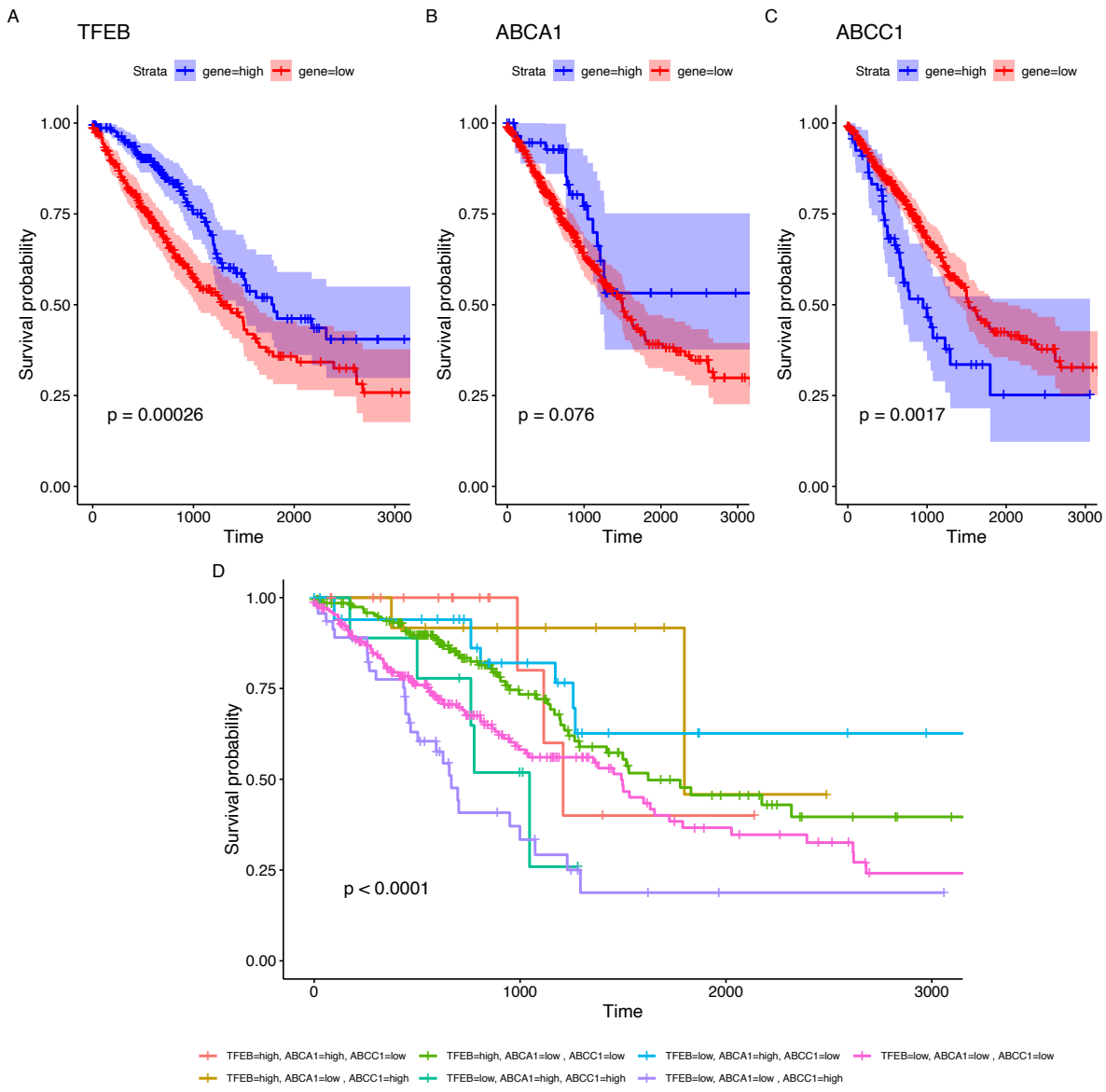

Figure 1: Impact of the expression of the TFEB, ABCA1, ABCC1 on overall survival (OS) in TCAGA LUAD Cohort. (A) High TFEB predicts better survival. (B) High ABCA1 predicts a better survival, although it was not significant. (C) Low ABCC1 predicts better survival. (D) In co-expression analysis, $TFEB^{low}ABCA1^{low}ABCC1^{high}$ is the poorest phenotype, $TFEB^{high}ABCA1^{high}ABCC1^{low}$ is the best phenotype in terms of OS.

Next, we validated these results in a NSCLC patient with unresectable diseases, treated with chemotherapy (32 patients) or ICI-based on Pembrolizumab (43 patients) as first line treatments (Fig 2). PFS, OS and expression of TFEB, ABCC1 and ABCA1 mRNA in samples of each patient are reported in Table 7.

				Relative expression		
Patient	**1st line treatment**	**TTP (months)**	**OS (months)**	**TFEB**	**ABCC1**	**ABCA1**
ITACA 242	PT-based chemotherapy	18	21	2.13	0.52	2.29
ITACA 348	PT-based chemotherapy	24	26	2.56	0.41	3.29
ITACA 426	PT-based chemotherapy	8	5	0.15	2.96	0.21
ITACA 544	PT-based chemotherapy	12	21	2.58	0.61	1.98
ITACA 623	PT-based chemotherapy	23	26	3.51	0.42	3.15
ITACA 624	PT-based chemotherapy	23	30	3.69	0.28	4.05
ITACA 631	PT-based chemotherapy	21	28	3.01	1.04	3.24
ITACA 641	PT-based chemotherapy	20	24	2.14	0.62	2.56
ITACA 670	PT-based chemotherapy	37	46	4.01	0.14	4.5
ITACA 671	PT-based chemotherapy	35	54	6.12	0.29	4.11
ITACA 690	PT-based chemotherapy	21	26	2.95	0.61	3.59
ITACA 715	PT-based chemotherapy	23	23	2.54	0.42	2.93
ITACA 745	PT-based chemotherapy	20	26	3.02	0.69	3.17
ITACA 759	PT-based chemotherapy	18	28	2.04	0.46	2.51

SI ITACA	PT-based chemotherapy	27	38	3.24	0.84	3.54
ITACA 24	PT-based chemotherapy	9	19	1.47	0.54	1.97
ITACA 15	PT-based chemotherapy	22	29	2.08	0.59	2.11
ITACA 206	PT-based chemotherapy	41	53	3.96	0.04	4.96
ITACA 446	PT-based chemotherapy	8	15	0.42	1.56	0.51
ITACA 607	PT-based chemotherapy	58	71	4.92	0.14	5.36
ITACA 87	PT-based chemotherapy	24	31	2.11	0.39	2.58
ITACA 157	PT-based chemotherapy	22	27	2.56	0.42	2.14
ITACA166	PT-based chemotherapy	51	59	4.85	0.18	5.46
ITACA301	PT-based chemotherapy	29	50	3.28	0.28	4.02
ITACA636	PT-based chemotherapy	6	20	1.14	0.14	1.47
ITACA 383	PT-based chemotherapy	3	9	0.15	2.15	0.26
ITACA 587	PT-based chemotherapy	14	22	0.81	0.97	1.36
ITACA 292	PT-based chemotherapy	23	28	0.96	1.13	1.82
ITACA 205	PT-based chemotherapy	24	45	1.25	0.42	1.98
ITACA 244	PT-based chemotherapy	35	49	2.28	0.21	2.45
ITACA 135	PT-based chemotherapy	15	55	3.15	0.17	3.85
ITACA 757	PT-based chemotherapy	21	30	2.84	0.52	3.24
MOLEC. 1	ICI-based therapy	4	5	0.08	2.36	0.12
MOLEC. 2	ICI-based therapy	1	2	0.45	3.18	0.39
17-C-04697	ICI-based therapy	11	23	1.91	1.15	2.15

17-I-12406	ICI-based therapy	32	46	3.15	0.18	3.58
18-I-01832	ICI-based therapy	2	5	0.08	2.89	0.14
16-C-00249	ICI-based therapy	29	63	4.16	0.09	4.28
18-I-05255	ICI-based therapy	9	19	1.28	1.47	1.58
20-I-4408	ICI-based therapy	9	11	1.11	1.63	1.23
17-I-00793A2	ICI-based therapy	43	53	4.52	0.05	4.65
20-C-02138	ICI-based therapy	5	11	0.81	1.51	1.12
18-C-01105 B	ICI-based therapy	45	63	5.11	0.17	5.64
20-I-2504	ICI-based therapy	4	14	0.76	1.28	0.85
19-C-5330	ICI-based therapy	1	7	0.38	2.41	0.25
20-C-2023	ICI-based therapy	4	11	0.94	1.48	0.62
20-I-00644 B1	ICI-based therapy	6	15	0.56	1.52	0.78
20-I-00099	ICI-based therapy	15	16	0.81	1.34	0.72
18-I-02470A2	ICI-based therapy	2	19	1.17	0.91	1.58
19-I-08588	ICI-based therapy	3	5	0.29	2.25	0.09
19-I-01684	ICI-based therapy	14	19	2.15	0.81	1.85
19-I-5272	ICI-based therapy	1	2	0.17	3.26	0.23
19-C-01646	ICI-based therapy	1	3	0.26	3.82	0.07
17-C-04337	ICI-based therapy	1	6	0.11	2.81	0.19
17-C-04914 B	ICI-based therapy	2	3	0.18	3.45	0.08
17-C-05257 A	ICI-based therapy	29	45	3.69	0.15	4.28

17-I-10421	ICI-based therapy	1	2	0.48	4.11	0.19
17-I-10155	ICI-based therapy	12	30	2.54	1.25	3.15
17-I-12748	ICI-based therapy	1	3	0.23	0.46	0.42
17-I-12097 B1	ICI-based therapy	2	5	0.28	0.28	0.53
17-C-007826	ICI-based therapy	29	41	3.46	0.21	3.78
17-I-13622A2	ICI-based therapy	8	23	2.07	1.14	2.14
18-I-00097 B	ICI-based therapy	2	6	0.31	2.58	0.32
17-I-14050	ICI-based therapy	3	6	0.46	2.46	0.25
18-I-10670	ICI-based therapy	47	130	5.28	0.09	6.12
18-I-06387 B2	ICI-based therapy	3	11	0.72	1.34	0.81
18-C-04699	ICI-based therapy	30	33	2.16	1.22	2.98
18-C-00265	ICI-based therapy	27	40	3.59	0.32	4.15
18-I-05700A2	ICI-based therapy	1	6	0.14	2.15	0.22
18-C-05582 B	ICI-based therapy	22	32	2.19	0.76	2.76
20-I-04286	ICI-based therapy	15	28	2.04	0.92	2.15
18-C-04462	ICI-based therapy	14	16	1.92	0.72	1.15
18-I-11188	ICI-based therapy	2	4	0.41	3.15	0.36
17-I-13953 A	ICI-based therapy	9	17	1.12	1.08	1.24
18-I-07856	ICI-based therapy	21	33	2.73	0.78	2.84

Table 7: Clinical follow-up and gene expression data in the retrospective cohort of NSCLC patients analyzed at the Department of Oncology, University of Torino.

Patients were divided between $TFEB^{high}ABCA1^{high}ABCC1^{low}$ versus $TFEB^{low}ABCA1^{low}ABCC1^{high}$. In the cisplatin-received patient group, PFS (Fig 2A) and OS (Fig 2B) were better for $TFEB^{high}ABCA1^{high}ABCC1^{low}$ phenotype compared to $TFEB^{low}ABCA1^{low}ABCC1^{high}$. The same trend was observed also in the immunotherapy-received patients (Fig 2C-2D).

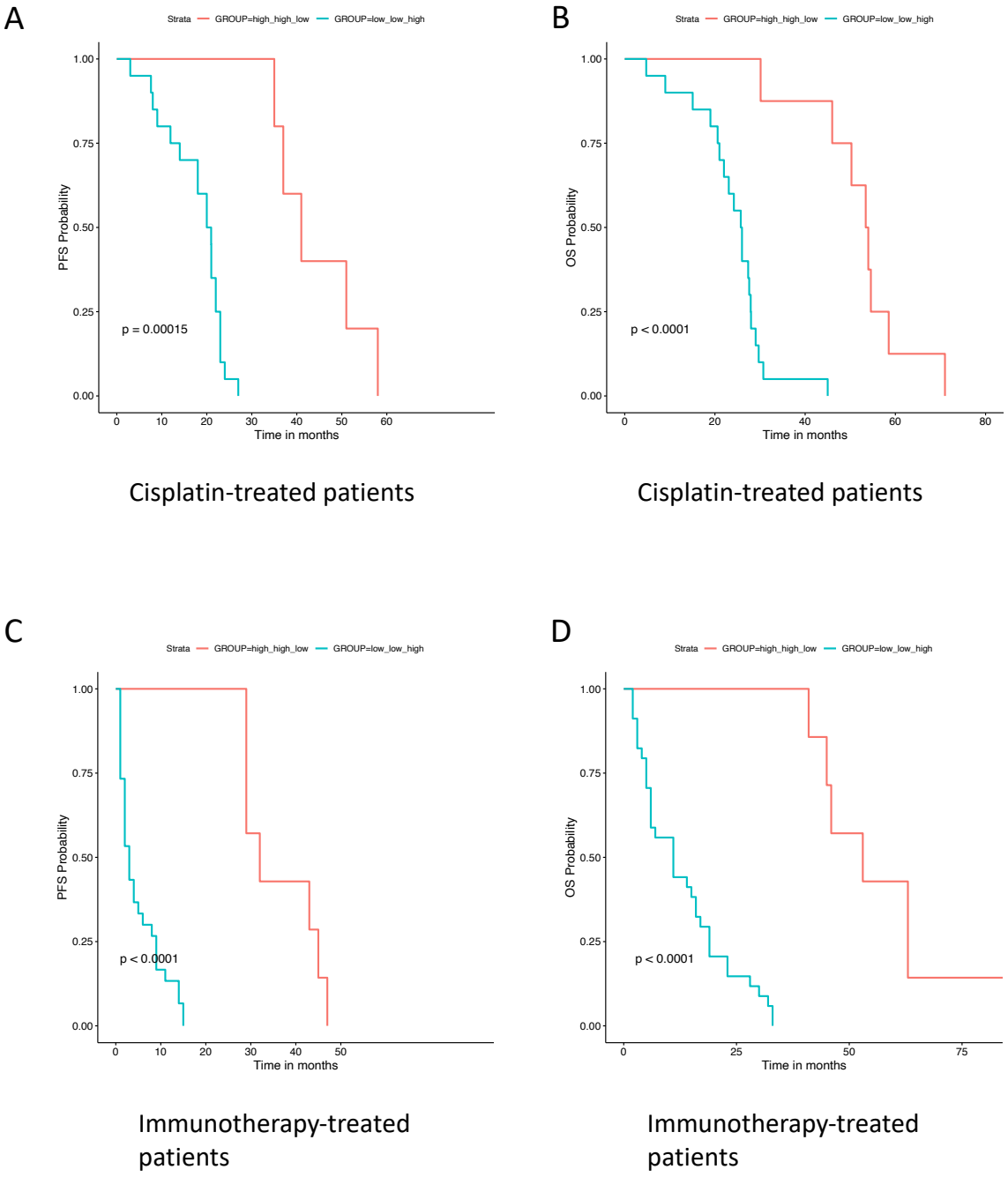

Figure 2: Impact of the expression of the TFEB^{high}ABCA1^{high}ABCC1^{low} on progression-free survival and overall survival. TFEB^{high}ABCA1^{high}ABCC1^{low} phenotype predicts better PFS (A) and OS (B) for the cisplatin chemotherapy patients. The same trend was observed also for the immunotherapy patients (C-D).

4.2 TFEB is positively correlated with ABCA1 and negatively correlated with ABCB1/ABCC1 in non-small cell cancer cells

Next, we started investigating both genetic and protein expressions of our genes of interest in 6 wild-type (WT) NSCLC cell lines, that we previously known characterized by medium-high resistance to cisplatin and resistance to immunokilling by Vγ9δ2 T-lymphocytes[74]. In flow cytometry assays, all the NSCLC cells had low levels of ABCA1 and high but different levels of ABCB1 and ABCC1 (Fig. 3A). NCI-NCI-H441 had the lowest levels, while NCI-NCI-H2228 expressed comparable levels of ABCB1 and ABCC1. Then we measured mRNA levels of TFEB; since NCI-H4441 and NCI-H2228 cell lines had the highest levels of TFEB, the subsequent experiments were carried out on these two cell lines (Fig 3B).When we correlated the levels of TFEB mRNA with expression of the ABC transporters of interest in the panel of NSCLC, we found that ABCA1 and TFEB had a strong positive correlation, while correlation of ABCB1 and TFEB was strongly negative. The correlation between TFEB and ABCC1 was negative, although not significant (Fig 3C).

The efficacy of TFEB silencing was verified both at mRNA (Fig 3D) and protein levels (Fig 3E). Silenced TFEB cells also had significantly decreased ABCA1 mRNA and increased of ABCB1 and ABCC1 mRNAs (Fig 3F). A similar trend was observed for the protein expression of these ABC transporters (Fig 3G).

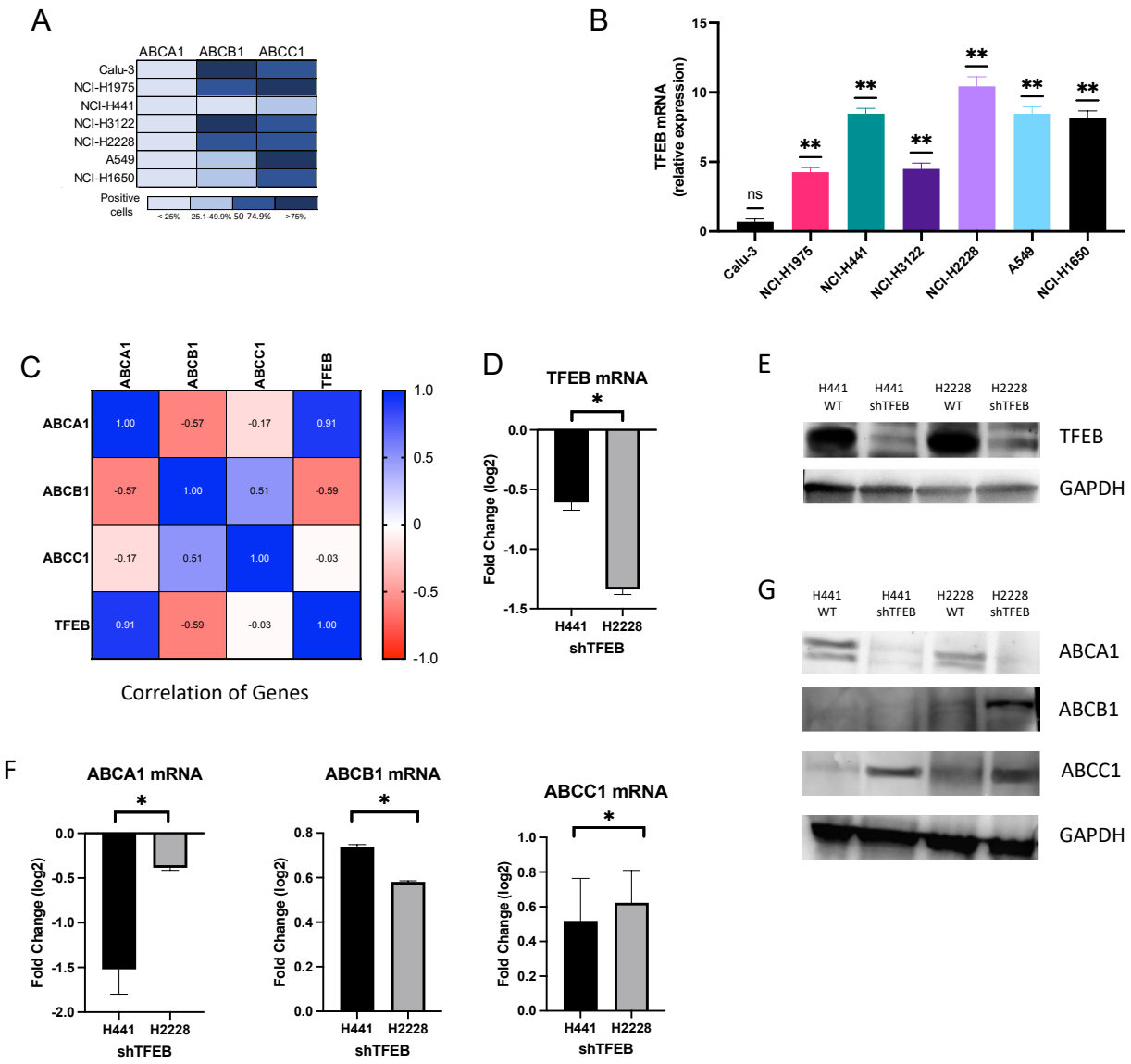

Figure 3: Changes in the expression levels of ABCA1, ABCB1, ABCC1 and TFEB in NCI-H441 and NCI-H2228 cells after TFEB silencing. mRNA expression of wild-type (WT) NSCLC of ABC transporters (A) and TFEB levels (B) in 6 NSCLC cell lines Data are means + SD (n=3), in duplicate. Correlation matrix between the expression levels of TFEB, ABCA1, ABCB1 and ABCC1 (C). mRNA (D) and protein (E) expression after TFEB silencing. mRNA data are means + SD (n=3), in duplicate: *p<0.05. The image is representative of 1 out of 3 independent experiments. Expression of ABCA1, ABCB1 and ABCC1 mRNA (F) and protein (G) in WT and shTFEB cells.

4.3. TFEB is a direct repressor of ABCA1 and an indirect inducer of ABCB1/ABCC1 via MAPK/HIF1-α and Akt/ HIF1-α Pathways

Moreover, we started to investigate how TFEB affects the expression of ABC transporters. First, we investigated if TFEB binds to promoter sites of ABCA1, ABCB1 or ABCC1, since previous data of ChIP sequencing in endothelial cells reported ABCA1 as a target gene of TFEB[95]. By scanning the promoters of ABC transporter gene with the JASPAR software, we found putative binding sites for TFEB on ABCA1 and ABCC1 promoters, not on ABCB1 promoter. We thus focused on the first two transporters to clarify if they were direct targets of TFEB in NSCLC cells. ChIP assay results indicated that TFEB binds to ABCA1 promoter site, as demonstrated by the reduced binding in shTFEB cells, meaning that ABCA1 is a direct target of TFEB, but it did not bound ABCC1 promoter (Fig 4A). Since HIF-1α is an up-regulator of ABCB1 and ABCC1[102] and it is phosphorylated and stabilized by MAPKs, ERK1/2 and Ras/Akt axes[73], we investigated whether the silencing of TFEB could reduce the phosphorylation and stabilization of HIF-1α mediated by one of these kinases.

TFEB silencing significantly downregulates the MAPK activity, taken as an index of ERK1/2 activity, to the same levels of wild-type cells treated with the commercial pan-ERK inhibitor (Fig 4B). Similarly, TFEB silencing reduced significantly Akt activity, although not as strongly as Akt inhibitor Capivasertib (Fig 4C). These results show that TFEB promote MAPK and Akt pathways. Then, we explored if these changes in MAP and Akt activity resulted in a change in stabilization and activation of HIF-1α. To measure phospho-HIF-1α, we immunoprecipitated the protein and decorated the blot with and phosphor-serine antibody. As shown in Fig. 4D, TFEB silencing showed a decreased HIF-1α phosphorylation, higher than the reduction in phosphorylation obtained by using pan-ERK inhibitor or Akt inhibitor separately. Also, TFEB silenced cells had

decreased nuclear translocation of HIF-1α (Fig 4E) and decreased binding to the promoters of ABCB1 and ABCC1 in ChIP assays (Fig 4f).

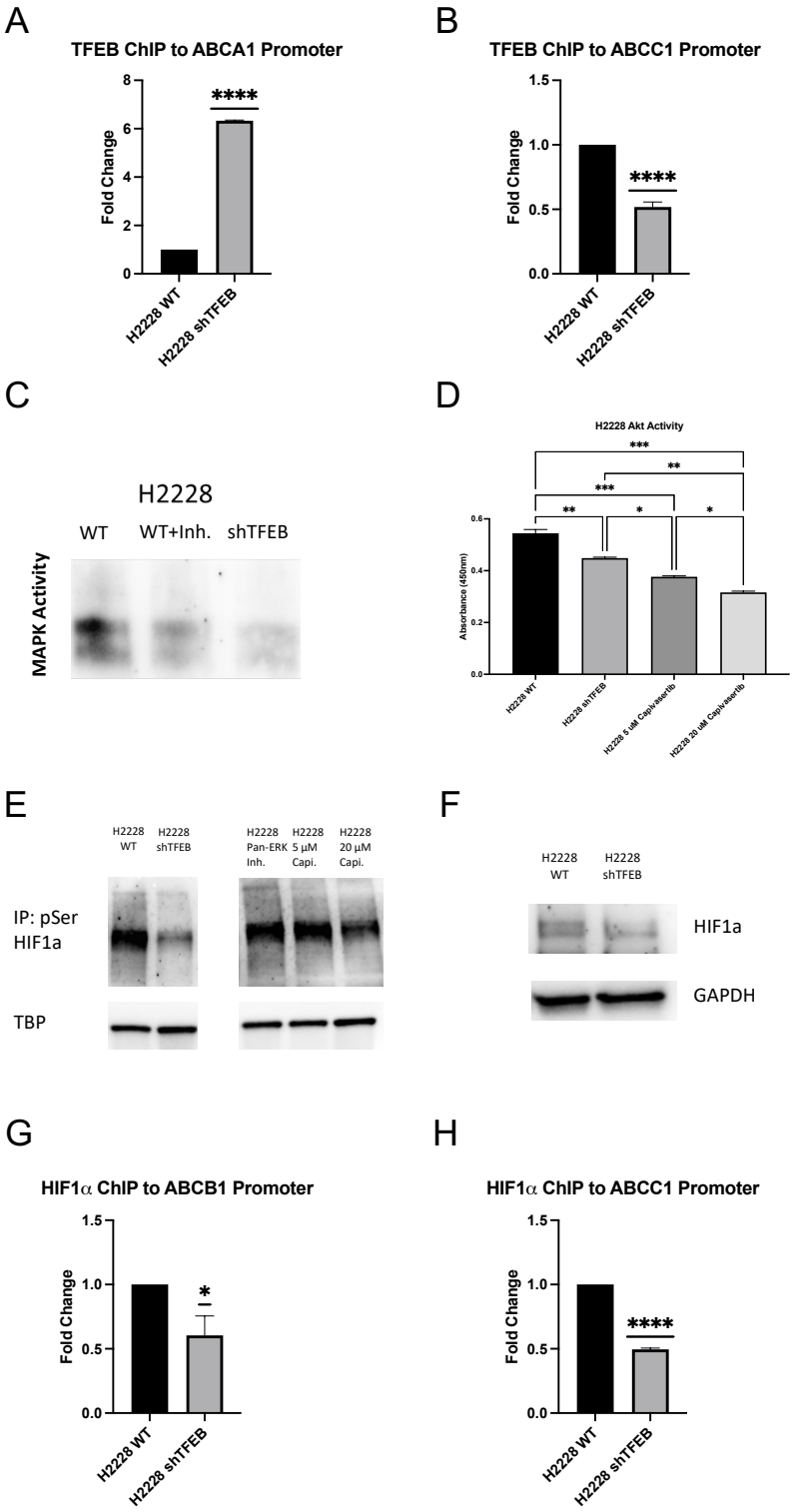

Figure 4: Mechanisms linking TFEB with expression of ABCA1, ABCB1, ABCC1.TFEB binding to ABCA1 (A) and ABCC1 (B) promoter in NCI-H2228 cells, wild-type (WT) and TFEB silenced (shTFEB). Data are means + SD (n=3), in duplicate. *p<0,05; **p<0,01; ***p<0,001; ****p<0,0001. MAPK (C) and Akt (D) activity in WT and shTFEB cells. As internal control, a pan-ERK inhibitor (Millipore pan-ERK inhibitor cocktail, 10 µL, 30 minutes) and the Akt inhibitor was added (Capivasertib, 5 and 20 µM, 24 h). Data are means + SD (n=3), in duplicate. *p<0,05; **p<0,01; ***p<0,001; ****p<0,0001. (E) HIF1α phosphorylation in WT NCI-H2228, grown in fresh medium (-) or treated with a pan-ERK inhibitor (Millipore pan-ERK inhibitor cocktail, 10 µL, 30 minutes) and the Akt inhibitor was added (Capivasertib, 5 and 20 µM, 24 h), and shTFEB NCI-H2228 cells. The blot is representative of 1 out of 3 images. (F) HIF1α nuclear translocation in WT and shTFEB cells. The blot is representative of 1 out of 3 images. HIF1α binding to ABCB1 (G) and ABCC1 (H) promoter by ChIP assay. Data are means + SD (n=3), in duplicate *p<0,05; **p<0,01; ***p<0,001; ****p<0,0001.

According to these data, we hypothesize that: TFEB is a transcriptional repressor of ABCA1, and indirect inducer of ABCB1/ABCC1, i.e., by activating MAPK and Akt that in turn phosphorylate HIF-1α, increasing its transcriptional activation on ABCB1 and ABCC1.

To verify if other post-translational modifications that may concur to decrease ABCA1 and increase ABCB1/ABCC1 protein in shTFEB cells may occur, we next measured their ubiquitination and phosphorylation that can modulate ABC transporters activity and stability. ABC transporters are also target for post-translational modifications namely phosphorylation and ubiquitination, phosphorylation is used to increase gating mechanisms of ABC transporters whereas ubiquitination of ABC transporters contributes to resistance to chemotherapeutics [103]. We did not find any sign of ubiquitination (Fig. 5A-C) nor phosphorylation (Fig. 5 D-F) on ABCA1, ABCB1 and ABCC1 upon TFEB silencing, excluding these post-translation modifications

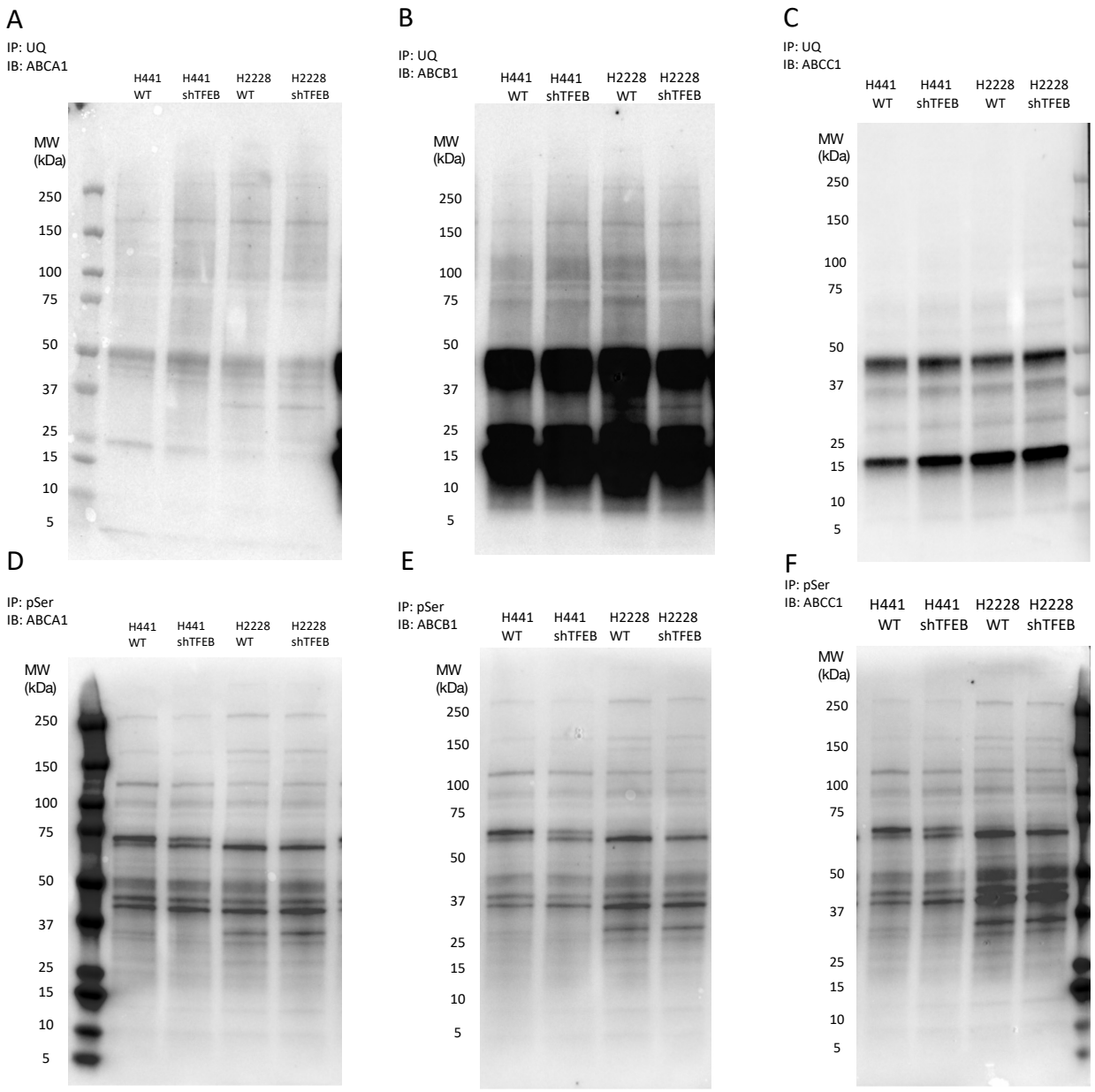

Figure 5: Ubiquitination (A-C) and phosphorylation (E-F) of ABCA1 (A), ABCB1 (B), and ABCC1 (C) in wild-type (WT) and TFEB silence (shTFEB) NCI-H441 and NCI-H2228 cells. Whole cell extracts were immunoprecipitated with an anti-poly-ubiquitination (UQ) or and anti-phosphoserine (pSer) antibody, then blotted for ABCA1, ABCB1, ABCC1. The blot is representative of 1 out of 3 images.

Since TFEB is closely associated with autophagy, we also evaluated if silencing influences on AMPK and ULK1 proteins that can in turn control mTOR/Akt and MAPK pathways[104]Western blot results showed that TFEB silencing did not change the protein levels of AMPK (Fig 6A), phospho-AMPK (Fig 6B), ULK1 (Fig 6C) and phospho-ULK1 (Fig 6D), meaning that TFEB acts on Akt/MAPK pathway independently from AMPK/ULK1 autophagic pathway.

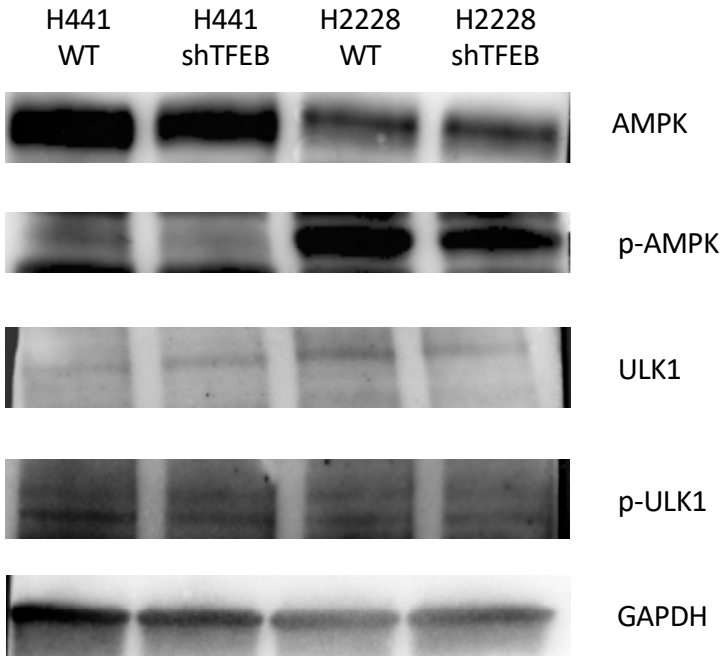

Figure 6: Western blot analysis of AMPK and ULK1 and their phosphorylated form upon TFEB silencing. The blot is representative of 1 out of 3 images.

4.4 By decreasing ERK1/2-mediated stabilization of SREBP2, TFEB regulates cholesterol homeostasis, IPP efflux via ABCA1 and IPP-mediated immune-killing

Since in melanoma cells, TFEB silencing is reported to reduce phosphorylation and activity of ERK1/2[105], and we observed a decrease in MAPK activity in NSCLC, we next deepened if the MAPK reduced by TFEB silencing was indeed ERK1/2. We observed that silencing TFEB downregulates

phospho-Erk as well as total Erk (Fig 7A). MAPK pathway regulates many cellular activities and one of them is cholesterol homeostasis: ERK1/2 is reported to phosphorylate SREBP2, the main transcription factor of cholesterol homeostasis genes, promoting its cleavage and activation[106]. To verify if p-ERK interacted with SREBP2 in NSCLC cells, phospho-Erk was immunoprecipitated from wild-type and TFEB silenced cells, then the samples were immunoblotted for SREBP2. In silence cells, we observed a TFEB decreased amount of SREBP2 precursor and its active form co-immunoprecipitated with phospho-Erk (Fig 7B). Consistently, PCR arrays indicated that many genes related to cholesterol uptake, synthesis and metabolism were downregulated when TFEB was silenced (Fig 7C; Table 6), suggesting that TFEB regulates cholesterol pathways. Although TFEB silencing did not change mRNA levels of HMGCR (Fig 7D), it decreased HMGCR activity (Fig 7E), and, consistently, cholesterol synthesis (Fig 7F) and efflux (Fig 7G), as well as the efflux of IPP efflux (Fig 7H), the intermediate in the cholesterol pathway that is an endogenous activator of Vγ9δ2 T-lymphocytes. To evaluate the impact on immune activation, Vγ9δ2 T-lymphocytes were isolated from the PBMC of healthy donors and co-cultured overnight with NCI-H441 and NCI-H2228 NSCLC cells. When Vγ9δ2 T-lymphocytes were co-cultured with shTFEB cells, their expansion was reduced (Figure 7I) and their anti-tumor capacities were significantly decreased (Figure 7J).

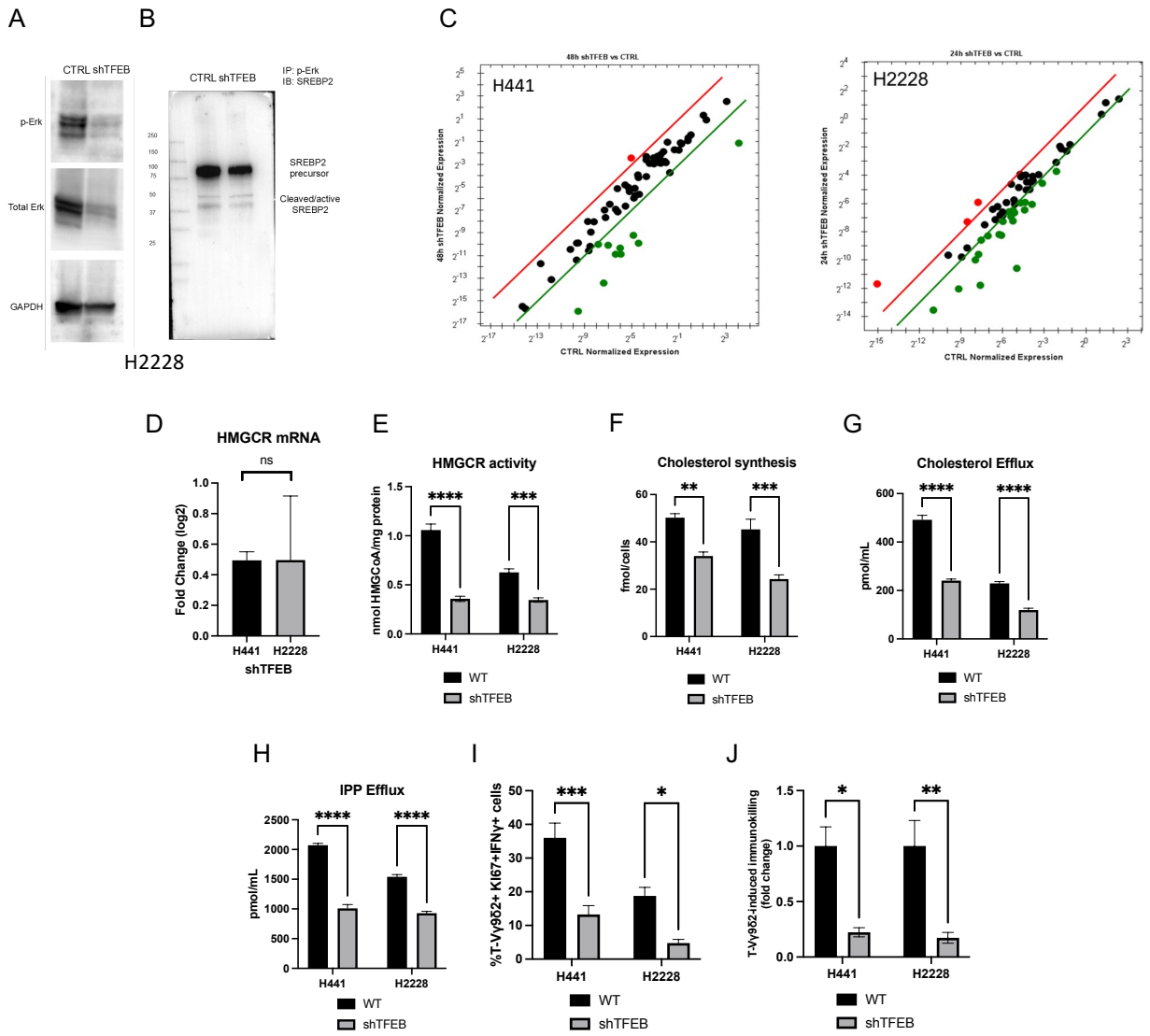

Figure 7: TFEB silencing modulates cholesterol homeostasis-related genes by reducing the activation of SREBP2. (A) Wild-type and TFEB silenced (shTFEB) NHCI-H2228 cells were lysed and subjected to immunoblotting for total Erk, phospho(Thr202/Tyr204)-Erk levels and SREBP2 (B), using an antibody recognizing both precursor and cleaved SREBP2. The blot is representative of 1 out of 3 images. (C). PCR-Array of cholesterol homeostasis-related genes in shTFEB-NCI-H441 and shTFEB-NCI-H2228 compared with wild-type cells. Red dot: significantly up-regulated genes; green dot: significantly down-regulated genes. (D-E). HMGCR mRNA levels and enzymatic activity. Data are means + SD (n=3), in duplicate. *p<0,05; **p<0,01; ***p<0,001; ****p<0,0001 (F-H). Cholesterol and IPP synthesis, and IPP efflux measured by metabolic radiolabeling. Data are means + SD (n=3), in duplicate. *p<0,05; **p<0,01; ***p<0,001; ****p<0,0001 (I-J). Co-cultures between NSCLC cells and Vγ9δ2 T-lymphocytes from healthy donors were set-up to

measure the expansion of Vγ9δ2 T-lymphocytes and the Vγ9δ2 T-lymphocyte-mediated NSCLC cell killing (I-J). Data are means + SD (n=3), in duplicate *p<0,05; **p<0,01; ***p<0,001; ****p<0,0001.

Upregulated	Downregulated
HMGCS1	ABCG1
	LCAT
	OSBPL5

Table 8: Commonly up/down-regulated genes in TFEB-silenced NCI-H441 and NCI-H2228 cell lines.

4.5 TFEB affects mitochondrial energetic metabolism and ABCB1/ABCC1 activity

We investigated the functional and metabolic cholesterol modulation followed by silencing of TFEB. The amount of total cholesterol in whole cell membranes (Fig 8A) and in mitochondria (Fig 8B) were notably decreased in shTFEB cells. On the other hand, electron transport chain (ETC) activity, whose efficiency is impaired by a high cholesterol content in mitochondria[107], was significantly increased in TFEB-silenced cells (Fig 8C) resulting in increased mitochondrial oxygen consumption rate (OCR; Fig 8D). Interestingly, while in wild-type cells OCR decreased with the progressive increase of cisplatin , in shTFEB cells, OCR remained high even in the presence of Cisplatin at IC75. The increase in the OCR is paralleled by significantly increased levels of mitochondrial ATP (Fig 8E), the main fuel of ABC transporters involved in drug efflux[108]. Accordingly, shTFEB cells had strikingly increased activities of ABCB1 (Fig 8F) and ABCC1 (Fig 8G), coupled with decreased intracellular retention carboplatin (Fig 8H).

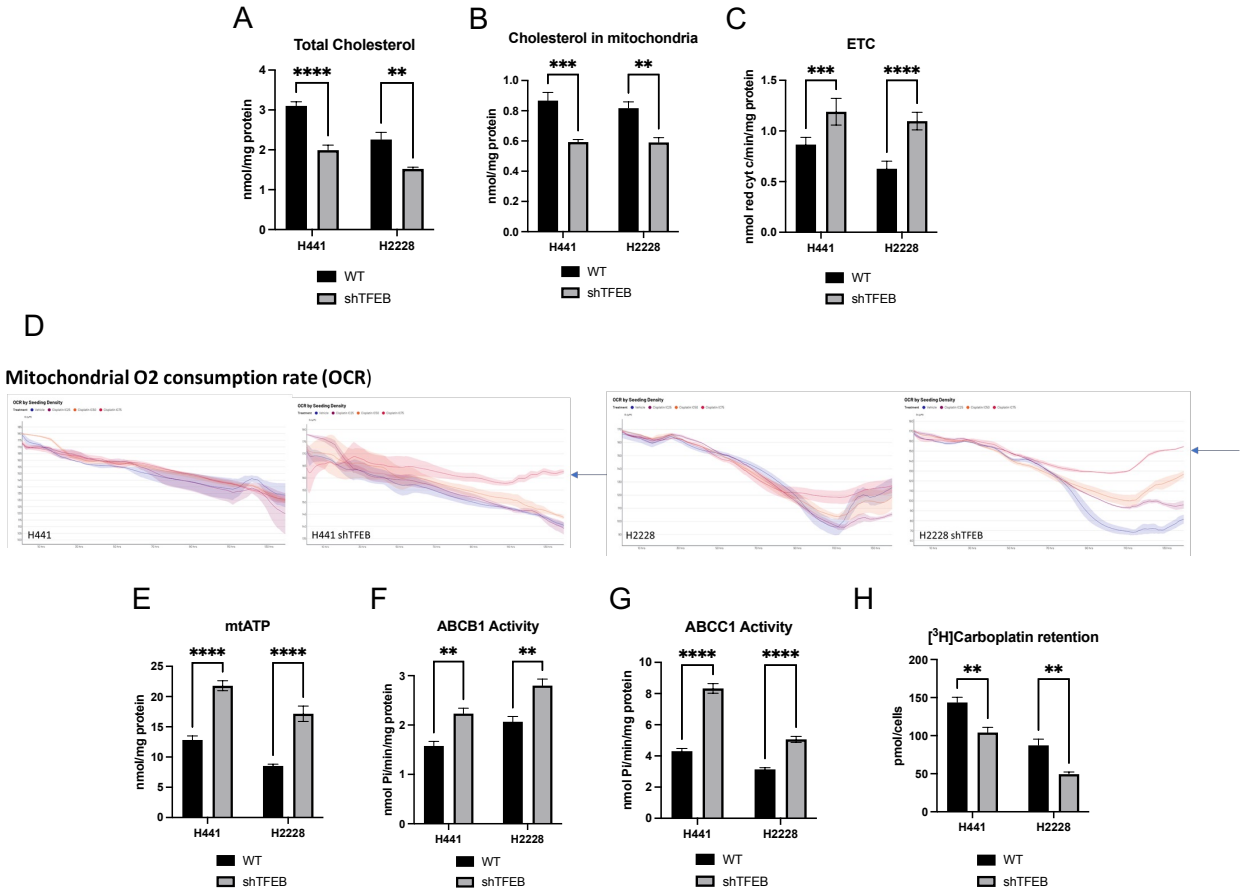

Figure 8: TFEB modulates mitochondrial cholesterol and metabolism, and ABC transporters activity. Modulation role of TFEB has functional results shown in the figure. Total cholesterol (A) and mitochondrial cholesterol (B) in decreased in NCHI-H441 and NCI-H2228 cells silenced for TFEB compared with wild-type (WT) cells. Data are means + SD (n=3), in duplicate *p<0,05; **p<0,01; ***p<0,001; ****p<0,0001 (C). ETC in WT and shTFEB cells. Data are means + SD (n=3), in duplicate *p<0,05; **p<0,01; ***p<0,001; ****p<0,0001 (M) were significantly increased (C). OCR monitored in live cells up to 120 h in WT and shTFEB cells incubated without (CTRL) or with cisplatin at IC25, IC50 and IC75 (determined in previous experiments). (E) Mitochondrial ATP. Data are means + SD (n=3), in duplicate. *p<0,05; **p<0,01; ***p<0,001; ****p<0,0001 (F-G). ABCB1 and ABCC1 catalytic activity. Data are means + SD (n=3), in duplicate. *p<0,05; **p<0,01; ***p<0,001; ****p<0,0001. (H) Intracellular retention of [^{14}C]-Carboplatin. Data are means + SD (n=3), in duplicate*p<0,05; **p<0,01; ***p<0,001; ****p<0,0001.

In line with these finding, TFEB silenced cells that had increased ABCB1 and ABCC1 activity had higher resistance to cisplatin, particularly in NCI-H2228 cells (Fig. 9A-B) and paclitaxel (Fig. 9C-D), although at lesser extent, increased in shTFEB.

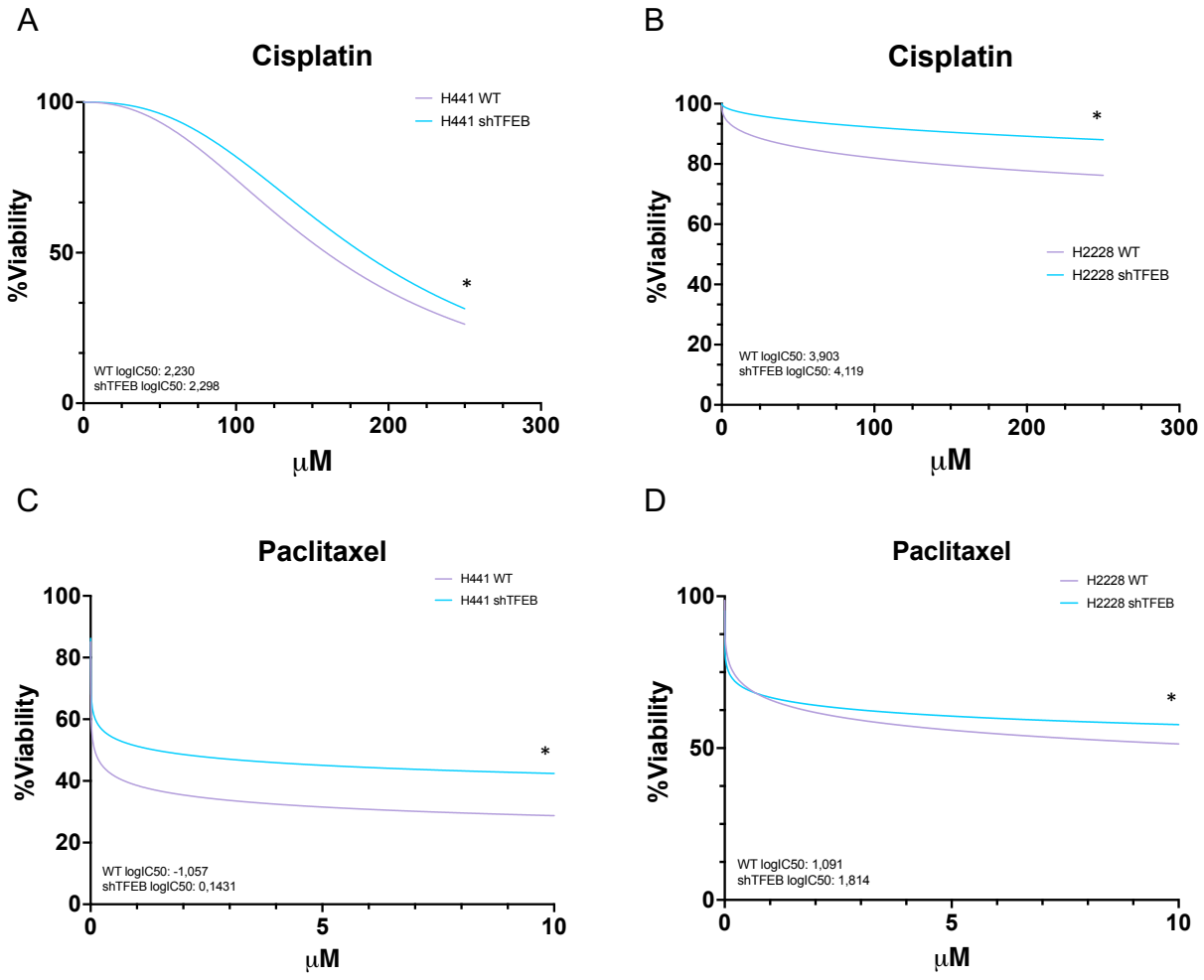

Figure 9: Dose-response viability in the presence of increasing concentration of cisplatin (250 µM, A-B) or paclitaxel (10 µM, C-D), measured in wild-type and TFEB-silenced NCI-H441 and NCI-H2228 cells. Data are means + SD (n=3), in quadruplicate *p<0,05.

So far, our data suggest that TFEB controls simultaneously the expression of ABCA1 via a direct transcriptional down-regulation, and the expression of ABCB1 and ABCC1 by activating their transcription via ERK1/2/HIF-1α and Akt/ HIF-1α axes. In addition, ERK1/2 phosphorylation of SREBP2, promoted by TFEB, favors the transcription of genes involved in cholesterol homeostasis, with at least two consequences: 1) the increased cholesterol and IPP efflux via ABCA1 that favors the immune-killing by Vγ9δ2 T-lymphocytes; 2) the decreased cholesterol content in mitochondria that reduces the ETC-dependent mitochondrial ATP, decreasing the efflux activity of ABCB1 and ABCC1. TFEB can be considered an inducer of chemo-immuno-sensitivity in NSCLC (Fig. 10), with cells with low TFEB are chemo-immuno-resistant.

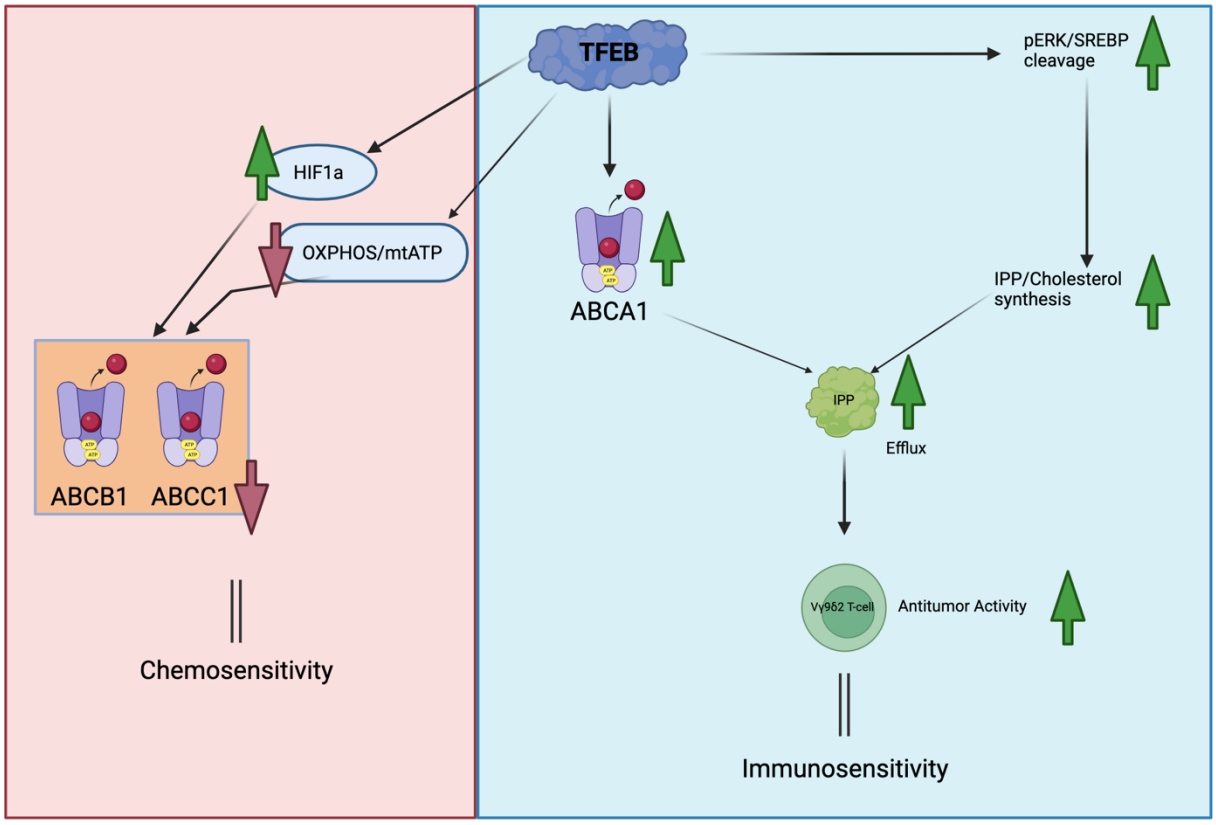

Figure 10: Mechanisms of TFEB as controllers of chemo- and immune-sensitivity in NSCLC cells.

4.6 Dissecting the dual role of TFEB by targeting cholesterol homeostasis with zoledronic acid: a new chemo-immuno-sensitizing strategy

Our results until now demonstrate that TFEB had a multifaceted role on chemo- and immune-sensitivity on NSCLC. Indeed, TFEB silencing induces decrease of IPP efflux and ABCA1 transcription, preventing the immune-killing mediated by Vγ9δ2 T-lymphocytes. Moreover, TFEB silencing transcriptionally upregulates ABCB1 and ABCC1 by activating HIF-1α and fuels their catalytic activity by increasing the efficiency of ETC and the production of mitochondrial ATP, two events that are likely consequence of the reduced cholesterol within mitochondria. We reasoned that to re-instate sensitization to cisplatin and Vγ9δ2 T-lymphocytes killing in NSCLC with low TFEB, we reasoned that a good strategy could be increasing the amount of IPP without reducing the amount of cholesterol. To this aim, we chose to use zoledronic acid, an aminobisphosphonate that is an inhibitor of farnesyl pyrophosphate synthase (FPPS), the enzyme downstream IPP production in the cholesterol synthesis[109]. By so doing, zoledronic acid increases the IPP accumulation and its efflux through ABCA1, promoting the expansion of Vγ9δ2 T-lymphocytes[71]. At the same time, since it does not target the pacemaker enzyme of cholesterol synthesis, we hypothesize that at low concentration it may increase IPP without significantly having effects on the level of cholesterol. Moreover, to maximize the tumor targeting limiting the uptake of the aminobisphosphonate by the bone, we used a self-assembled liposomal formulation of zoledronic acid (NanoZol, NZ), previously reported to have a better tumor-to bone ration than free drugs[110].

In preliminary experiment on NCI-H2228 cells, we set up NZ concentration that did not reduce cholesterol synthesis in shTFEB cells Fig. 11A), but increased IPP synthesis (Fig 11B) and IPP efflux (Fig 11C).Accordingly, this concentration . resulted in an increased percentage of activated Vγ9δ2 T-lymphocytes (Fig 11D) and increased immune-killing by Vγ9δ2 T-lymphocytes, both alone and in combination with cisplatin (Fig. 11E).

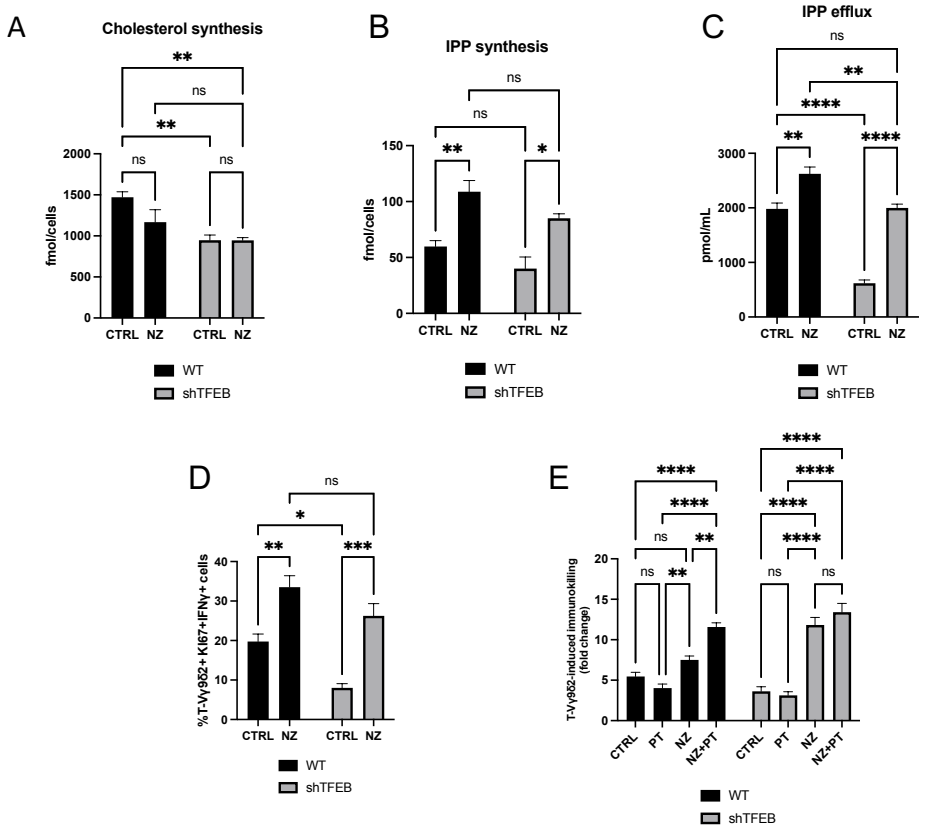
A
Cholesterol synthesis
fmol/cells
B
IPP synthesis
fmol/cells
C
IPP efflux
pmol/mL
D
%T-Vγ9δ2+ Ki67+IFNγ+ cells
E
T-Vγ9δ2-induced immunokilling (fold change)
CTRL
PT
NZ
NZ+PT
WT
shTFEB

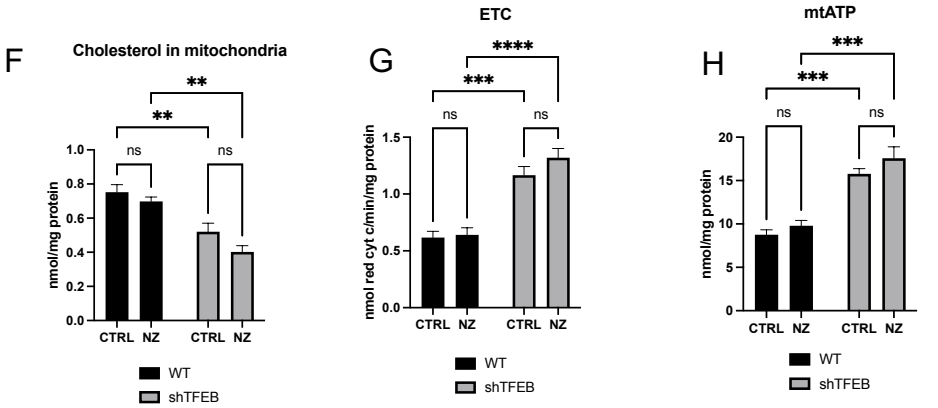
F
Cholesterol in mitochondria
nmol/mg protein
G
ETC
nmol red cyt c/min/mg protein
H
mtATP
nmol/mg protein
CTRL
NZ
WT
shTFEB

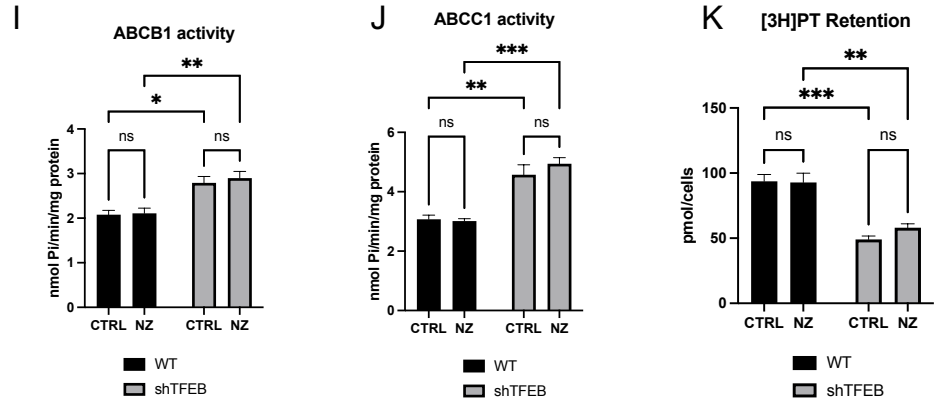
I
ABCB1 activity
nmol Pi/min/mg protein
J
ABCC1 activity
nmol Pi/min/mg protein
K
[3H]PT Retention
pmol/cells
CTRL
NZ
WT
shTFEB

Figure 11: Effects of NZ on cholesterol homeostasis and mitochondrial energetic metabolism. NCI-H2228 cells, wild-type (WT) or silenced for TFEB (shTFEB) were incubated 24 h with or without (CTRL) 100 nM NZ (A-B). Cholesterol and IPP synthesis. Data are means + SD (n=3), in quadruplicate. *p<0,05; **p<0,01; ***p<0,001; ****p<0,0001 (C). Expansion of proliferating (Ki67+) and activated (IFNγ+) t-lymphocytes, and immune-killing capabilities. Data are means + SD (n=3), in duplicate. *p<0,05; **p<0,01; ***p<0,001; ****p<0,0001 (D-E). Mitochondrial cholesterol, ETC and mitochondrial ATP (F-H). ABCB1 and ABCC1 activity (I-J). PT retention (K). Data are means + SD (n=3), in duplicate. *p<0,05; **p<0,01; ***p<0,001; ****p<0,0001.

Moreover, mitochondrial cholesterol was not decreased further in TFEB-silenced cells (Fig 11. F), nor was the ETC (Fig. 11 G) and ATP (Fig. 11H). Accordingly, ABCB1 and ABCC1 activity was not further increased (Fig. 11 I-J) and PT retention was not further decreased (Fig. 11K) in NZ-treated cells.

To prove that NZ could be a good agent that increases the immune-killing without impairing the efficacy of cisplatin in TFEB-silenced tumors cases, NZ treatment had no effect on these parameters in both xenografts.

We implanted wild-type and shTFEB NCI-H2228 tumors in NOD scid gamma mouse (NSG) bearing humanized immune system (Hu-CD34^{+} NSG strain) to mimic the immune response of humans. Wild-type (WT) and shTFEB NCI-H2228 NSCLC cell line xenografts were implanted subcutaneously and treated with saline solution, cisplatin, NZ, or their combination.

We noticed that shTFEB xenografts had less volume compared to WT counterparts (Fig 12A). In WT tumor, single treatments with cisplatin or NZ delayed tumor growth but did not reduce tumor volume at our end point (Fig. 12A-B). A similar trend was observed in shTFEB tumor. Notably, both in WT and in shTFEB tumors the combination of cisplatin + NZ strongly decreased tumor growth.

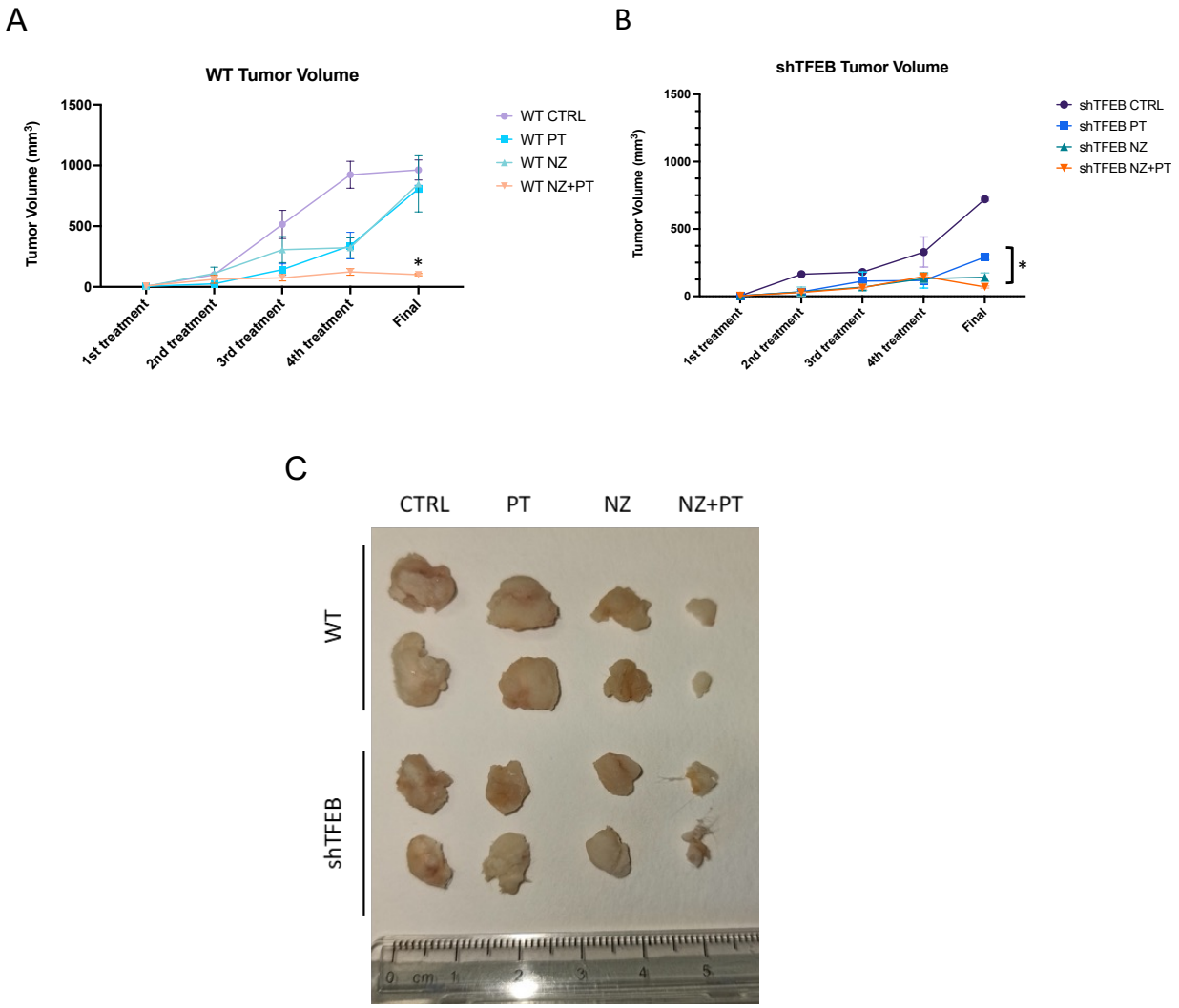

Figure 12: The combination of NZ and cisplatin is effective against chemo-immuno-resistant TFEB-silenced tumors. Wild-type (WT) and TFEB-silenced (shTFEB) NCI-H2228 tumors were implanted subcutaneously in Hu-CD34^{+}NSG mice and randomized when tumor volume reached 50 mm^3, animals were randomized and treated for 3 weeks as it follows: control group (CTRL), treated with 0.1ml saline solution intravenously (i.v.), once a week; cisplatin group (PT), treated with 2 mg/kg cisplatin i.v. once a week; Nanozol group (NZ), treated with 1 mg/kg i.v. NZ once a week; Nanozol and cisplatin (NZ+PT) group, receiving the same doses i.v. once a week simultaneously. Animals were euthanized at day 28 (A-B) Tumors growth was monitored by a caliper. Data are means + SD (n=3), in duplicate. *p<0.05. (C) Representative photos of excised tumors.

While non-appreciable differences in tumor histology were evident in hematoxylin-eosin staining, Ki67, an intratumor proliferation was reduced at the same level by cisplatin, NZ, or the combination in wild-type tumors. The reduction of Ki67 elicited by cisplatin was lower in shTFEB tumors, but NZ significantly decreased this parameter (Fig. 13A-B). The intratumor apoptosis, evaluated by TUNEL assay, was induced by cisplatin in wild-type but not in shTFEB tumors. In these tumors, only the combination of cisplatin and NZ produced a significant increase of apoptosis (Fig. 12C-E).

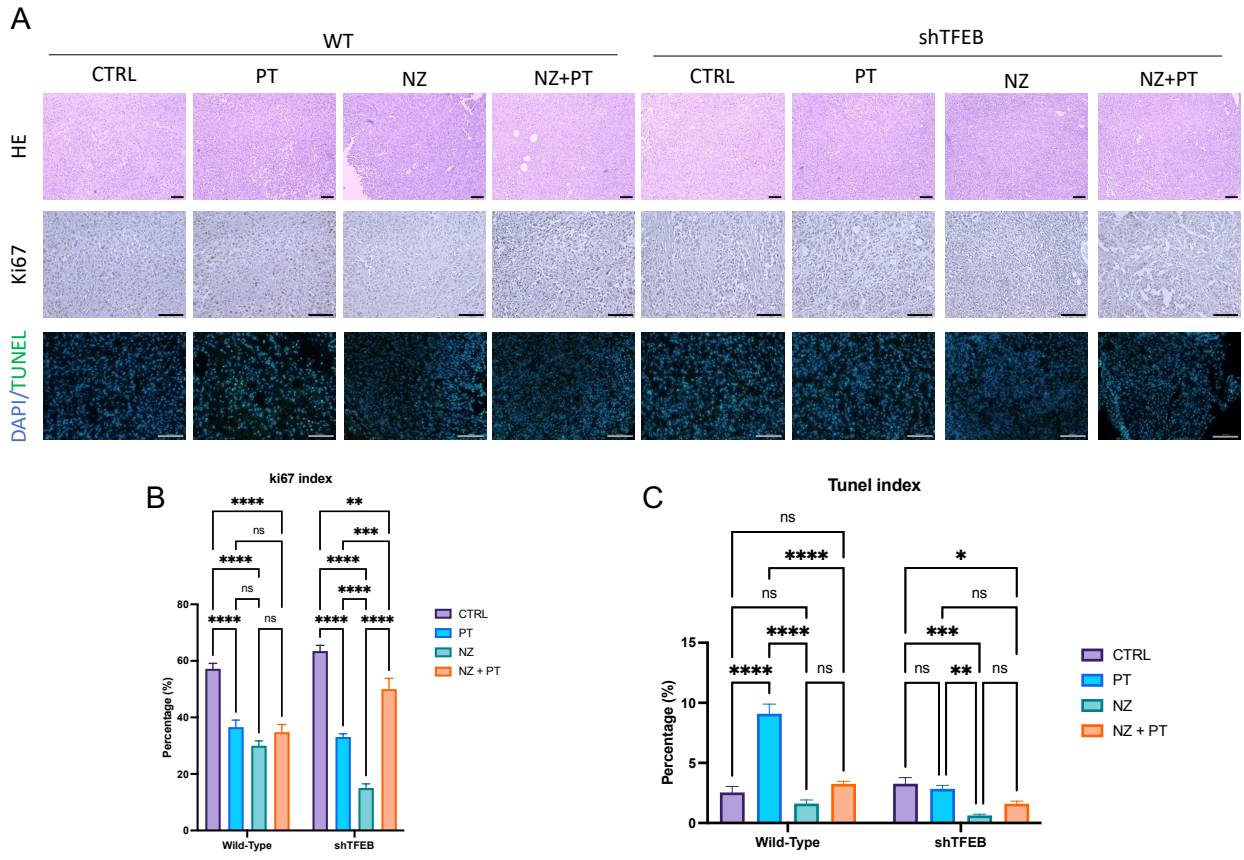

Figure 13: Hematoxylin-eosin staining, Ki67 staining and TUNEL staining or representative sections of tumors from each group. At least 4 tumors /group were examined (5 filed/each tumor). Objective: 10X; Ocular: 10X. Bar: 100 µm for HE, Objective: 20X; Ocular: 10X; Bar: 100 µm for Ki67 and DAPI/TUNEL (A) Percentage of $Ki67^{+}$cells/total nuclei and $TUNEL^{+}$ cells/total cells on 4 sections with an average number of 100 cells/section. *, ** $p < 0.05$. ***$p < 0.001$.

Finally, we verified the toxicity of our treatment options. The post-mortem pathological analysis of organs did not reveal appreciable histological alterations in heart, liver, lung, kidney, and spleen in each experimental group (Fig. 14). Similarly, the hematochemical parameters measured immediately after euthanasia indicated no signs of toxicity for bone marrow (RBC, Hb, WBC, PLT), liver (LDH, AST, ALT, AP), kidney (creatinine), muscles and heart (CPK) in each group of treatment (Table 9).

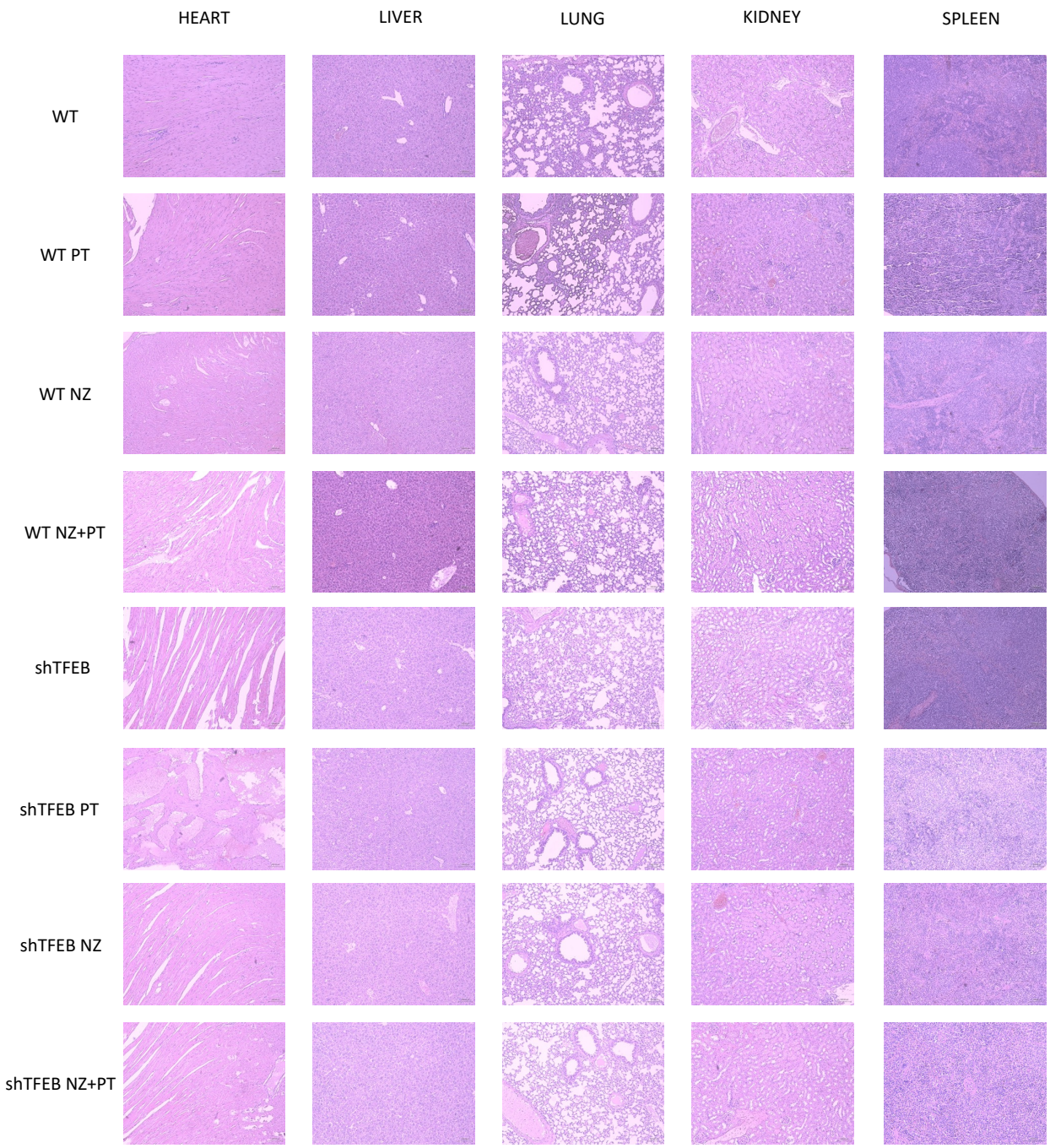

Figure 14: **Hematoxylin-eosin staining of heart, liver, lung, kidneys, and spleen collected post-mortem**. Objective:

Objective: 10X; Ocular: 10X; Bar: 100 µm.

Supplementary table SX (hematochemical parameteres)								
	WT				shTFEB			
	vehicle	PT	NZ	NZ+PT	vehicle	PT	NZ	NZ+PT
RBC (x 106/µl)	13.23 + 2.01	12.18 + 1.95	13.21 + 1.42	12.18 + 1.69	12.59 + 2.47	11.29 + 2.61	13.48 + 4.52	12.11 + 3.51
Hb (g/dl)	13.11 + 1.44	12.45 + 2.31	13.48 + 0.91	12.41 + 1.13	12.63 + 1.94	12.01 + 2.15	12.54 + 1.59	12.04 + 2.51
WBC (x 103/µl)	13.28 + 3.02	14.37 + 2.39	12.04 + 2.15	13.08 + 1.57	11.07 + 2.07	13.29 + 2.51	12.11 + 1.27	13.45 + 2.45
PLT (x 103/µl)	873 + 134	745 + 234	916 + 115	8566 + 152	896 + 205	792 + 184	809 + 152	701 + 172
LDH (U/l)	9823 + 548	10523 + 627	8912 + 604	7598 + 501	7984 + 412	8216 + 285	7452 + 205	7205 + 236
AST (U/l)	156 + 44	135+ 34	143 + 39	144 + 49	134+ 29	146 + 34	152 + 47	162 + 44
ALT (U/l)	36 + 14	45 + 11	45 + 19	54 + 23	44 + 18	37 + 11	49 + 15	53 + 11
AP (U/l)	114 + 22	127 + 28	129 + 342	113 + 205	128 + 33	108 + 27	119 + 37	109 + 48
Creatinine (mg/l)	0.071 + 0.009	0.082 + 0.007	0.069 + 0.011	0.079 + 0.009	0.074 + 0.007	0.079 + 0.010	0.072 + 0.008	0.0692 + 0.011
CPK (U/l)	231 + 22	256 + 42	282+ 48	304 + 55	205 + 38	249 + 52	281 + 61	298 + 84

Table 9: Hematochemical parameters of animals after euthanasia (n=4/each group of treatment).

4.7 Differentially Expressed Genes and Pathways between TFEB^{low}ABCA1^{low}ABCC1^{high} vs TFEB^{high}ABCA1^{high}ABCC1^{low}: an *in-silico* analysis

In the last part of my project thesis, I enlarged the analysis of the gene network linking TFEB, ABCA1, ABCB1 and ABCC1, with the goal of finding further pathways explaining the chemo-immuno-resistance of TFEB^{low} tumors and identifying new druggable targets. To this aim, we re-analyzed the TCGA-LUAD dataset. First, we evaluated the changes in their expression in lung tumors versus non-tumor tissues: violin plots revealed that TFEB (Fig 15A), ABCA1 (Fig 15B) ABCB1 (Fig 15C) expression was downregulated significantly in tumors, while ABCC1 did not change (Fig 15D).

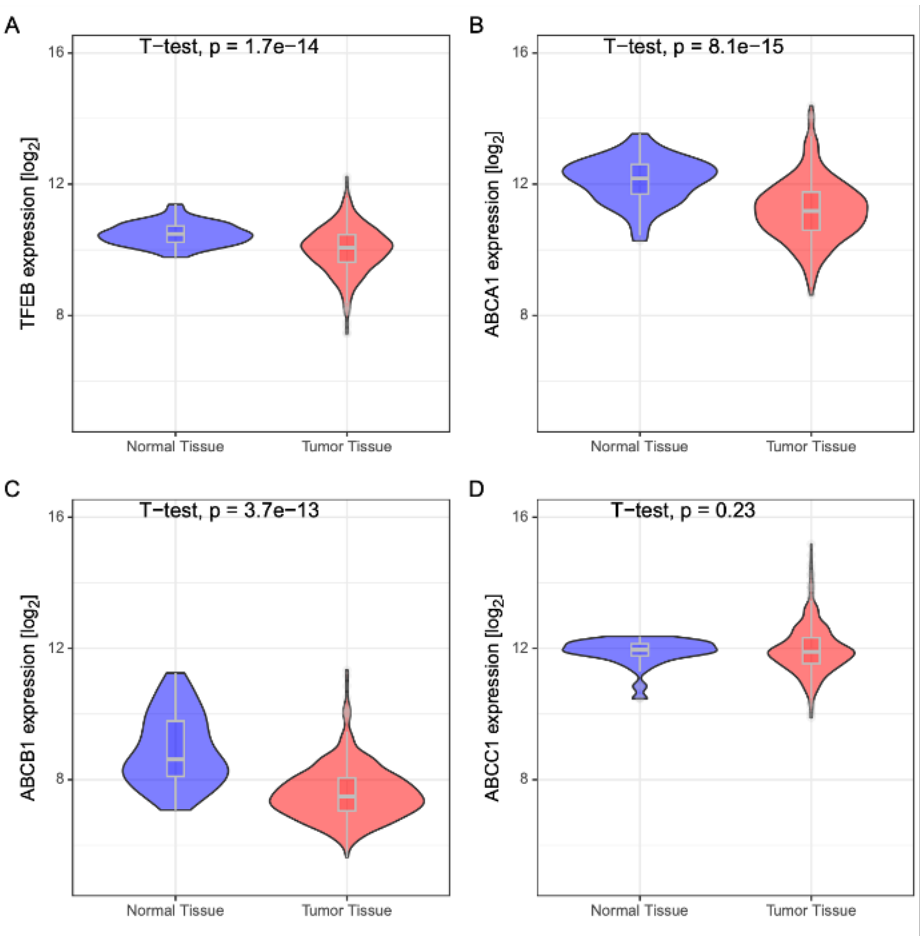

Figure 15: Changes in TFEB (A) and ABCA1 (B), ABCB1 (C), and ABCC1 (D) in primary tumors versus normal tissue (TCGA-LUAD).

Next, we investigated the DEGs between $TFEB^{low}ABCA1^{low}ABCC1^{high}$ and $TFEB^{high}ABCA1^{high}ABCC1^{low}$ phenotypes, i.e., the most negative and most positive prognostic phenotypes in the TCGA-LUAD cohort. ~19174 genes resulted differentially expressed. The most up-and downregulated genes in both phenotypes are shown in Fig. 16A. Based on the DEGs, Kegg Pathways (Fig. 16B), Wikipathways (Fig. 16C) and Gene Ontology Biological Process (Fig. 16D) enrichment analysis were performed.

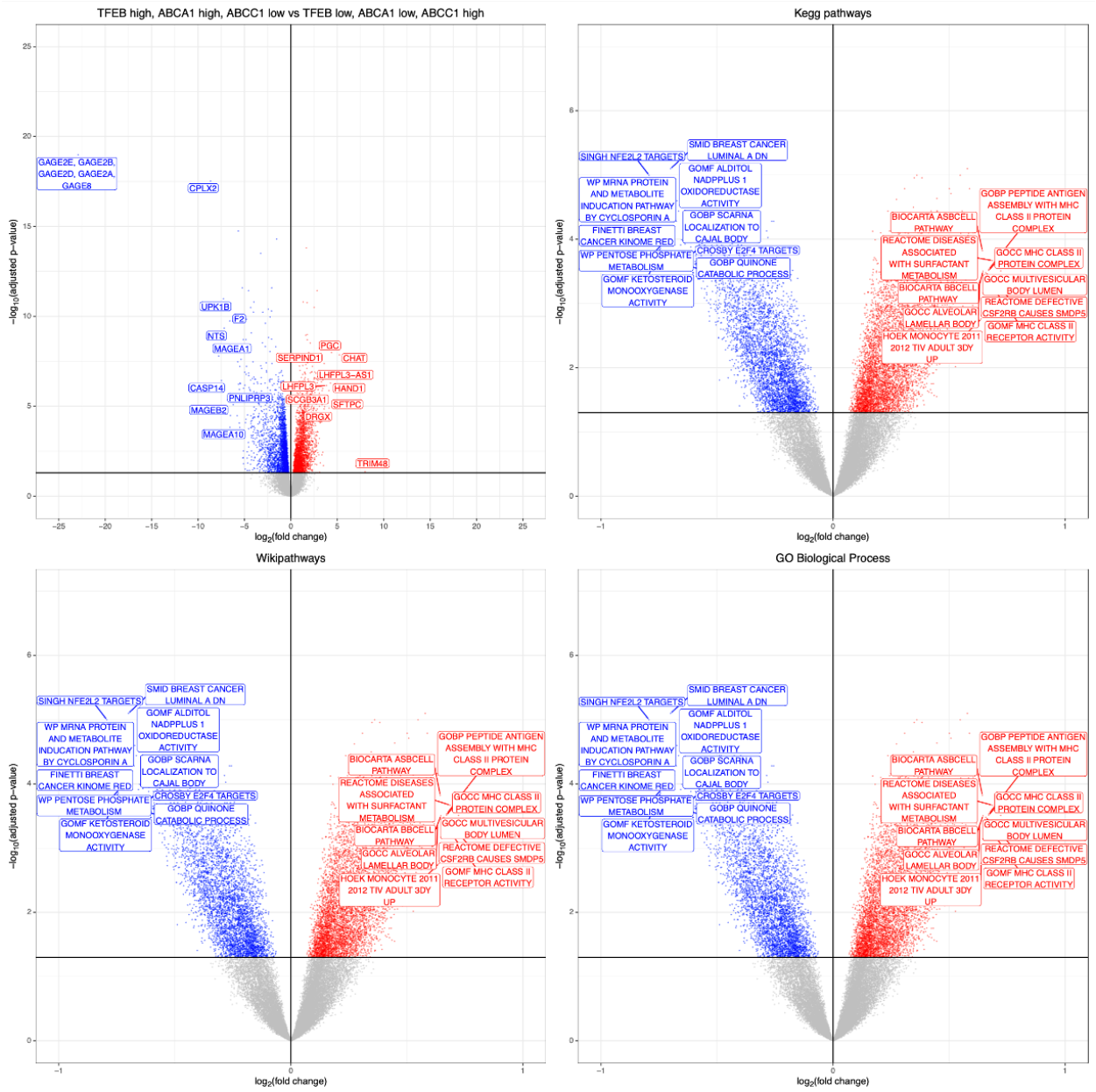

Figure 16: (A) Differentially expressed genes of TFEB^{low}ABCA1^{low}ABCC1^{high} versus TFEB^{high}ABCA1^{high}ABCC1^{low} (A). Differentially expressed pathways based on Kegg (B), Wikipathways (C), and GO Biological Process (D) tools.

Strikingly, all three tools indicated that TFEB^{low}ABCA1^{low}ABCC1^{high} tumors shared the following pathways/biological processes upregulated: Peptide Antigen Assembly with MHC Class II Protein

Complex, Negative Regulation of Interleukin 18 Production, Regulation of Cellular Response to Macrophage Colony Stimulating Factor Stimulus, Leukotriene Signaling Pathway, and Antigen Processing and Presentation Endogenous Lipid Antigen Via MHC Class IB. By contrast, common downregulated pathways/biological process were Quinone catabolic process, Scarna localization to Cajal body, Positive regulation of establishment of protein localization to telomere, Menaquinone metabolic process, Meiotic sister chromatid cohesion centromeric, Cytolysis by host of symbiont cells, Positive regulation of blood vessel remodeling.

4.8. Construction of Weighted Gene Coexpression Network

The data were cleaned from microRNA, small nucleolar RNA, long intergenic non-protein coding RNAs and uncharacterized RNAs followed by low abundance gene filtering. After this step, WGCNA was performed based on the DEGs of between $TFEB^{low}ABCA1^{low}ABCC1^{high}$ and $TFEB^{high}ABCA1^{high}ABCC1^{low}$ phenotypes. The analysis was performed based on a signed network and “biweight midcorrelation (bicor)” were chosen as correlation type. The power of $\beta = 7$ was chosen as soft threshold. 34 modules were created based on phenotyping, and expression of TFEB, ABCA1 and ABCC1 (Fig. 17A). Survival times were not significant according to the hierarchical clustering tree of the dendrogram (Fig. 17B). Depending on t-statistics, genes in M23 and M31 modules were significantly upregulated in the $TFEB^{low}ABCA1^{low}ABCC1^{high}$ group, while genes in M1 and M10 were significantly downregulated (Fig. 18).

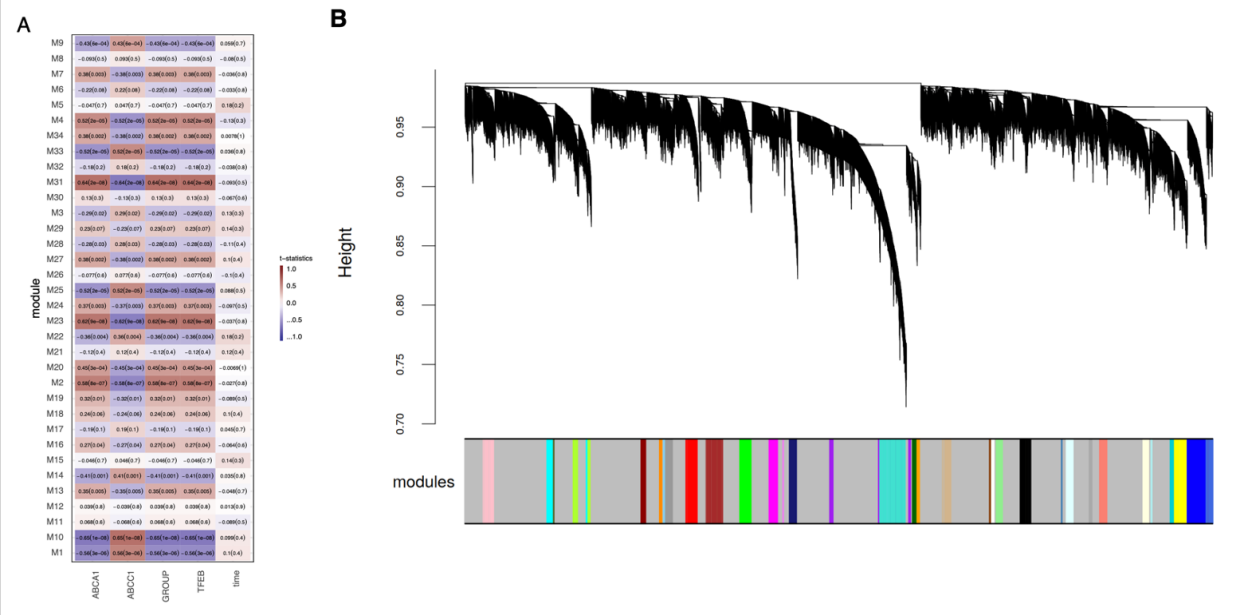

Figure 17: (A) Network analysis showing upregulated and downregulated modules. (B) Hierarchical clustering tree of the dendrogram were created based on gene expression rather than survival time.

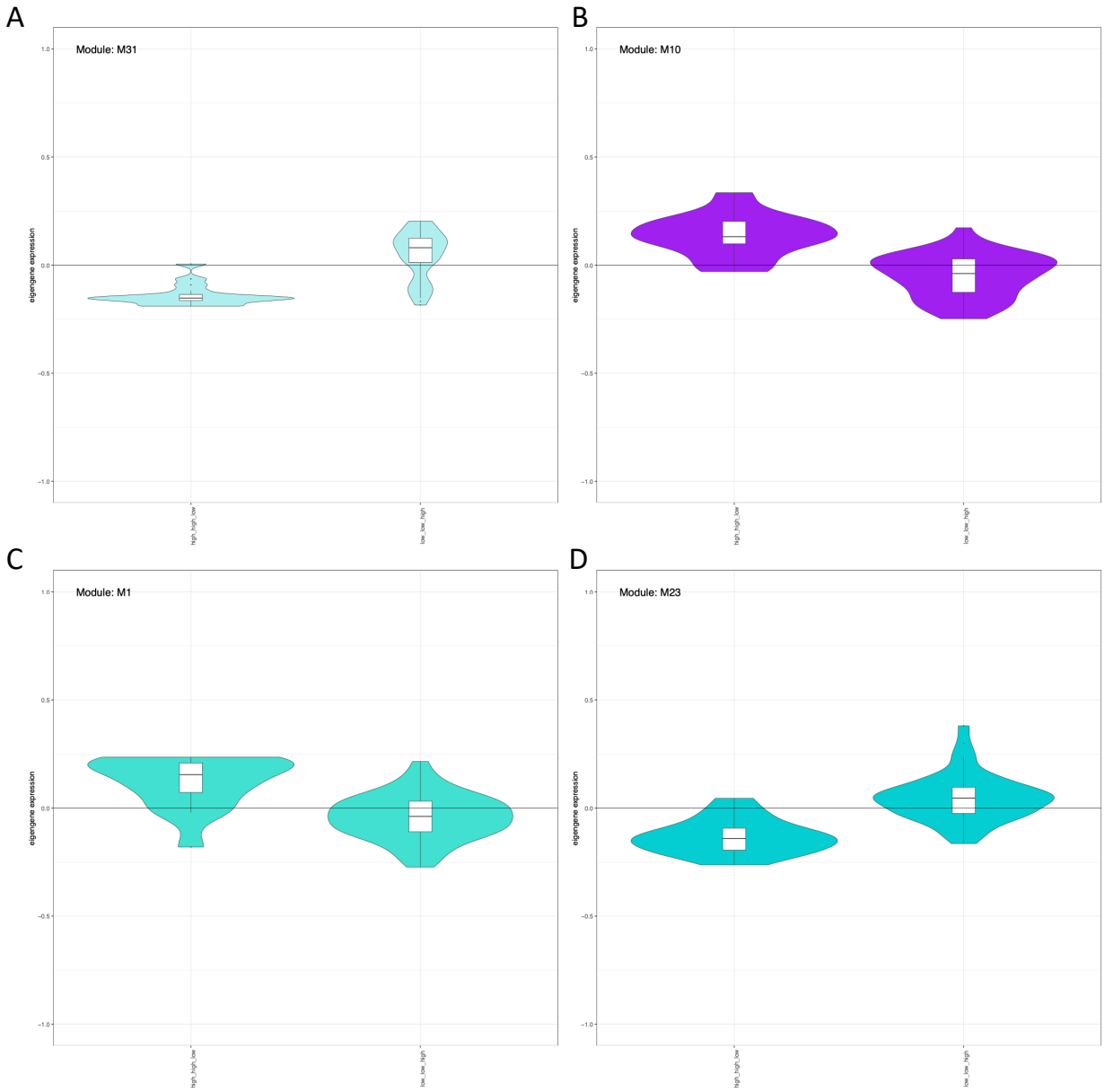

Figure 18: Top 4 modules with the most significant changes. Modules M31 (A) and M23 (D) were upregulated in TFEB^{low}ABCA1^{low}ABCC1^{high} phenotype, M10 (B) and M1 (C) were downregulated significantly.

4.9. Network analysis shows that ABC transporters are involved in the immune response

Hence, we focused on the genes belonging to these four networks. Oxidative stress-sensitive genes, such as induced growth inhibitor 1 (OSGIN1), cytochrome p450 4F11 (CYP4F11) and

Phosphogluconate Dehydrogenase (PGD) were strongly associated in the M31 module (Fig 19A). GO-BP clusters show that genes in the M31 module regulate the cellular response to oxidative stress, oligopeptide transport, hormone stimulus and metabolic processes involving $NADP^+$, xenobiotics and progesterone (Fig. 19B).

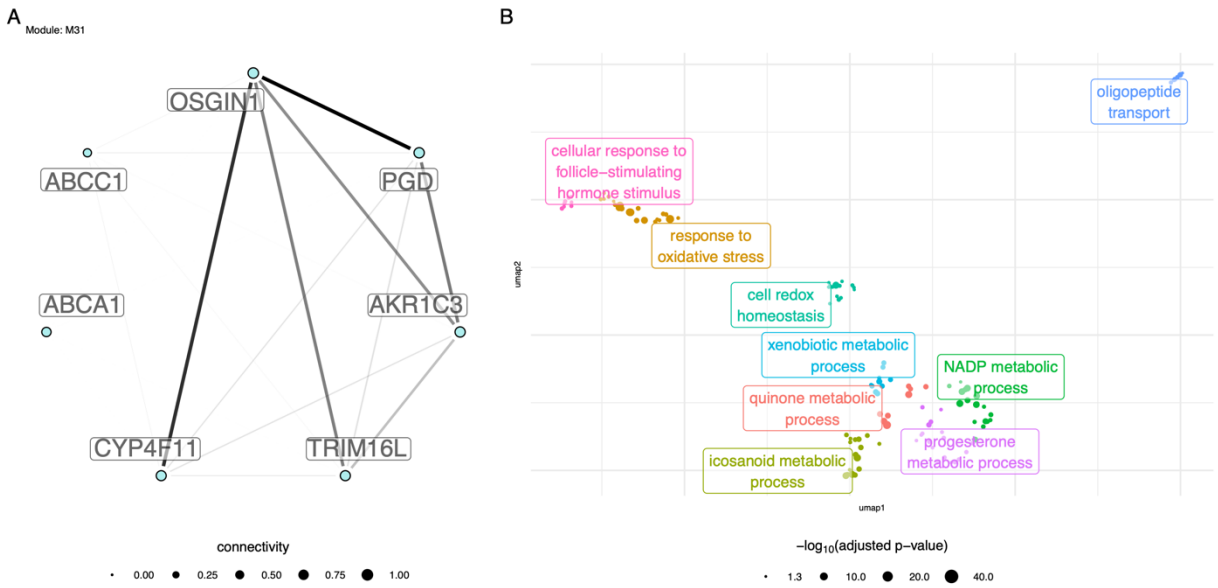

Figure 19: (A) Connectivity of ABCA1 and ABCC1 to OSGIN1 and PGD. (B) Pathways in the network of M31

The second upregulated module, M23 (Fig. 20A), included genes such as General Transcription Factor IIA Subunit 2 (GTF2A2), PCNA Clamp Associated Factor (PCLAF) and ATP Synthase Membrane Subunit C Locus 3 (ATP5MC3) that are linked to mitochondrial transporters, mitochondrial membrane organization and ATP synthesis (Fig. 20B). Overall, these profiles indicate that $TFEB^{low}ABCA1^{low}ABCC1^{high}$ may have higher protection from oxidative stress, and higher oxide-reductive and mitochondrial metabolisms, all features that sustain a chemo-immuno-resistant phenotype, as we observed in TFEB silenced NSCLC cells.

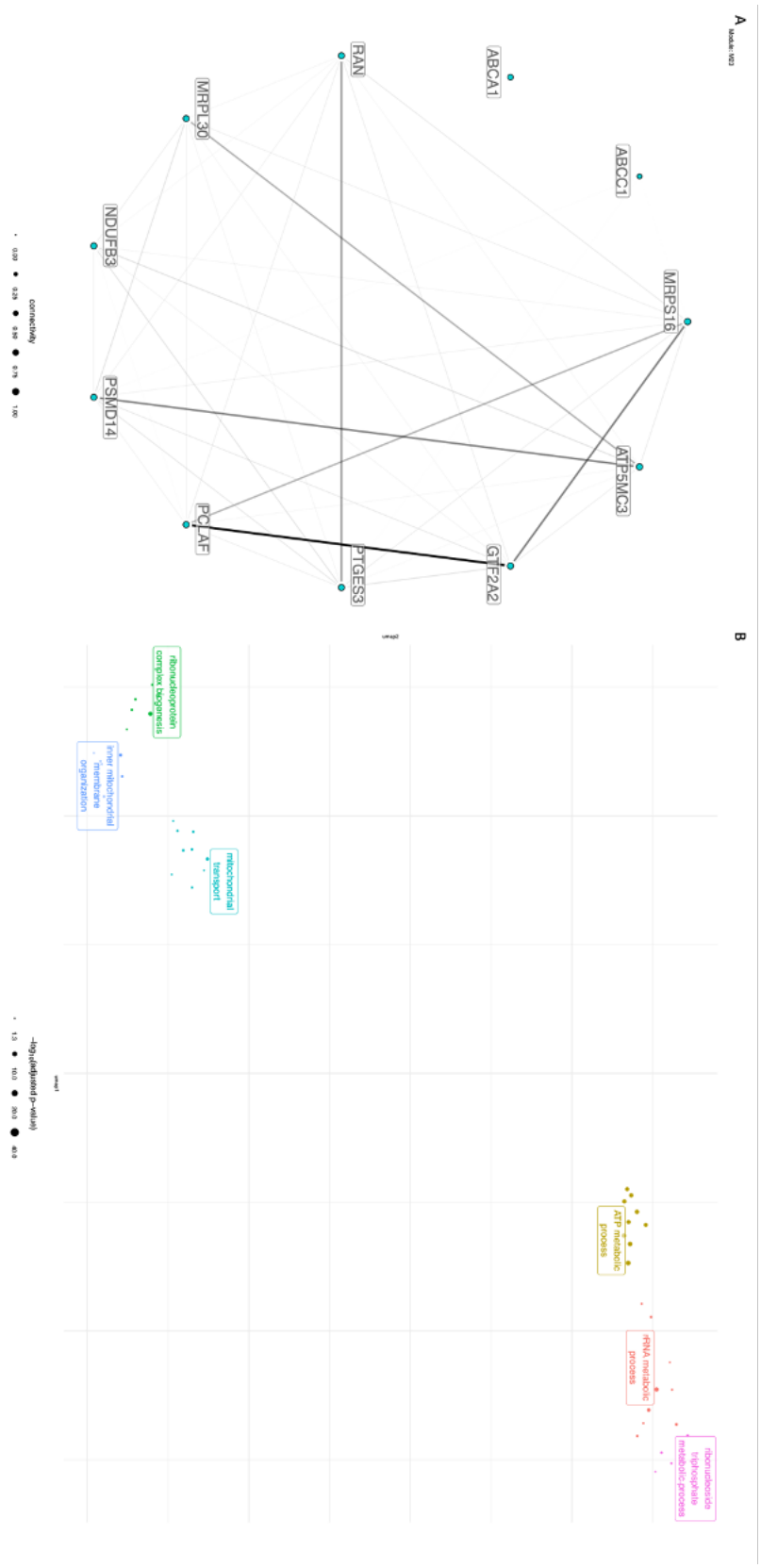

Figure 20: (A) Connectivity of ABCA1 and ABCC1 to GTF2A2 and PCLAF. (B) Pathways in the network of M23.

Analyzing the downregulated modules, Adhesion G protein-coupled receptor F5 (ADGRF5) and Folliculin Interacting Protein 2 (FNIP2) had a strong association in the module M10 (Fig 21A). These genes are involved in the regulation of GTPase activity and downstream signal transduction, as well as in cell−extracellular matrix adhesion and cell-cell junction (Fig 21B).

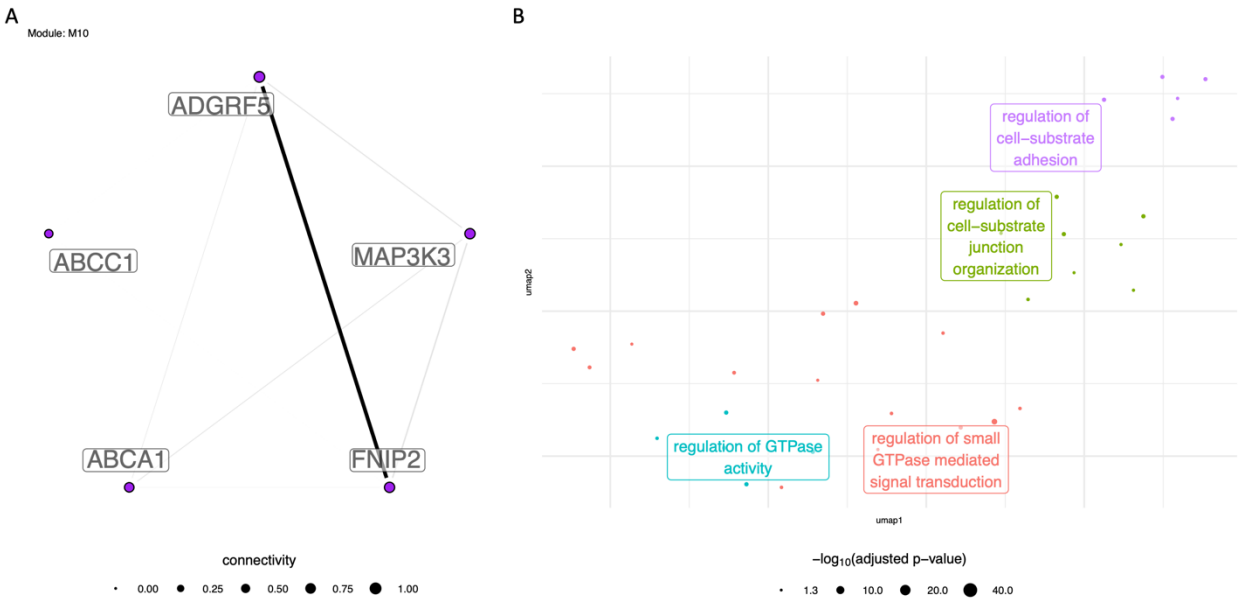

Figure 21: (A) Connectivity of ABCA1 and ABCC1 to ADGRF5 and FNIP2. (C) Pathways in the network of M10.

Finally, in M1, SAM And SH3 Domain Containing 3 (SASH3) gene was found to be connected strongly to Leukocyte surface antigen CD53, IKAROS Family Zinc Finger 1 (IKZF1) and Sorting Nexin 20 (SNX20), which is connected to Leupaxin (LPXN). Interleukin 10 Receptor Subunit α (IL10RA) gene was also regulated within M1 (Fig 22A). The extensive network of genes in M1 and M10 plays different roles in the immune system, such as cell chemotaxis, regulation of immune response, antigen processing and presentation, activation and differentiation of T-cells, and

cytokine production (Fig 22B). The downregulation of these genes is consistent with the immuno-evasive profile of $TFEB^{low}ABCA1^{low}ABCC1^{high}$ NSCLC cells[74]. ABC transporters ABCA1 and ABCC1 resulted present, albeit with low connectivity and association, in all modules, while TFEB did not, suggesting that there is not a direct correlation between TFEB and the DEGs identified, but the effects of TFEB are mediated by downstream controller processes. We are validating which of this biological process, beyond the mitochondria energy metabolism that already emerged in the represent work, could link TFEB with the expression levels of ABCA1 and ABCC1, determine chemo-immuno-sensitivity or resistance.

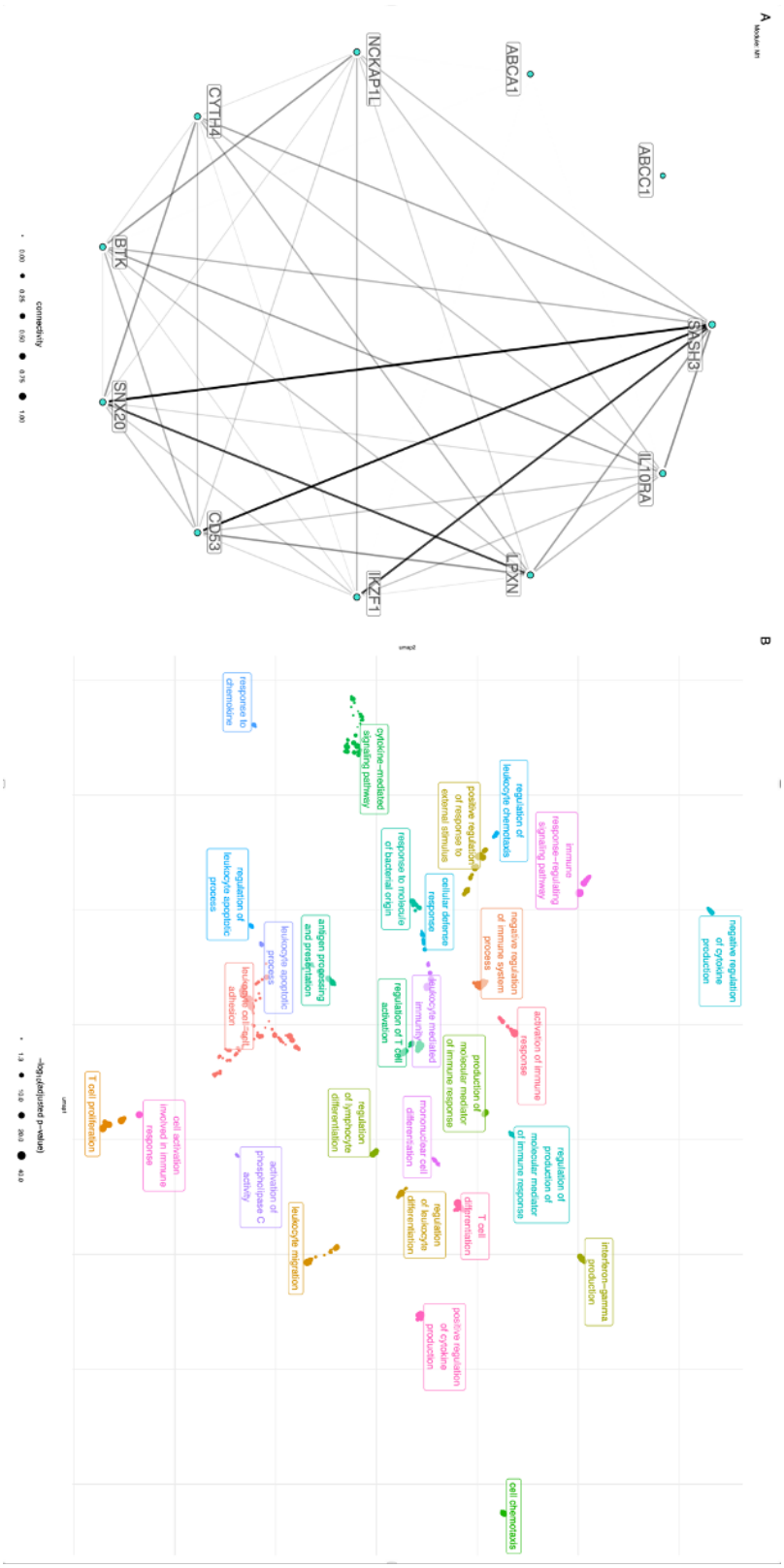

Figure 22: (A) Connectivity of ABCA1 and ABCC1 to SASH3 and SNX20. (B) Pathways in the network of M1.

5. Discussion

Multidrug resistance (MDR), is often caused by the overexpression of ABC transporters and hinders the success of chemotherapy in NSCLC[111,112]. More than thirty years passed from the development of the first ABC inhibitors but still many of the attempts failed during clinical trials, because of poor specificity and high toxicity, indicating the need of new approaches to overcome MDR[113]. Considering that among the main drivers of lung cancer formation and progression, there are genomic instability and mutations[114], molecular techniques are extremely relevant and genetic profiling - together with other OMIC-techniques (transcriptomics, proteomics or metabolomics) - might have great potential to identify new pathways and gene networks[115] that can be targeted to overcome MDR. In this project we dissected the role of TFEB on regulation of ABC transporters to investigate investigated if TFEB affects the response to chemotherapy and to Vγ9δ2 T-lymphocytes in NSCLC, starting from the analysis of transcriptomic databases of large cohort of patients, analyzing the molecular mechanisms underlying, finding a new pharmacological chemo-immuno-sensitizing approach, and finally expanding our knowledge on putative factors connected with TFEB and involved in chemo-immuno-resistance, to have an in silico prediction of new biomarkers and actionable targets.

First, we evaluated the effect of our genes of interest (the transcription factor TFEB, the drug efflux transporters ABCB1/ABCC1, the immune-sensitizing transporter ABCA1) on survival, analyzing the TCGA LUAD cohort. The effects of TFEB on cancer biology and progression are reported to be likely tumor-type-dependent. Giatromanolaki et al. reported that TFEB is increased in NSCLC patients and, along with LAMP2a and Cathepsin D, is correlated with poor prognosis. The overexpression of TFEB and subsequent activation of autophagy were also reported in

glioblastoma and early stages of breast cancer[85,116,117]. A high expression of TFEB is also linked with poor prognosis in colorectal cancer patients, where, contrarily to lung cancer, TFEB was expressed at lower levels in cancer tissues compared to normal tissues[118]. Given the fact that autophagy has conversing roles in cancer, either promoting cancer cell survival under stress conditions or inhibiting oncogenesis[119], TFEB and its influence on autophagy might have different effects on cancer progression under different situations such as the basal levels of TFEB, the basal activation of autophagy machinery, the stage of the tumor, etc., explaining the contrasting evidence existing in literature.

ABCB1 and ABCC1 are recognized among the main mediators for chemoresistance in most cancers. Both transporters are upregulated in tumors followed by chemotherapy and induce chemotherapeutic failure by actively transporting the drugs outside the cell[69,111]. Even in chemo-naïve tumors, ABCB1 and ABCC1 expressions were higher in NSCLC tumors compared to normal tissue[120,121], and this overexpression was linked with poor prognosis in NSCLC[122]. Although we did not find a significant difference between normal tumor and tissue in TCGA LUAD cohort, ABCC1^{high} phenotype is indeed linked with lower OS in these patients.

Contrarily to what was expected from literature, ABCB1 was downregulated in tumor tissues versus normal tissue in the TCGA-LUAD dataset. However, it should be noted that in each cancer type, expressions of ABC transporters may vary [112]. We recently observed that in a panel of 28 NSCLC cell lines, we had a wide range of expression of ABCB1 and ABCC1[74]. However, the levels of ABCB1/ABCC1 were always inversely related to that of [74], the main effluxer of cholesterol and IPP, promoting immune-killing of tumor cell. Cholesterol enables cell differentiation and cancer growth[123] through the Hedgehog pathway, Wnt and mTORC1, which in turn controls TFEB[124,125].

It has been proposed that ABCA1 has antitumoral activity by increasing cholesterol efflux, because ABCA1 deficiency or downregulation leads to accumulation of mitochondrial cholesterol that in return increases the cell survival in colon and pancreatic cancer[126,127]. This finding is in line with our observations in TCGA LUAD cohort reporting that ABCA1^{high} phenotype had the best OS. Liu et al.,[128] reported that miRNA-200b-3 promotes the proliferation and metastasis of lung adenocarcinoma cells by suppressing ABCA1, suggesting that high levels ABCA1 might have a positive biological meaning in NSCLC. However, also for the role of ABCA1 the scenario is multifaceted. For instance, ABCA1 upregulation was linked to poor survival in ovarian cancer[129]. We found that ABCA1 was significantly downregulated in TCGA LUAD cohort, although ABCA1 levels are not significantly associated with OS. Since TFEB and ABC transporters examined individually have controversial results on survival in TCGA LUAD cohort, we examined the impact of their associations. We found that the TFEB^{low}ABCA1^{low}ABCC1^{high} phenotype is associated with the poorest survival. By contrast, the TFEB^{high}ABCA1^{high}ABCC1^{low} phenotype had a better overall survival. The LUAD cohort data were next validated in two smaller cohorts present at our department, who has received chemotherapy or immunotherapy as first-line treatment. In both cisplatin -and immunotherapy-treated groups TFEB^{high}ABCA1^{high}ABCC1^{low} phenotype offered a better and significant progression free survival and overall survival, suggesting that it has a chemo-immuno-sensitizing role in NSCLC.

Following bioinformatics analysis, we focused on the relationship between TFEB and ABC transporters. Our NSCLC cells expressed TFEB and ABC transporters at various levels, but when we silenced TFEB in the two cell lines with the highest levels of expression, we obtained an upregulation of ABCB1 and ABCC1, and a downregulation of ABCA1, suggesting that ABC

transporters' expression could be controlled by TFEB. Our correlation matrix shows a positive association between TFEB and ABCA1, and our ChIP data further supports ABCA1 as a probable direct target of TFEB. However, TFEB was not a direct transcriptional controller of ABCB1 and ABCC1. We thus investigated an indirect mechanism. It is widely reported that TFEB controls Akt and ERK1/2 activity[105,130]. In neurons, Akt/TFEB leads to the phosphorylation of HIF-1α[131]. In heart, ERK1/2 controls HIF-1α when autophagic conditions (i.e., high TFEB activity) occur[132]. To the best of our knowledge, this is the first time that TFEB is reported to modulate Akt/HIF-1α and ERKs/HIF-1α in NSCLC. In TFEB silenced cells, we found lower activation of Akt and ERK1/2, and lower phosphorylation of HIF-1α that was translated in a reduced transcriptional activity. Since HIF-1α was a master controller of ABCB1 and ABCC1[102], this mechanism can explain the reduced expression of ABCB1 and ABCC1 upon silencing of TFEB. Hence, while ABCA1 is a direct target of TFEB, which acts as a negative regulator, the transcription of ABCB1 and ABCC1 is indirectly controlled by TFEB, i.e., through the activation of Akt/HIF-1α and ERKs/HIF-1α axis.

HIF-1α is often induced in the tumor microenvironment under low oxygen availability in solid tumors[133]. PI3K/Akt/mTOR and RAS/Raf/ERK1/2 pathways are well known activators of HIF-1α[134,135]. Our findings support this observations: indeed, in the reduced Akt and ERK1/2 activity produced upon TFEB silencing led to decreased HIF-1α phosphorylation and transcriptional activity, resulting in a downregulation of its target genes ABCB1 and ABCC1[136,137]. Since the role of TFEB is tightly connected to lysosomal bioprocesses, it also controls cholesterol homeostasis. It has been found that TFEB is influenced by nutritional state of the cell and regulates the genes involved in the lipid catabolism[138]. Previous microarray research showed that whereas TFEB overexpression enhances cellular lipid metabolism, it also perturbates lipid biosynthesis,

including steroid, lipid, and isoprenoid biosynthetic processes[138]. When we silenced TFEB in NSCLC cells, we observed a higher number of downregulated genes than upregulated genes involved in cholesterol synthesis. Among them HMGCS1 (Hydroxymethylglutaryl-CoA synthase), which transforms Acetyl-CoA into HMG-CoA, was upregulated[139]. The expression of HMGCS1 was found to be changed in many cases and one proteomics analysis revealed that generation of Abraxane-resistant A549 cells had dysregulated lipid metabolism and the most overexpressed gene was HMGCS1[140]. On the other hand, HMGCR activity was reduced leading to a decreased cholesterol synthesis, without changing in its mRNA. This decrease in HMGCR activity may be a compensatory response to the upregulation of HMGCS1 or to the increase of esterified cholesterol species, in line with the increase of LCAT, that promote a negative allosteric feed-back on HMGCR activity.

Lung cancer is not often associated with cholesterol levels, however it has been found that low HDL-cholesterol levels were linked with increased lung cancer risk[141,142]. LDL, HDL and triglyceride homeostasis is directly controlled by SREBP isoforms 1c and 2, which can also negatively regulate the expression of ABCA1 through their introns miR-33a/b[143]. Nuclear translocation and activation of SREBP2 has been shown to be induced by ERK1/2; also PKC β increased SREBP2's nuclear translocation through a mechanism mediated by MEK/ERK and JNK[144]. In line with these findings, we found that TFEB silencing decreased total ERK as well as its phosphorylated active form in our NSCLC. SREBP2 was co-expressed with p-ERK and TFEB silenced cells, where ERK1/2 activity and expression were lower, consistently showed reduced SREBP2 activation and cholesterol synthesis. It has been previously reported that TFEB silenced D4M metastatic melanoma cells had significantly decreased levels of phosphor-ERK and total ERK as well as reduced SREBP2

precursors compared to wild-type cells[105]. shTFEB-D4M cells also had downregulated HMGCR and TCA flux which resulted with low cholesterol synthesis, suggesting the negative effects of TFEB on cholesterol pathway is not cell or cancer specific rather general. Together with the lower synthesis, cholesterol was less efflux as IPP. This event can be due to the lower endogenous synthesis and/or to the lower expression of ABCA1 in shTFEB cells. This sequence of events is not new, although it has reported in NSCLC for the first time. Indeed, in a study investigating the effects of hypericin-mediated sonodynamic therapy in atherosclerotic plaques, the treatment caused THP-1 macrophages produced reactive oxygen species (ROS) which increased nuclear translocation of TFEB, expression of ABCA1 and cholesterol efflux[145]. Since our shTFEB cells had lower ABCA1 expression and IPP efflux when in co-cultures with Vγ9Vδ2 T cells, lymphocytes displayed significantly reduced activation and immune-killing in silenced TFEB compared to wild-type cells.

While there are many studies exploring the link between autophagy and MDR, our is the first study demonstrating that TFEB controls the expression of ABC transporters involved in chemo-immuno-resistance. In our study, TFEB silencing increased the expression of ABCB1 and ABCC1, in an independent way from its role in nutrient stress and autophagy, as there were no changes in AMPK/ULK1 expression. Accordingly, shTFEB cells had increased resistance to Cisplatin and Paclitaxel. This is the first report of a potential role of TFEB as chemo-sensitizer. We are aware that the direct proof of this linkage should be represented by cells overexpressing TFEB; however, TFEB overexpression deeply impact on membrane proteins endocytosis, recycling, and autophagy[146]. These effects also involve ABC transporters, making difficult the interpretation of

the mechanisms (changes in internalization, autophagosomal degradation, or transcription) and of the functional consequences on chemoresistance.

Beside the increase in transcription of ABCB1 and ABCC1, we also noticed a significant increase in the mitochondrial oxygen consumption in shTFEB cells treated with cisplatin, that reduces this parameter in wild-type cells. Indeed, part of the toxic effect of cisplatin is also due to mitochondrial damage in sensitive cells[147]. We thus wondered how TFEB silencing impacts on mitochondria energetic metabolism and has a chemoprotective role.

As cholesterol plays an important role in other compartments of the body, it is also used in the mitochondria in the production of products such as oxysterols, steroids and hepatic bile acid; on the other hand, high intracellular cholesterol in the mitochondria leads to mitochondrial dysfunction, bioenergetic failure, and eventually cell death[148]. Mitochondria uses oxidative phosphorylation to generate ATP and ETC is a crucial step in the mitochondria energy generation[149]. During carcinogenesis, cancer cells often switch from aerobic glycolysis to anaerobic glycolysis. Although this switch was attributed to mitochondria impairment, accumulating evidence show that mitochondria also contributes to cancer progression[150]. Recently, Giddings and colleagues reported that increased ETC activity and ATP production in mitochondria were observed in chemoresistance-generated cancer cell lines and this activity fuels the activity of ABC transporters, hence attenuating mitochondrial respiration decreased drug efflux through low ABC transporter activity[108]. In line with these findings, our shTFEB cells, which had lower cholesterol in their mitochondria that allowed an elevated ETC activity and mitochondrial ATP, display also increased activity of ABCB1 and ABCC1 and lower retention of cisplatin. This is an additional mechanism determining chemoresistance in shTFEB silenced cells.

Since the synthesis of the cholesterol-upstream metabolite IPP promotes immune-killing, but a low level of cholesterol may trigger chemoresistance, we next set up a pharmacological strategy that increased IPP leaving unaltered cholesterol. Since statins produce a decrease in both IPP and cholesterol, we chose nanoformulations of zoledronic acid that - at low doses -did not change cholesterol levels but was sufficient to increase IPP, since it inhibited the FPPS, leading to the accumulation of IPP. After verifying in vitro that NZ produced indeed immune-sensitizing effects, without increasing the activity of ABC transporters, we validated our findings in vivo using humanized Hu-CD34^{+} NSG mice bearing the highly chemo-immuno-resistant NCI-H2228 xenografts, wild-type or silenced for TFEB.

According to mice study of shTFEB D4M melanoma cells, TFEB downregulates the tumor growth [105], also In our previous study, we found that NZ was able to resensitize doxorubicin-resistant osteosarcoma and reduce tumor growth by increasing Vγ9Vδ2 T lymphocyte activation [73]. Similar to Nanozol-Doxorubicin combination in resistant-osteosarcoma model[73], combining NZ with cisplatin had the best anti-tumor effects on wild-type and particularly in shTFEB xenografts, without any significant side-effect.. This could be due to the restored activity of Vγ9Vδ2 T lymphocytes and/or to the amplification of the effects of cisplatin.

To identify additional mechanisms by which TFEB can further contribute to chemo and immune-resistance, we further re-analyzed the TCGA LUAD cohort to pick up possible gene signatures characterizing TFEB^{high}ABCA1^{high}ABCC1^{low} (i.e., chem-immuno-sensitive) and TFEB^{low}ABCA1^{low}ABCC1^{high} (i.e., chem-immuno-resistant) tumors.

Our KEGG, Wikipathways and GO pathway enrichment analysis indicated that differentially expressed genes between TFEB^{low}ABCA1^{low}ABCC1^{high} versus TFEB^{high}ABCA1^{high}ABCC1^{low} are

strongly correlated to the immune system. Indeed, beyond their role in drug efflux, ABC transporters are also involved in the modulation of the immune system activity that leads to cancer formation and progression. One of the endogenous substrates of ABCC1 is LTC4 which is released from mast cells and basophils to constrict the bronchi and enable the migration of inflammatory cells to lymph nodes[133,134]. In NSCLC, LTC4 is used by cancer cells and infiltrating monocytes to produce LTD4, which in turn supports cancer cell migration and cell survival[136]. In line with these findings, the leukotriene signaling pathway is upregulated in resistant $TFEB^{low}ABCA1^{low}ABCC1^{high}$ tumors.

Among the other genes associated with the $TFEB^{low}ABCA1^{low}ABCC1^{high}$ phenotype, IL-18 is a proinflammatory cytokine produced by macrophages and dendritic cells, involved in T cell subtype activation and differentiation. Most notably, IL-18, together with IL12, activates the Th1 response, which promotes tumor immune-surveillance[137,151]. IL-18 is also essential for $CD8^+$ T cell activation against NSCLC[152]. On the other hand, IL-18/IL-12 combination downregulates ABCA1 in human monocytes[153], and this may impair the anti-tumor activity of Vγ2Vδ9 T-lymphocytes, the immune population most associated with good prognosis of NSCLC [154]. Through this mechanism, IL-18 axis may negatively impair tumor immune-environment (TIME), explaining why it is associated with the $TFEB^{low}ABCA1^{low}ABCC1^{high}$, characterized by poor survival.

We further expanded the network analysis to identify possible interactors of the DEGs identified, explaining the poor survival of patients with $TFEB^{low}ABCA1^{low}ABCC1^{high}$ phenotype. First, ABCA1 and ABCC1 were found to be connected to OSGIN1, which is in turn strongly connected to PGD and CYP4F11. To our knowledge, this is the first study correlating these three genes. OSGIN1 is upregulated in endothelial cells under stress, it can prevent apoptosis by interacting with p53

and controlling cytochrome c release from mitochondria[155]. It may represent a key player in lung cancer cell apoptosis or survival in response to stress as chemotherapy. PGD gene encodes the 6PGD enzyme which is responsible for producing ribulose 5-phosphate and NADPH, essential for nucleic acid synthesis, lipogenesis, and protection from oxidative stress. Lipogenesis was reported to be upregulated in lung adenocarcinoma, and to promote tumor growth, becoming an interesting new target for lung cancer treatment [156–158]. Recently, it has been demonstrated that Liver X Receptor Alpha (LXRα) gene, which induces ABCA1 expression, also controls CYP4F11 expression[159,160], whose function is needed for NRF2-dependent lung cancer growth[161]. It has been proposed that in highly CYP4F11-expressing lung cancer cells, CYP4F11 products inhibit irreversibly stearoyl CoA desaturase, which generate unsaturated fatty acids, required for proliferation[162]. Overall, the first three players identified in one module upregulated in $TFEB^{low}ABCA1^{low}ABCC1^{high}$ NSCLC – OSGIN1, PGD and CYP4F11 – may have different and interconnected roles in preventing apoptosis and promoting proliferation, synthesizing building blocks, and protecting cancer cells from oxidative stress and unfavorable conditions as exposure to chemotherapy.

ADGRF5 and FNIP2 genes were the hub genes most significantly upregulated in the second module associated with $TFEB^{low}ABCA1^{low}ABCC1^{high}$ phenotype, and they had strongly associated each other. ADGRF5 is a poorly characterized receptor, which is highly expressed in lung and kidneys, where it is responsible for cell adhesion to extracellular matrix and cell-cell interaction[163]. The loss of function or downregulation of ADGRF5 were linked to increased airway inflammation or pulmonary alveolar proteinosis[164,165]. One in silico analysis showed that ADGRF5 is overexpressed in colorectal cancer and is associated with PI3K/Akt/mTOR pathway[166], which is a

critical pro-survival pathway also in lung cancer[167]. The second hub gene of this module, FNIP2, is associated with Birt–Hogg–Dubé syndrome, which is characterized by renal tumors, pulmonary cysts. and pneumothorax. It binds to folliculin (FLCN) to create the FLCN/FNIP1/FNIP2 complex that mediates mTORC1-dependent cell proliferation[168]. Interestingly, this axis represses TFEB activity[169]. Although there are no studies performed on the association between FNIP2 and ADGRF5, the mTORC1-dependent pathway, which acts downstream FNIP2 and ADGRF5, might be the linking player between these two genes, and with TFEB and its target ABCA1.

GTF2A2, also known as transcription factors II A2, is the hub gene of a module down-regulated in $TFEB^{low}ABCA1^{low}ABCC1^{high}$ phenotype. GTF2A2 interacts with the transcription factor TBP2 and mediates the initiation of RNA polymerase II transcription[170]. It is a target gene of STAT5, which is needed for cell survival, proliferation, angiogenesis, and metastasis in solid[171] and hematopoietic[172] cancers. There was no study explaining the relationship between GTF2A2 and ABC transporters. However, Ou-Yang and Dai[173] reported that GTF2A2 interacts with adipogenesis-related genes[174]. Since ABCA1 regulates adipocyte lipogenesis and lipid accumulation, both GTF2A2 and ABCA1 may be under the control of common homeostatic or transcriptional mechanisms, explaining why GTF2A2 is downregulated in tumors with low ABCA1.

Lastly, we discovered an immune-related extensive network down-regulated in $TFEB^{low}ABCA1^{low}ABCC1^{high}$ phenotype, led by SASH3 gene, which was strongly associated with SNX20, CD53 and IKZF1. SASH3 is one of the key players in the signal transduction in lymphocytes, and its deficiency or mutations led to impaired development of T- and B-cells, as well as NK cells[175]. Moreover, in one study correlating high JAK1 expression to good prognosis in breast cancer, infiltrating lymphocytes of JAK1-expressing tumor co-expressed SASH3, CD53 and IL10RA,

indicating that these genes are essential for immune response in breast cancer[176,177]. IKZF1 is essential for hematopoiesis and is especially involved in lymphoid differentiation[178]. A high IKZF1 expression, together with SASH3 and IL10RA, is associated with a good prognosis of head and neck squamous cell carcinoma [179], but its role in cancer is controversial and tumor dependent. Indeed, it acts as tumor-suppressor on B-cell precursor in acute lymphoblastic leukemia[180]; on the other hand, it upregulates Ikaros, which promotes migration and invasion in lung and ovarian cancer cells[181,182]. Another immune-related gene in this cluster was SNX20[183]. A high expression of SNX20 has been associated with anti-tumor TIME and better OS in lung adenocarcinoma patients[184]. Moreover, high SNX20 and PDL1 levels were proposed as a prognostic marker for lung adenocarcinoma patients who undergo PD1-inhibitor therapy[185]. SNX20 is also strongly connected with LPXN, which is in turn connected to SASH3 and CD53. LPXN encodes for leupaxin, which is a focal adhesion protein expressed in hematopoietic cells[186]. Overall, the downregulation of this extensive immune-related network – including SASH3, SNX20, CD53, IKZF1 and LPX - is consistent with the moderately immune evasive nature of NSCLC[187] and provides a further explanation of the low survival of $TFEB^{low}ABCA1^{low}ABCC1^{high}$ NSCLC patients.

6. Conclusion and Future Perspective

In this study we described that TFEB^{low}ABCA1^{low}ABCC1^{high} phenotype is an indicator of a poor prognosis in NSCLC. The association of this phenotype with poor survival may be due to the up- or downregulation of multiple gene networks controlling cell proliferation, migration, and TIME. Since TFEB and ABC transporters can be commonly detected by quantitative RT-PCR or immunohistochemistry, their measure could be included in the future diagnostic workflow of NSCLC, particularly for those patients' candidate to receive chemotherapy or immunotherapy, as good predictor of response.

This works connects TFEB with the modulation of ABCA1, which mediates immune-recognition, and ABCB1/ABCC1, that induces chemoresistance. This is the first report of TFEB as a controller of chemo-and immune-resistance in NSCLC. We are now investigating – by dry and wet biology approaches – If this linkage is limited to NSCLC or could be extended to other tumors. Until now, TFEB has been deeply connected with lysosome biogenesis and metabolism. Our work demonstrated that the effects of TFEB goes beyond lysosomal activities. For instance, it is an upstream controller of Akt/HIF-1α and ERK1/2/ HIF-1α. Moreover, we report that it has an important role in downregulating cholesterol synthesis and increasing mitochondrial energy metabolism. These two events impact on immunokilling and chemosensitivity of NSCLC. The analysis of the mechanisms linking TFEB with ABC transporters also paved the way to the use of NZ, a patented formulation of zoledronic acid in clinical trial in glioblastoma, as novel chemo-immuno-sensitizer agents in NSCLC tumors with low TFEB levels.

Moreover, our network analyses picked-up specific genes associated with the TFEB^{low}ABCA1^{low}ABCC1^{high} phenotype led to the identification of a huge number of biological

process and gene network analysis that could be responsible for the immune-evasive and chemoresistant profile. This in silico analysis is the premise to the future analysis of novel biomarkers of chemo-immuno-resistance in NSCLC, but also of a plethora of potentially actionable targets. To further understand the pleiotropic mechanism of TFEB, we are subjecting the wild-type and shTFEB tumors treated with cisplatin, NZ or their combination to single-cell RNA-Seq analysis, to better understand the qualitative and quantitative changes that high or low tumoral TFEB induces in TIME, the cell-cell network mechanisms underlining the chemo-immuno-resistance/sensitivity, identify potential gene signature predictive of chemo-immuno-sensitivity/resistance and further enlarge the spectrum of possibility sensitizing agents.

In conclusion, we identified a new function of TFEB as a driver of chemo-immuno-resistance in NSCLC. We believe that the identification of intracellular and intercellular signaling pathways up-regulating TFEB or controlled by TFEB may lead to the discovery of unexpected and novel chemo-immune-sensitizer agents.

7. Bibliography

1. Global cancer data by country | World Cancer Research Fund International. *WCRF International* https://www.wcrf.org/cancer-trends/global-cancer-data-by-country/.
2. Lung cancer statistics | World Cancer Research Fund International. *WCRF International* https://www.wcrf.org/cancer-trends/lung-cancer-statistics/.
3. Cancer today. http://gco.iarc.fr/today/home.
4. I numeri del cancro in Italia. *AIOM* https://www.aiom.it/i-numeri-del-cancro-in-italia/.
5. Passiglia, F. *et al.* Lung Cancer in Italy. *J. Thorac. Oncol.* **14**, 2046–2052 (2019).
6. Gandini, S. *et al.* Tobacco smoking and cancer: A meta-analysis. *Int. J. Cancer* **122**, 155–164 (2008).
7. Fleiss, J. L. & Gross, A. J. Meta-analysis in epidemiology, with special reference to studies of the association between exposure to environmental tobacco smoke and lung cancer: A critique. *J. Clin. Epidemiol.* **44**, 127–139 (1991).
8. Akhtar, N. & Bansal, J. G. Risk factors of Lung Cancer in nonsmoker. *Curr. Probl. Cancer* **41**, 328–339 (2017).
9. Marques, P., Piqueras, L. & Sanz, M.-J. An updated overview of e-cigarette impact on human health. *Respir. Res.* **22**, 151 (2021).
10. Abelia, X. A., Lesmana, R., Goenawan, H., Abdulah, R. & Barliana, M. I. Comparison impact of cigarettes and e-cigs as lung cancer risk inductor: a narrative review. *Eur. Rev. Med. Pharmacol. Sci.* **27**, 6301–6318 (2023).
11. Hill, W. *et al.* Lung adenocarcinoma promotion by air pollutants. *Nature* **616**, 159–167 (2023).

12. Cogliano, V. J. *et al.* Preventable Exposures Associated With Human Cancers. *JNCI J. Natl. Cancer Inst.* **103**, 1827–1839 (2011).

13. Coté, M. L. *et al.* Increased risk of lung cancer in individuals with a family history of the disease: a pooled analysis from the International Lung Cancer Consortium. *Eur. J. Cancer Oxf. Engl. 1990* **48**, 1957–1968 (2012).

14. Bailey-Wilson, J. E. *et al.* A major lung cancer susceptibility locus maps to chromosome 6q23-25. *Am. J. Hum. Genet.* **75**, 460–474 (2004).

15. Pillai, R. M. & Nair, S. A. Polymorphism of p53 in cancer prognosis. *Indian J. Med. Res.* **144**, 314–316 (2016).

16. Who Should Be Screened for Lung Cancer? | CDC. https://www.cdc.gov/cancer/lung/basic_info/screening.htm (2022).

17. Amicizia, D. *et al.* Systematic Review of Lung Cancer Screening: Advancements and Strategies for Implementation. *Healthc. Basel Switz.* **11**, 2085 (2023).

18. Pastorino, U. *et al.* Prolonged lung cancer screening reduced 10-year mortality in the MILD trial: new confirmation of lung cancer screening efficacy. *Ann. Oncol.* **30**, 1162–1169 (2019).

19. McCormick, F. KRAS as a Therapeutic Target. *Clin. Cancer Res. Off. J. Am. Assoc. Cancer Res.* **21**, 1797–1801 (2015).

20. Jančík, S., Drábek, J., Radzioch, D. & Hajdúch, M. Clinical Relevance of KRAS in Human Cancers. *J. Biomed. Biotechnol.* **2010**, 150960 (2010).

21. Bublil, E. M. & Yarden, Y. The EGF receptor family: spearheading a merger of signaling and therapeutics. *Curr. Opin. Cell Biol.* **19**, 124–134 (2007).

22. Moody, T. W., Ramos-Alvarez, I. & Jensen, R. T. Peptide G-Protein-Coupled Receptors and ErbB Receptor Tyrosine Kinases in Cancer. *Biology* **12**, 957 (2023).

23. O'Leary, C. *et al.* Epidermal Growth Factor Receptor (EGFR)-Mutated Non-Small-Cell Lung Cancer (NSCLC). *Pharmaceuticals* **13**, 273 (2020).

24. Pillai, R. N. *et al.* HER2 mutations in lung adenocarcinomas: A report from the Lung Cancer Mutation Consortium. *Cancer* **123**, 4099–4105 (2017).

25. Huang, H. Anaplastic Lymphoma Kinase (ALK) Receptor Tyrosine Kinase: A Catalytic Receptor with Many Faces. *Int. J. Mol. Sci.* **19**, 3448 (2018).

26. Kwak, E. L. *et al.* Anaplastic Lymphoma Kinase Inhibition in Non–Small-Cell Lung Cancer. *N. Engl. J. Med.* **363**, 1693–1703 (2010).

27. Sabir, S. R., Yeoh, S., Jackson, G. & Bayliss, R. EML4-ALK Variants: Biological and Molecular Properties, and the Implications for Patients. *Cancers* **9**, 118 (2017).

28. Yan, N. *et al.* BRAF-Mutated Non-Small Cell Lung Cancer: Current Treatment Status and Future Perspective. *Front. Oncol.* **12**, 863043 (2022).

29. Bracht, J. W. P. *et al.* BRAF Mutations Classes I, II, and III in NSCLC Patients Included in the SLLIP Trial: The Need for a New Pre-Clinical Treatment Rationale. *Cancers* **11**, 1381 (2019).

30. Bergethon, K. *et al.* ROS1 Rearrangements Define a Unique Molecular Class of Lung Cancers. *J. Clin. Oncol.* **30**, 863–870 (2012).

31. Dyrbekk, A. P. H. *et al.* "Evaluation of ROS1 expression and rearrangements in a large cohort of early-stage lung cancer". *Diagn. Pathol.* **18**, 70 (2023).

32. Rodriguez-Canales, J., Parra-Cuentas, E. & Wistuba, I. I. Diagnosis and Molecular Classification of Lung Cancer. *Cancer Treat. Res.* **170**, 25–46 (2016).

33. Travis, W. D., Brambilla, E. & Riely, G. J. New pathologic classification of lung cancer: relevance for clinical practice and clinical trials. *J. Clin. Oncol. Off. J. Am. Soc. Clin. Oncol.* **31**, 992–1001 (2013).

34. Nicholson, A. G. *et al.* The 2021 WHO Classification of Lung Tumors: Impact of Advances Since 2015. *J. Thorac. Oncol.* **17**, 362–387 (2022).

35. Pikor, L. A., Ramnarine, V. R., Lam, S. & Lam, W. L. Genetic alterations defining NSCLC subtypes and their therapeutic implications. *Lung Cancer Amst. Neth.* **82**, 179–189 (2013).

36. Guo, Q. *et al.* Current treatments for non-small cell lung cancer. *Front. Oncol.* **12**, 945102 (2022).

37. Restrepo, J. C., Dueñas, D., Corredor, Z. & Liscano, Y. Advances in Genomic Data and Biomarkers: Revolutionizing NSCLC Diagnosis and Treatment. *Cancers* **15**, 3474 (2023).

38. The American Joint Committee on Cancer: the 7th edition of the AJCC cancer staging manual and the future of TNM - PubMed. https://pubmed.ncbi.nlm.nih.gov/20180029/.

39. Rami-Porta, R., Asamura, H., Travis, W. D. & Rusch, V. W. Lung cancer — major changes in the American Joint Committee on Cancer eighth edition cancer staging manual. *CA. Cancer J. Clin.* **67**, 138–155 (2017).

40. Socinski, M. A. *et al.* IMpower150 Final Overall Survival Analyses for Atezolizumab Plus Bevacizumab and Chemotherapy in First-Line Metastatic Nonsquamous NSCLC. *J. Thorac. Oncol.* **16**, 1909–1924 (2021).

41. Kogure, Y. *et al.* Efficacy and safety of carboplatin with nab-paclitaxel versus docetaxel in older patients with squamous non-small-cell lung cancer (CAPITAL): a randomised, multicentre, open-label, phase 3 trial. *Lancet Healthy Longev.* **2**, e791–e800 (2021).

42. Lackey, A. & Donington, J. S. Surgical Management of Lung Cancer. *Semin. Interv. Radiol.* **30**, 133–140 (2013).

43. Megyesfalvi, Z. *et al.* Clinical insights into small cell lung cancer: Tumor heterogeneity, diagnosis, therapy, and future directions. *CA. Cancer J. Clin.* (2023) doi:10.3322/caac.21785.

44. Ko, E. C., Raben, D. & Formenti, S. C. The Integration of Radiotherapy with Immunotherapy for the Treatment of Non-Small Cell Lung Cancer. *Clin. Cancer Res. Off. J. Am. Assoc. Cancer Res.* **24**, 5792–5806 (2018).

45. Dasari, S. & Tchounwou, P. B. Cisplatin in cancer therapy: molecular mechanisms of action. *Eur. J. Pharmacol.* **740**, 364–378 (2014).

46. Ghosh, S. Cisplatin: The first metal based anticancer drug. *Bioorganic Chem.* **88**, 102925 (2019).

47. Tan, N. *et al.* Navitoclax Enhances the Efficacy of Taxanes in Non–Small Cell Lung Cancer Models. *Clin. Cancer Res.* **17**, 1394–1404 (2011).

48. Tan, T. *et al.* Efficacy and safety of nab-paclitaxel plus platinum in non-small cell lung cancer: a meta-analysis. *Front. Med.* **10**, 1139248 (2023).

49. Ramalingam, S. & Belani, C. P. Carboplatin/gemcitabine combination in advanced NSCLC. *Oncol. Williston Park N* **18**, 21–26 (2004).

50. Hazarika, M., White, R. M., Johnson, J. R. & Pazdur, R. FDA drug approval summaries: pemetrexed (Alimta). *The Oncologist* **9**, 482–488 (2004).

51. Hanna, N. *et al.* Randomized Phase III Trial of Pemetrexed Versus Docetaxel in Patients With Non-Small-Cell Lung Cancer Previously Treated With Chemotherapy. *J. Clin. Oncol. Off. J. Am. Soc. Clin. Oncol.* **41**, 2682–2690 (2023).

52. Gadgeel, S. *et al.* Updated Analysis From KEYNOTE-189: Pembrolizumab or Placebo Plus Pemetrexed and Platinum for Previously Untreated Metastatic Nonsquamous Non-Small-Cell Lung Cancer. *J. Clin. Oncol. Off. J. Am. Soc. Clin. Oncol.* **38**, 1505–1517 (2020).

53. Cheng, Y., Zhang, T. & Xu, Q. Therapeutic advances in non-small cell lung cancer: Focus on clinical development of targeted therapy and immunotherapy. *MedComm* **2**, 692–729 (2021).

54. Mamdani, H., Matosevic, S., Khalid, A. B., Durm, G. & Jalal, S. I. Immunotherapy in Lung Cancer: Current Landscape and Future Directions. *Front. Immunol.* **13**, 823618 (2022).

55. Han, Y., Liu, D. & Li, L. PD-1/PD-L1 pathway: current researches in cancer. *Am. J. Cancer Res.* **10**, 727–742 (2020).

56. Salmaninejad, A. *et al.* PD-1 and cancer: molecular mechanisms and polymorphisms. *Immunogenetics* **70**, 73–86 (2018).

57. Shiravand, Y. *et al.* Immune Checkpoint Inhibitors in Cancer Therapy. *Curr. Oncol.* **29**, 3044–3060 (2022).

58. Lesokhin, A. M., Callahan, M. K., Postow, M. A. & Wolchok, J. D. On being less tolerant: enhanced cancer immunosurveillance enabled by targeting checkpoints and agonists of T cell activation. *Sci. Transl. Med.* **7**, 280sr1 (2015).

59. Paulsen, E.-E. *et al.* CTLA-4 expression in the non-small cell lung cancer patient tumor microenvironment: diverging prognostic impact in primary tumors and lymph node metastases. *Cancer Immunol. Immunother.* **66**, 1449–1461 (2017).

60. Vellanki, P. J. *et al.* FDA Approval Summary: Nivolumab with Ipilimumab and Chemotherapy for Metastatic Non-Small Cell Lung Cancer, a Collaborative Project Orbis Review. *Clin. Cancer Res. Off. J. Am. Assoc. Cancer Res.* **27**, 3522–3527 (2021).

61. Bou Antoun, N. & Chioni, A.-M. Dysregulated Signalling Pathways Driving Anticancer Drug Resistance. *Int. J. Mol. Sci.* **24**, 12222 (2023).

62. Wang, X., Zhang, H. & Chen, X. Drug resistance and combating drug resistance in cancer. *Cancer Drug Resist.* **2**, 141–160 (2019).

63. Robey, R. W. *et al.* Revisiting the role of ABC transporters in multidrug-resistant cancer. *Nat. Rev. Cancer* **18**, 452–464 (2018).

64. Cole, S. P. C. Multidrug Resistance Protein 1 (MRP1, ABCC1), a "Multitasking" ATP-binding Cassette (ABC) Transporter. *J. Biol. Chem.* **289**, 30880–30888 (2014).

65. Dean, M., Rzhetsky, A. & Allikmets, R. The human ATP-binding cassette (ABC) transporter superfamily. *Genome Res.* **11**, 1156–1166 (2001).

66. Kachalaki, S., Ebrahimi, M., Mohamed Khosroshahi, L., Mohammadinejad, S. & Baradaran, B. Cancer chemoresistance; biochemical and molecular aspects: a brief overview. *Eur. J. Pharm. Sci.* **89**, 20–30 (2016).

67. Zhang, Q. *et al.* Apatinib Reverses Paclitaxel-resistant Lung Cancer Cells (A549) Through Blocking the Function of ABCB1 Transporter. *Anticancer Res.* **39**, 5461–5471 (2019).

68. Hu, P. *et al.* Clinical relevance of the multidrug resistance-associated protein 1 gene in non-small cell lung cancer: A systematic review and meta-analysis. *Oncol. Rep.* **40**, 3078–3091 (2018).

69. Adorni, M. P. *et al.* A New ABCB1 Inhibitor Enhances the Anticancer Effect of Doxorubicin in Both In Vitro and In Vivo Models of NSCLC. *Int. J. Mol. Sci.* **24**, 989 (2023).

70. Wu, K., Zou, L., Lei, X. & Yang, X. Roles of ABCA1 in cancer. *Oncol. Lett.* **24**, 349 (2022).

71. Castella, B. *et al.* The ATP-binding cassette transporter A1 regulates phosphoantigen release and Vγ9Vδ2 T cell activation by dendritic cells. *Nat. Commun.* **8**, 15663 (2017).

72. Jacobo-Albavera, L., Domínguez-Pérez, M., Medina-Leyte, D. J., González-Garrido, A. & Villarreal-Molina, T. The Role of the ATP-Binding Cassette A1 (ABCA1) in Human Disease. *Int. J. Mol. Sci.* **22**, 1593 (2021).

73. Belisario, D. C. *et al.* ABCA1/ABCB1 Ratio Determines Chemo- and Immune-Sensitivity in Human Osteosarcoma. *Cells* **9**, 647 (2020).

74. Salaroglio, I. C. *et al.* Mitochondrial ROS drive resistance to chemotherapy and immune-killing in hypoxic non-small cell lung cancer. *J. Exp. Clin. Cancer Res. CR* **41**, 243 (2022).

75. Ma, Y., Li, X., Cheng, S., Wei, W. & Li, Y. MicroRNA-106a confers cisplatin resistance in non-small cell lung cancer A549 cells by targeting adenosine triphosphatase-binding cassette A1. *Mol. Med. Rep.* **11**, 625–632 (2015).

76. Vargas, T. *et al.* ColoLipidGene: signature of lipid metabolism-related genes to predict prognosis in stage-II colon cancer patients. *Oncotarget* **6**, 7348–7363 (2015).

77. Pan, H. *et al.* Expression of LXR-β, ABCA1 and ABCG1 in human triple-negative breast cancer tissues. *Oncol. Rep.* **42**, 1869–1877 (2019).

78. He, L. *et al.* Autophagy: The Last Defense against Cellular Nutritional Stress. *Adv. Nutr. Bethesda Md* **9**, 493–504 (2018).

79. Zhang, L., Li, Z., Zhang, L., Qin, Y. & Yu, D. Dissecting the multifaced function of transcription factor EB (TFEB) in human diseases: From molecular mechanism to pharmacological modulation. *Biochem. Pharmacol.* **215**, 115698 (2023).

80. Settembre, C. & Ballabio, A. Lysosome: regulator of lipid degradation pathways. *Trends Cell Biol.* **24**, 743–750 (2014).

81. Napolitano, G. & Ballabio, A. TFEB at a glance. *J. Cell Sci.* **129**, 2475–2481 (2016).

82. Settembre, C. *et al.* TFEB links autophagy to lysosomal biogenesis. *Science* **332**, 1429–1433 (2011).

83. Settembre, C. *et al.* A lysosome-to-nucleus signalling mechanism senses and regulates the lysosome via mTOR and TFEB. *EMBO J.* **31**, 1095–1108 (2012).

84. Martina, J. A., Chen, Y., Gucek, M. & Puertollano, R. MTORC1 functions as a transcriptional regulator of autophagy by preventing nuclear transport of TFEB. *Autophagy* **8**, 903–914 (2012).

85. Giatromanolaki, A. *et al.* Increased expression of transcription factor EB (TFEB) is associated with autophagy, migratory phenotype and poor prognosis in non-small cell lung cancer. *Lung Cancer* **90**, 98–105 (2015).

86. Wang, L. *et al.* Down Regulation of SIRT2 Reduced ASS Induced NSCLC Apoptosis Through the Release of Autophagy Components via Exosomes. *Front. Cell Dev. Biol.* **8**, (2020).

87. Li, M., Wang, Z., Wang, P., Li, H. & Yang, L. TFEB: A Emerging Regulator in Lipid Homeostasis for Atherosclerosis. *Front. Physiol.* **12**, (2021).

88. Li, Y. *et al.* TFEB is a master regulator of tumor-associated macrophages in breast cancer. *J. Immunother. Cancer* **8**, e000543 (2020).

89. Alexa-Stratulat, T., Pešić, M., Gašparović, A. Č., Trougakos, I. P. & Riganti, C. What sustains the multidrug resistance phenotype beyond ABC efflux transporters? Looking beyond the tip of the iceberg. *Drug Resist. Updat. Rev. Comment. Antimicrob. Anticancer Chemother.* **46**, 100643 (2019).

90. Carlson, M. org.Hs.eg.db. *Bioconductor* http://bioconductor.org/packages/org.Hs.eg.db/ (2019).

91. Love, M. I., Huber, W. & Anders, S. Moderated estimation of fold change and dispersion for RNA-seq data with DESeq2. *Genome Biol.* **15**, 550 (2014).

92. Hänzelmann, S., Castelo, R. & Guinney, J. GSVA: gene set variation analysis for microarray and RNA-Seq data. *BMC Bioinformatics* **14**, 7 (2013).

93. Ritchie, M. E. *et al.* limma powers differential expression analyses for RNA-sequencing and microarray studies. *Nucleic Acids Res.* **43**, e47 (2015).

94. Langfelder, P. & Horvath, S. WGCNA: an R package for weighted correlation network analysis. *BMC Bioinformatics* **9**, 559 (2008).

95. Doronzo, G. *et al.* TFEB controls vascular development by regulating the proliferation of endothelial cells. *EMBO J.* **38**, e98250 (2019).

96. Campia, I. *et al.* Digoxin and ouabain induce the efflux of cholesterol via liver X receptor signalling and the synthesis of ATP in cardiomyocytes. *Biochem. J.* **447**, 301–311 (2012).

97. Castella, B. *et al.* Immune modulation by zoledronic acid in human myeloma: an advantageous cross-talk between Vγ9Vδ2 T cells, αβ CD8+ T cells, regulatory T cells, and dendritic cells. *J. Immunol. Baltim. Md 1950* **187**, 1578–1590 (2011).

98. Xu, X. *et al.* HSD17B7 gene in self-renewal and oncogenicity of keratinocytes from Black versus White populations. *EMBO Mol. Med.* **13**, e14133 (2021).

99. Spinelli, J. B. *et al.* Fumarate is a terminal electron acceptor in the mammalian electron transport chain. *Science* **374**, 1227–1237 (2021).

100. Cimini, E. *et al.* Zoledronic acid enhances Vδ2 T-lymphocyte antitumor response to human glioma cell lines. *Int. J. Immunopathol. Pharmacol.* **24**, 139–148 (2011).

101. Kopecka, J. *et al.* Zoledronic acid-encapsulating self-assembling nanoparticles and doxorubicin: a combinatorial approach to overcome simultaneously chemoresistance and immunoresistance in breast tumors. *Oncotarget* **7**, 20753–20772 (2016).

102. Belisario, D. C. *et al.* Hypoxia Dictates Metabolic Rewiring of Tumors: Implications for Chemoresistance. *Cells* **9**, 2598 (2020).

103. Czuba, L. C., Hillgren, K. M. & Swaan, P. W. Post-translational Modifications of Transporters. *Pharmacol. Ther.* **192**, 88–99 (2018).

104. Paquette, M. *et al.* AMPK-dependent phosphorylation is required for transcriptional activation of TFEB and TFE3. *Autophagy* **17**, 3957–3975 (2021).

105. Ariano, C. *et al.* TFEB inhibition induces melanoma shut-down by blocking the cell cycle and rewiring metabolism. *Cell Death Dis.* **14**, 314 (2023).

106. Arito, M., Horiba, T., Hachimura, S., Inoue, J. & Sato, R. Growth factor-induced phosphorylation of sterol regulatory element-binding proteins inhibits sumoylation, thereby stimulating the expression of their target genes, low density lipoprotein uptake, and lipid synthesis. *J. Biol. Chem.* **283**, 15224–15231 (2008).

107. Monteiro, J. P., Oliveira, P. J. & Jurado, A. S. Mitochondrial membrane lipid remodeling in pathophysiology: a new target for diet and therapeutic interventions. *Prog. Lipid Res.* **52**, 513–528 (2013).

108. Giddings, E. L. *et al.* Mitochondrial ATP fuels ABC transporter-mediated drug efflux in cancer chemoresistance. *Nat. Commun.* **12**, 2804 (2021).

109. Räikkönen, J. *et al.* Correlation between time-dependent inhibition of human farnesyl pyrophosphate synthase and blockade of mevalonate pathway by nitrogen-containing bisphosphonates in cultured cells. *Biochem. Biophys. Res. Commun.* **407**, 663–667 (2011).

110. Ristori, S. *et al.* Structural Characterization of Self-Assembling Hybrid Nanoparticles for Bisphosphonate Delivery in Tumors. *Mol. Pharm.* **15**, 1258–1265 (2018).

111. Mohammad, I. S., He, W. & Yin, L. Understanding of human ATP binding cassette superfamily and novel multidrug resistance modulators to overcome MDR. *Biomed. Pharmacother.* **100**, 335–348 (2018).

112. Wang, Y. *et al.* The role of non-coding RNAs in ABC transporters regulation and their clinical implications of multidrug resistance in cancer. *Expert Opin. Drug Metab. Toxicol.* **17**, 291–306 (2021).

113. Palmeira, A., Sousa, E., Vasconcelos, M. H. & Pinto, M. M. Three Decades of P-gp Inhibitors: Skimming Through Several Generations and Scaffolds. *Curr. Med. Chem.* **19**, 1946–2025.

114. Hanahan, D. Hallmarks of Cancer: New Dimensions. *Cancer Discov.* **12**, 31–46 (2022).

115. Vailati-Riboni, M., Palombo, V. & Loor, J. J. What Are Omics Sciences? in *Periparturient Diseases of Dairy Cows: A Systems Biology Approach* (ed. Ametaj, B. N.) 1–7 (Springer International Publishing, 2017). doi:10.1007/978-3-319-43033-1_1.

116. Giatromanolaki, A. *et al.* Autophagy and lysosomal related protein expression patterns in human glioblastoma. *Cancer Biol. Ther.* **15**, 1468–1478 (2014).

117. Giatromanolaki, A., Sivridis, E., Kalamida, D. & Koukourakis, M. I. Transcription Factor EB Expression in Early Breast Cancer Relates to Lysosomal/Autophagosomal Markers and Prognosis. *Clin. Breast Cancer* **17**, e119–e125 (2017).

118. Liang, J., Jia, X., Wang, K. & Zhao, N. High expression of TFEB is associated with aggressive clinical features in colorectal cancer. *OncoTargets Ther.* **11**, 8089–8098 (2018).

119. Bahrami, A., Bianconi, V., Pirro, M., Orafai, H. M. & Sahebkar, A. The role of TFEB in tumor cell autophagy: Diagnostic and therapeutic opportunities. *Life Sci.* **244**, 117341 (2020).

120. Munoz, M., Henderson, M., Haber, M. & Norris, M. Role of the MRP1/ABCC1 multidrug transporter protein in cancer. *IUBMB Life* **59**, 752–757 (2007).

121. Vesel, M. *et al.* ABCB1 and ABCG2 drug transporters are differentially expressed in non-small cell lung cancers (NSCLC) and expression is modified by cisplatin treatment via altered Wnt signaling. *Respir. Res.* **18**, 52 (2017).

122. Fang, L. *et al.* Prognostic role of multidrug resistance-associated protein 1 expression and platelet count in operable non-small cell lung cancer. *Oncol. Lett.* **16**, 1123–1132 (2018).

123. Maslyanko, M., Harris, R. D. & Mu, D. Connecting Cholesterol Efflux Factors to Lung Cancer Biology and Therapeutics. *Int. J. Mol. Sci.* **22**, 7209 (2021).

124. Halimi, H. & Farjadian, S. Cholesterol: An important actor on the cancer immune scene. *Front. Immunol.* **13**, 1057546 (2022).

125. Liu, X. *et al.* Tubeimoside-1 induces TFEB-dependent lysosomal degradation of PD-L1 and promotes antitumor immunity by targeting mTOR. *Acta Pharm. Sin. B* **11**, 3134–3149 (2021).

126. Lee, B. H. *et al.* Dysregulation of cholesterol homeostasis in human prostate cancer through loss of ABCA1. *Cancer Res.* **73**, 1211–1218 (2013).

127. Smith, B. & Land, H. Anticancer Activity of the Cholesterol Exporter ABCA1 Gene. *Cell Rep.* **2**, 580–590 (2012).

128. Liu, K., Zhang, W., Tan, J., Ma, J. & Zhao, J. MiR-200b-3p Functions as an Oncogene by Targeting ABCA1 in Lung Adenocarcinoma. *Technol. Cancer Res. Treat.* **18**, 1533033819892590 (2019).

129. Chien, J. *et al.* Analysis of gene expression in stage I serous tumors identifies critical pathways altered in ovarian cancer. *Gynecol. Oncol.* **114**, 3–11 (2009).

130. Hu, J.-H. *et al.* TFEB: a double-edged sword for tumor metastasis. *J. Mol. Med. Berl. Ger.* **101**, 917–929 (2023).

131. Cen, J. *et al.* A Water-Soluble Quercetin Conjugate with Triple Targeting Exerts Neuron-Protective Effect on Cerebral Ischemia by Mitophagy Activation. *Adv. Healthc. Mater.* **11**, e2200817 (2022).

132. Popov, S. V. *et al.* Regulation of autophagy of the heart in ischemia and reperfusion. *Apoptosis Int. J. Program. Cell Death* **28**, 55–80 (2023).

133. Fan, J., To, K. K. W., Chen, Z.-S. & Fu, L. ABC transporters affects tumor immune microenvironment to regulate cancer immunotherapy and multidrug resistance. *Drug Resist. Updat.* **66**, 100905 (2023).

134. Sim, S., Choi, Y. & Park, H.-S. Immunologic Basis of Type 2 Biologics for Severe Asthma. *Immune Netw.* **22**, e45 (2022).

135. Kietzmann, T., Mennerich, D. & Dimova, E. Y. Hypoxia-Inducible Factors (HIFs) and Phosphorylation: Impact on Stability, Localization, and Transactivity. *Front. Cell Dev. Biol.* **4**, 11 (2016).

136. Lukic, A. *et al.* Exosomes and cells from lung cancer pleural exudates transform LTC4 to LTD4, promoting cell migration and survival via CysLT1. *Cancer Lett.* **444**, 1–8 (2019).

137. Kaplanski, G. Interleukin-18: Biological properties and role in disease pathogenesis. *Immunol. Rev.* **281**, 138–153 (2018).

138. Settembre, C. *et al.* TFEB controls cellular lipid metabolism through a starvation-induced autoregulatory loop. *Nat. Cell Biol.* **15**, 647–658 (2013).

139. Fragki, S. *et al.* Systemic PFOS and PFOA exposure and disturbed lipid homeostasis in humans: what do we know and what not? *Crit. Rev. Toxicol.* **51**, 141–164 (2021).

140. Zhao, M. *et al.* Quantitative Proteomic Analysis of Cellular Resistance to the Nanoparticle Abraxane. *ACS Nano* **9**, 10099–10112 (2015).

141. Ding, X., Zhang, W., Li, S. & Yang, H. The role of cholesterol metabolism in cancer. *Am. J. Cancer Res.* **9**, 219–227 (2019).

142. Kucharska-Newton, A. M. *et al.* HDL-cholesterol and the incidence of lung cancer in the Atherosclerosis Risk in Communities (ARIC) study. *Lung Cancer Amst. Neth.* **61**, 292–300 (2008).

143. Ma, W. *et al.* Methyl protodioscin increases ABCA1 expression and cholesterol efflux while inhibiting gene expressions for synthesis of cholesterol and triglycerides by suppressing SREBP transcription and microRNA 33a/b levels. *Atherosclerosis* **239**, 566–570 (2015).

144. Wong, T. Y., Tan, Y. Q., Lin, S.-M. & Leung, L. K. Phorbol 12-myristate 13-acetate promotes nuclear translocation of hepatic steroid response element binding protein-2. *Int. J. Biochem. Cell Biol.* **75**, 1–10 (2016).

145. Li, X. *et al.* Hypericin-mediated sonodynamic therapy induces autophagy and decreases lipids in THP-1 macrophage by promoting ROS-dependent nuclear translocation of TFEB. *Cell Death Dis.* **7**, e2527 (2016).

146. Appelqvist, H., Wäster, P., Kågedal, K. & Öllinger, K. The lysosome: from waste bag to potential therapeutic target. *J. Mol. Cell Biol.* **5**, 214–226 (2013).

147. Gao, X. *et al.* Fucoidan-proanthocyanidins nanoparticles protect against cisplatin-induced acute kidney injury by activating mitophagy and inhibiting mtDNA-cGAS/STING signaling pathway. *Int. J. Biol. Macromol.* **245**, 125541 (2023).

148. Goicoechea, L., Conde de la Rosa, L., Torres, S., García-Ruiz, C. & Fernández-Checa, J. C. Mitochondrial cholesterol: Metabolism and impact on redox biology and disease. *Redox Biol.* **61**, 102643 (2023).

149. Ahmad, M., Wolberg, A. & Kahwaji, C. I. Biochemistry, Electron Transport Chain. in *StatPearls* (StatPearls Publishing, 2023).

150. Zong, W.-X., Rabinowitz, J. D. & White, E. Mitochondria and Cancer. *Mol. Cell* **61**, 667–676 (2016).

151. Novick, D., Kim, S., Kaplanski, G. & Dinarello, C. A. Interleukin-18, more than a Th1 cytokine. *Semin. Immunol.* **25**, 439–448 (2013).

152. Timperi, E. *et al.* IL-18 receptor marks functional CD8+ T cells in non-small cell lung cancer. *Oncoimmunology* **6**, e1328337 (2017).

153. Yu, X.-H. *et al.* Interleukin-18 and interleukin-12 together downregulate ATP-binding cassette transporter A1 expression through the interleukin-18R/nuclear factor-κB signaling pathway in THP-1 macrophage-derived foam cells. *Circ. J. Off. J. Jpn. Circ. Soc.* **76**, 1780–1791 (2012).

154. Gentles, A. J. *et al.* The prognostic landscape of genes and infiltrating immune cells across human cancers. *Nat. Med.* **21**, 938–945 (2015).

155. Khoi, C.-S., Xiao, C.-Q., Hung, K.-Y., Lin, T.-Y. & Chiang, C.-K. Oxidative Stress-Induced Growth Inhibitor (OSGIN1), a Target of X-Box-Binding Protein 1, Protects Palmitic Acid-Induced Vascular Lipotoxicity through Maintaining Autophagy. *Biomedicines* **10**, 992 (2022).

156. Satanowski, A. *et al.* Awakening a latent carbon fixation cycle in Escherichia coli. *Nat. Commun.* **11**, 5812 (2020).

157. Jiang, X. *et al.* Systematic Analysis and Validation of the Prognosis, Immunological Role and Biology Function of the Ferroptosis-Related lncRNA GSEC/miRNA-101-3p/CISD1 Axis in Lung Adenocarcinoma. *Front. Mol. Biosci.* **8**, 793732 (2021).

158. Khan, G. B., Qasim, M., Rasul, A., Ashfaq, U. A. & Alnuqaydan, A. M. Identification of Lignan Compounds as New 6-Phosphogluconate Dehydrogenase Inhibitors for Lung Cancer. *Metabolites* **13**, 34 (2022).

159. He, P., Gelissen, I. C. & Ammit, A. J. Regulation of ATP binding cassette transporter A1 (ABCA1) expression: cholesterol-dependent and – independent signaling pathways with relevance to inflammatory lung disease. *Respir. Res.* **21**, 250 (2020).

160. Zhang, T. *et al.* Regulation of cytochrome P450 4F11 expression by liver X receptor alpha. *Int. Immunopharmacol.* **90**, 107240 (2021).

161. Bar-Peled, L. *et al.* Chemical Proteomics Identifies Druggable Vulnerabilities in a Genetically Defined Cancer. *Cell* **171**, 696-709.e23 (2017).

162. Theodoropoulos, P. C. *et al.* Discovery of tumor-specific irreversible inhibitors of stearoyl CoA desaturase. *Nat. Chem. Biol.* **12**, 218–225 (2016).

163. Einspahr, J. M. & Tilley, D. G. Pathophysiological impact of the adhesion G protein-coupled receptor family. *Am. J. Physiol. Cell Physiol.* **323**, C640–C647 (2022).

164. Fukuzawa, T. *et al.* Lung Surfactant Levels are Regulated by Ig-Hepta/GPR116 by Monitoring Surfactant Protein D. *PLOS ONE* **8**, e69451 (2013).

165. Kubo, F. *et al.* Loss of the adhesion G-protein coupled receptor ADGRF5 in mice induces airway inflammation and the expression of CCL2 in lung endothelial cells. *Respir. Res.* **20**, 11 (2019).

166. Kang, H., Fichna, J., Matlawska-Wasowska, K. & Jacenik, D. The Expression Pattern of Adhesion G Protein-Coupled Receptor F5 Is Related to Cell Adhesion and Metastatic

Pathways in Colorectal Cancer-Comprehensive Study Based on In Silico Analysis. *Cells* **11**, 3876 (2022).

167. Tan, A. C. Targeting the PI3K/Akt/mTOR pathway in non-small cell lung cancer (NSCLC). *Thorac. Cancer* **11**, 511–518 (2020).

168. Hasumi, H., Baba, M., Hasumi, Y., Furuya, M. & Yao, M. Birt–Hogg–Dubé syndrome: Clinical and molecular aspects of recently identified kidney cancer syndrome. *Int. J. Urol.* **23**, 204–210 (2016).

169. Fenner, A. Differential mTORC1 pathways in BHD. *Nat. Rev. Urol.* **17**, 485–485 (2020).

170. Pangas, S. A. & Rajkovic, A. Chapter 21 - Follicular Development: Mouse, Sheep, and Human Models. in *Knobil and Neill's Physiology of Reproduction (Fourth Edition)* (eds. Plant, T. M. & Zeleznik, A. J.) 947–995 (Academic Press, 2015). doi:10.1016/B978-0-12-397175-3.00021-1.

171. Ren, Z. *et al.* Phosphorylated STAT5 regulates p53 expression via BRCA1/BARD1-NPM1 and MDM2. *Cell Death Dis.* **7**, e2560 (2016).

172. Girardot, M. *et al.* Persistent STAT5 activation in myeloid neoplasms recruits p53 into gene regulation. *Oncogene* **34**, 1323 (2015).

173. Y, O.-Y. & Mm, D. Screening for genes, miRNAs and transcription factors of adipogenic differentiation and dedifferentiation of mesenchymal stem cells. *J. Orthop. Surg.* **18**, (2023).

174. Cuffe, H. *et al.* Targeted deletion of adipocyte Abca1 impairs diet-induced obesity. *Arterioscler. Thromb. Vasc. Biol.* **38**, 733–743 (2018).

175. Delmonte, O. M. *et al.* SASH3 variants cause a novel form of X-linked combined immunodeficiency with immune dysregulation. *Blood* **138**, 1019–1033 (2021).

176. Bai, M., Pan, Q. & Sun, C. Tumor Purity Coexpressed Genes Related to Immune Microenvironment and Clinical Outcomes of Lung Adenocarcinoma. *J. Oncol.* **2021**, 9548648 (2021).

177. Chen, B. *et al.* JAK1 as a prognostic marker and its correlation with immune infiltrates in breast cancer. *Aging* **11**, 11124–11135 (2019).

178. Yang, L., Luo, Y. & Wei, J. Integrative genomic analyses on Ikaros and its expression related to solid cancer prognosis. *Oncol. Rep.* **24**, 571–577 (2010).

179. Wang, J. *et al.* Establishment and validation of immune microenvironmental gene signatures for predicting prognosis in patients with head and neck squamous cell carcinoma. *Int. Immunopharmacol.* **97**, 107817 (2021).

180. Marke, R., Leeuwen, F. N. van & Scheijen, B. The many faces of IKZF1 in B-cell precursor acute lymphoblastic leukemia. *Haematologica* **103**, 565–574 (2018).

181. He, L.-C. *et al.* Ikaros inhibits proliferation and, through upregulation of Slug, increases metastatic ability of ovarian serous adenocarcinoma cells. *Oncol. Rep.* **28**, 1399–1405 (2012).

182. Zhao, W., Chen, T. & Wang, H. Ikaros is heterogeneously expressed in lung adenocarcinoma and is involved in its progression. *J. Int. Med. Res.* **48**, 0300060520945860 (2020).

183. Schaff, U. Y. *et al.* SLIC-1/Sorting Nexin 20: A novel sorting nexin that directs subcellular distribution of PSGL-1. *Eur. J. Immunol.* **38**, 550–564 (2008).

184. Wu, G. J. *et al.* SNX20 Expression Correlates with Immune Cell Infiltration and Can Predict Prognosis in Lung Adenocarcinoma. *Int. J. Gen. Med.* **14**, 7599–7611 (2021).

185. Fan, L. *et al.* Increased SNX20 and PD-L1 Levels Can Predict the Clinical Response to PD-1 Inhibitors in Lung Adenocarcinoma. *OncoTargets Ther.* **13**, 10075–10085 (2020).

186. Tanaka, T., Moriwaki, K., Murata, S. & Miyasaka, M. LIM domain-containing adaptor, leupaxin, localizes in focal adhesion and suppresses the integrin-induced tyrosine phosphorylation of paxillin. *Cancer Sci.* **101**, 363–368 (2010).

187. Anichini, A., Perotti, V. E., Sgambelluri, F. & Mortarini, R. Immune Escape Mechanisms in Non Small Cell Lung Cancer. *Cancers* **12**, 3605 (2020).

First and foremost, I would like to thank my PhD supervisor Prof. Chiara Riganti for her constant support, guidance and encouragement that have been invaluable throughout my entire PhD journey. I feel incredibly fortunate to have had her guidance and mentorship. I also would like to thank Iris Chiara Salaroglio, Joanna Kopecka, and Costanzo Costamagna for helping me with my never-ending questions. I am grateful to everyone I've collaborated with externally; Prof. Federico Bussolino, Dr. Gabriella Doronzo, and Camilla Ariano at Candiolo Cancer Institute for their help with my TFEB project.

My research has led me to countless places to visit and learn new things, but one has a significant place in my heart, Vienna. I've been incredibly lucky to have Dr. Thomas Mohr as a mentor for not only in bioinformatics but also in life, and Dr. Tatiana Chontorotsea for her help with our scRNA-seq projects.

I am indebted to my exceptional lab mates Martina, Simona and Sabrina, and Giulia whose support has been a constant source of motivation. You're the best PhD crew that one can only imagine, it's been great fun working with you all! I'll fondly remember all our successes and failures at our lab and cherish them forever.

To my better half Seren, words cannot express how much your unwavering belief in me has meant. You have been my biggest cheerleader throughout this journey, and I cannot thank you enough for your love and support. Your everlasting support brought me success and made me excel at not only academia but also life.

Finally, I would like to thank my family for believing in me and for their encouragement to pursue my dreams. Their belief in me has kept my spirits and motivation high during this process.